NTNU – Trondheim
Norwegian University of
Science and Technology

Condition Assessment of Medium Voltage Cable Joints

Dielectric Spectroscopy of field grading materials

Mai-Linn Sanden

Master of Energy and Environmental Engineering
Submission date: June 2015
Supervisor: Frank Mauseth, ELKRAFT
Co-supervisor: Sverre Hvidsten, SINTEF Energy Research

Norwegian University of Science and Technology
Department of Electric Power Engineering

Project description

A significant part of the Norwegian medium voltage cable distribution net is older than the expected lifetime of 30 years. Cable joints have a shorter expected lifetime than the cable. In case of heat-shrink joints installed in the 80's, many service failures have occurred due to over-heating of the metallic connector. In general, the condition of the insulation of the joints can be assessed by partial discharge measurements or dielectric spectroscopy.

For joints and terminations, field grading materials (FGM) are often used to achieve the wanted field distribution to avoid local field enhancement and partial discharges. The dielectric properties of the FGM will also be influenced by the frequency of the applied voltage, but also humidity and temperature will influence the resulting field distribution.

The project work will be mainly experimental. Field grading material will be characterized as function of frequency and electric field. The influence of humidity is also important and will also be investigated during the master work.

Preface

This master thesis is written during spring semester of 2015. The thesis is a final assignment of a five years M.Sc. in Energy and Environmental engineering at the Norwegian University of Science and Technology. The thesis is carried out at the Department of Electric Power Engineering in collaboration with SINTEF Energy Research.

The master work has mostly been experimental, with numerous hours spent in the laboratory. A parallel experiment was performed at SINTEF Energy research, with measurements performed on the same test objects utilized in this thesis. Measurement results found by SINTEF Energy Research is thereby to be used in this thesis for analysis of the obtained values here.

Trondheim, June 2015

Mai-Linn Sanden

Acknowledgement

I would like to thank my supervisor Frank Mauseth at NTNU and co-supervisor Sverre Hvidsten at SINTEF Energy Research. For guidance and help throughout the master work, insightful advises and practical assistance in laboratory.

Thanks to Henrik Enoksen for help with preparing and conditioning the test objects correctly before measurements, in addition to helpful information through the master work. I would also thank Torbjørn Andersen Ve for help in the laboratory when performing water uptake measurements, and Jorunn Hølto with guidance during differential scanning calorimetry measurements.

I must thank my fellow students at NTNU, especially my four closest girlfriends, for good times and many wonderful memories during these five years.

I would wish to express my deepest appreciation to Yngve, for your support and patience throughout the semester. For encouraging and helping me when I needed it and for all those hours you have spent reading and correcting my thesis. I valuable your advices and critical comments.

At last, I would like express a sincere gratitude to my family. For love and support throughout the years, and all the possibilities you have provided me.

(PS: Frank, I still got my long nails.)

Abstract

This thesis examines the electrical properties of a commonly used stress control tube for medium voltage heat-shrink joints using non-destructive methods in laboratory. The electrical properties of the tube were determined by use of dielectric spectroscopy while changing the temperature, AC electric field and humidity level. In order to characterize the material, both differential scanning calorimetry and water uptake measurements was performed on samples of stress control tube.

Two similar test objects were used in order to obtain a higher electric field strength at the same applied AC voltage. A Raychem stress control tube was shrunk on the outside of a cylindrical shape consisting of two metal electrodes and a PTFE rod separating them. The length of the PTFE rod was 100 mm for Object L, while only 20 mm for Object S providing a higher field strength.

Water uptake measurement was performed in order to determine the stress control tube's ability to diffuse water. Measurement results imply that the water uptake is dependent of both the degree of shrinkage and the temperature. The highest water content is observed for a virgin stress control tube kept at 90 ℃, with a concentration of 8 % after 105 days. None on the test samples reached saturation during the experimental work.

Differential scanning calorimetry measurement was performed in order to examine if the stress control tube had any phase transitions changing the electrical properties of the stress control tube. Samples of stress control tube were examined in the temperature range of 20 ℃ to 200 ℃. Results indicate that the stress control tube, independent of the degree of shrinkage, has an endothermic melting transition in the temperature range of 94 ℃ to 114 ℃. Dielectric response measurements show that the thermal transition of the stress control tube will provide an increased conductivity. This is likely caused by a change from semi-crystalline to amorphous state, releasing trapped charge carriers and providing the material to become more electrical conductive.

Dielectric spectroscopy was performed on both test objects in the electric field range from 0.025 – 1.0 kV_{peak}/mm for Object S and 0.005 – 0.01 kV_{peak}/mm for Object L. Frequency was varied from 100 Hz to 1 mHz.

A temperature dependence was observed for dielectric loss tangent, in addition to large values up to 1000. At higher temperatures, the dielectric loss tangent was observed independent of the electric field. For measurements at 40 ℃, an electric field dependence is observed for field strengths above 0.5 kV_{peak}/mm.

The results show that the conductivity is dependent of the temperature. After exposed to 150 ℃, the temperature is decreased to 40 ℃ and a new measurement is performed. Hysteresis effect is then observed as the conductivity attains a higher value than before exposed to high temperatures.

The conductivity is found independent at the electrical field at high temperatures. At low temperatures, the electrical field dependence is observed for field strengths above 0.5 kV_{peak}/mm.

Observations made imply that the conductivity is strongly dependent of the humidity level. When performing dielectric response measurement on a wet test object, the conductivity experienced a significant increase from 10^{-11} to 10^{-5} S/m.

Wet stress control tube was dissected after complete dielectric response measurement. There was not observed signs of tracking, causing the electrodes to be short-circuited during measurements.

Sammendrag

Denne masteroppgaven vil ta for seg laboratorieundersøkelser av de elektriske egenskapene til kommersiell feltstyrende strømpe brukt i mellomspenningskabelskjøter. Dielektrisk responsmåling i frekvensdomenet ble brukt for å bestemme de elektriske egenskapene til strømpen som en funksjon av temperatur, AC elektrisk felt og fuktighet. For å karakterisere strømpen ble det utført differensiell skannings-kalorimetri og vannopptaksmålinger.

Testobjektet brukt i oppgaven bestod av to metallelektroder montert sammen med en PTFE stav. På utsiden var det krympet på en Raychem feltstyrende strømpe. Det var valgt to ulike lengder, 100 mm og 20 mm, på PTFE staven for å oppnå høyere feltstyrker.

Fra vannopptaksmålingene ble det observert at vannopptaket var avhengig av både temperatur og grad av krymping. Det høyeste vanninnhold er observert for en ukrympet strømpe ved en temperatur på 90 ℃, hvor konsentrasjonen etter 105 dager hadde økt med 8 % av tørrvekten. Ingen av prøvene gikk i metning under det eksperimentelle arbeidet.

Differensiell skannings-kalorimetri ble utført for å undersøke om den feltstyrende strømpen hadde noen faseoverganger som kunne endre de elektriske egenskapene under dielektrisk spektroskopi målingene. Resultatet fra målingene indikerer at strømpen, uavhengig av krympenivå, har et smeltepunkt i temperaturområdet fra 94 til 114 ℃. Dielektriske responsmålinger viser at faseovergangen gir økt ledningsevne. Dette er sannsynligvis forårsaket av en endring fra semi-krystallinsk til amorf tilstand som vil frigjøre ladningsbærere og øke ledningsevnen til strømpen.

Dielektrisk spektroskopi ble utført på begge testobjektene. Den elektriske feltstyrken påtrykket Objekt S og Objekt L er henholdsvis 0,025 - 1,0 kV_{peak}/mm og 0,005 - 0,01 kV_{peak}/mm. Frekvensen ble variert fra 100 Hz til 1 mHz.

En temperaturavhengighet ble observert for den dielektrisk tapstangenten, og ved 1 mHz ble det målt verdier opp til 1000. Tapstangenten er vil være uavhengig av feltstyrken ved høye temperaturer. Målinger utført ved 40 ℃ indikerer en elektrisk feltavhengighet for feltstyrker over 0,5 kV_{peak}/ mm.

Resultatene viser at ledningsevnen er avhengig av temperaturen. Etter å ha blitt påtrykket temperatur opp til 150 ℃, blir temperaturen redusert til 40 ℃ og en ny måling utført. En hysterese-effekt blir så observert, hvor konduktiviteten holder en høyere verdi enn før utsatt for høy temperatur.

Konduktiviteten er funnet at uavhengig av feltstyrken ved høye temperaturer. Målinger ved lavere temperaturer vil en feltavhengighet være synlig for feltstyrker over 0,5 kV_{peak}/ mm.

Observasjoner antyder at konduktiviteten er sterkt avhengig av fuktnivået i strømpen. Sammenlikning av resultater for tørt og vått objekt viser en betydelig økning i ledningsevnen, fra 10^{-11} til 10^{-5} S / m.

Etter måling blir det våte objektet dissekert. Det blir ikke observert tegn som indikerer at elektrodene har vært kortsluttes i løpet av målingene.

Abbreviations

DSC	Differential scanning calorimetry
FD	Frequency domain
FGM	Field grading material
PTFE	Polytetrafluoroethylene
SCT	Stress control tube
TD	Time domain
XLPE	Crossed linked polyethylene

Table of contents

Chapter 1

1 Introduction

1.1 Background

In Norway, a significant part of the medium voltage (12 and 24 kV) cable distribution systems have reached its expected lifetime. Observations indicate that several cable sections containing heat shrink joints have suffered from overheating. Observations imply that these joints still seems to withstand the service conditions. However, if the current loading in the cable network increases, additional joints can experience critical overheating. [1]

This overheating is probably caused by a high contact resistance in the metallic connector. Overheating can be expected to increase the temperature within the cable section to temperatures well above the rated temperature. It has been proposed that such joints have a very low electrical resistance. [1]

Joints and terminations are considered as the weakest parts of the cable system. In order to avoid field enhancement, leading to partial discharges and possible premature failure, these sections can be equipped with a field grading tube. The function of this tube is to obtain a more uniform field distribution along the cable length and further reduce the probability of an enhancement.

This thesis will examine a field grading tube is commonly used in joints that have experienced overheating. The aim is to examine how the tube behaves as the temperature is increased up to 150 ℃. Analysis will mainly concern if such high temperatures can cause critical changes in the electrical properties of the material. The paper is part of a larger work trying to elucidate the mechanisms causing low insulation resistance in medium voltage cable joints.

1.1.1 Condition assessment

In order to determine in which state the cable system is, several non-destructive tests can be performed. The collective term of this investigation is called condition assessment, and has the past decade managed to achieve a high focus and great priority in the industry. A proper understanding of the power system and its failure characteristics is desirable knowledge. This can be used to provide a comprehensive estimate of the condition and the remaining lifetime of the system.

If condition assessment is performed throughout the lifetime and the obtained information is used properly, an increased reliability of the system can be achieved. This information provides an opportunity to schedule maintenance and replacement at the most suitable time. Additionally, the assessment can state which component in need for a replacement and thus avoiding changing of a healthy component and unnecessary costs.

The challenge regarding condition assessment is to determine the indicators that reveal a critical system state. Efforts have been put into the discovery of the failure indicators and which of the parameters that differ from the normal condition and thus can be used in evaluations. Laboratory tests are performed with an aim to develop a recommended diagnostic method with an interpretation of the evaluation criteria. This will provide realistic replacement measures for the cable system.

For a cable system, the two most common non-destructive tests performed are dielectric response and partial discharge measurement. Dielectric response measurements are based on the changes in dielectric properties and are dependent on several factor. These factors can be frequency or time, temperature and chemical composition of the dielectric [2]. Partial discharge measurements can thus be used to find internal weak spots, e.g. voids, cracks and impurities.

However, when measuring dielectric loss tangent for a cable section containing cable joint, large values can be observed. This can lead to erroneous assessment of the cable condition, e.g. stating that the cable suffer from severely water treeing. [3]

1.2 Hypothesis

This master thesis will examine the temperature, humidity and electric field dependence of a commercial field grading tube used in medium voltage XLPE cable installed in the 80s. Both measurement of the diffusion and differential scanning calorimetry is performed to characterize the material, while the main focus of this thesis will be on dielectric response measurements. Experimental work has been performed in order to test the following hypothesis.

1. Diffusion
    i. Both the temperature and degree of shrinkage effects the stress control tube's ability to diffuse water.
    ii. Samples of stress control tube will reach saturation during master work. This result can further be used in order to conditioning the test object into having a humidity level of $>$90 %.

2. Differential scanning calorimetry
    i. The stress control tube does not have any phase transition at temperatures below 150 ℃, which causes the electrical properties of the stress control tube to change.

3. Dielectric response measurements
    i. Dielectric loss tangent, $\tan\delta$, for the stress control tube has a high value that can cause erroneous assessment of cable condition containing a cable joint.
    ii. When increasing the temperature, the stress control tube's conductivity will increase.
    iii. Hysteresis effects are not present in the stress control tube. The material has a reversibly change of the conductivity after being subjected to high temperatures.
    iv. Having an increased humidity of the test object, the stress control tube's conductivity will increase.

Chapter 2

2 Theory

2.1 XLPE-cable systems

Cross-linked polyethylene, often referred to as XLPE or PEX, are thermosetting polymers that has been through a vulcanization process. The process establishes crosslinks between the molecules which removes the material's plasticity when heated. This type of polymer will not reshape during overheating such as thermoplastic polymers does. Thus, a higher operation temperature can be achieved for XLPE than for ordinary polyethylene (PE).

Thus, the continuous operation temperatures of the cables are in international norms set to be 70 ℃ for PE, and 90 ℃ for XLPE. After XLPE cables were introduced, it has been the most commonly used material in cable insulation. [4]

PE and XLPE cables are on the other hand sensitive to partial discharges, which can have a considerable influence on the cable's lifetime. Great effort is therefore focused on preventing voids and protrusions. [5]

XLPE cables were introduced in 1968 in Norway. These cables were not water tight, causing them to be vulnerable to water tree degradation. In the beginning of 1980s, the cables were produced with a dry vulcanization, but still without a watertight design. From 1990, XLPE cables were produced to be both axially and radially watertight and are the design used today. [6]

The failure rate of XLPE cables is relatively low, but when considering the entire system, including terminations and joints, the failure rate increases [3].

2.1.1 Cable joints

Cables are manufactured in factories under a clean and controlled environment. Several factors limit the length of cables during manufacturing, and long cables are therefore produced in several sections. Dividing the cable into sections also eases the process of service and repair. Installation of those two sections is performed at site and they are connected with a joint providing a protected and insulated connection.

The cables are stripped down to the conductors by removing the insulation and are electrically connected by e.g. a metal connector. By screwing or pressing, the connector tightens and creates an electrical connection between the two cable sections. Outside the metal connector, the cable layers are connected to make a protected and insulated layer. A moisture barrier should also be added to avoid water diffusion into the joint.

When joining cables at site, a clean environment and experienced personnel are required. Caution must be taken to avoid improperly installation, as poor workmanship tends to increase local stress. Examples of poor workmanship are cuts on the cable during the shield cutback operation, contaminations or weak connection between the conductors.

The weak connection in the metal connector provides a high transition resistance and an increased heat generation inside the joint. If the heat generated exceeds the heat dissipated to the environment the temperature will increase. As the temperature becomes higher than the rated temperature of the cable system, degradation of the insulation material will increase rapidly. Degradation weakens the electrical and mechanical properties of the material and initiates partial discharges that might lead to breakdown. For this reason, jointing two cables should be performed with caution. [5]

Heat-shrink joints made of shrinkable plastic are commonly used and are especially useful when re-insulating jointed cables. They have the advantage to be made in a different size from the conductors and can be applied in a short time and adjusted to fit the conductors [7]. However, many medium voltage cable sections with these joints have suffered from overheating, especially XLPE cables installed in the 1980s. [3]

2.1.2 Field grading

In order to join the two cable sections, each cable has to be stripped down exposing its conductor. For a uniform coaxial cable, the electric field distribution along its length is radial. However, for a termination or joint the electric field will no longer be one-directional. The electric field will now have both a component in the radial and tangential direction at the cutback. This causes a field enhancement at the edge of the semi-conducting layer, which is illustrated in Figure 1. [8]

Although the insulation and boundary surfaces are designed for a high withstand strength, a field enhancement will cause partial discharges to be a problem even at voltages below rated value. These can propagate leading to lower breakdown strength and damage the insulation, and possibly result in a premature failure in the cable system.

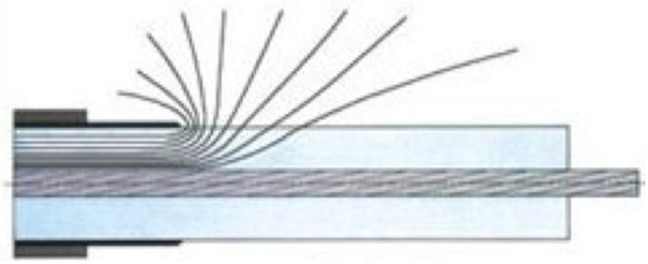

Figure 1: Equipotential lines on a stripped cable. An enhancement occurs at the edge of the semi-conductive layer. [9]

Figure 1 illustrates the change of the equipotential lines from only being in the radial direction to have both a radial and tangential component whilst reaching the cable termination. The equipotential lines have a higher density giving field enhancement, which can reach untenable levels.

In order to reduce of the electric field's tangential component, field grading is introduced. The usual method to obtain field grading is by application of a material that utilizes a more even voltage distribution along the cable's length, e.g. stress control tube. With a sufficient voltage distribution, the electric field becomes reduced and the enhancement becomes within safe values.

As the stress control tube is applied outside the insulation, the distribution of equipotential lines changes. This is illustrated in Figure 2, where the lines become more evenly distributed, which prevents high enhancement at the edge.

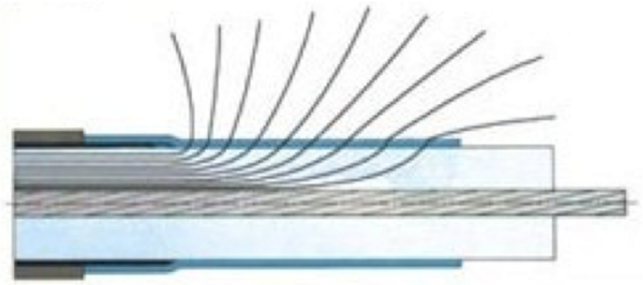

Figure 2: Equipotential lines when a stress control tube is applied. Field grading gives a more uniform distribution and a less enhancement at the edge. [9]

Field grading, or stress control, can be achieved in several different ways. The methods to achieve field grading are normally divided into two main mechanisms that can be distinguished by the dominating component of the current, e.g. resistive or capacitive current. These two mechanisms are (1) capacitive field grading and (2) resistive field grading.

Capacitive field grading concerns the material's dielectric constant (ε) and includes geometrical electrode grading and condenser grading. For capacitive grading, the dielectric constant will be sufficiently high to distribute the field longitudinally. [10]

Resistive field grading is controlled by the conductivity (σ) of the material, and is mostly used in the form of special materials comprising the desired current-field characteristic. This is to achieve a voltage distribution less dependent of the frequency by having a resistivity that is independent of the field strength. Figure 3 shows an example of a current-field characteristic where the field strength is independent of the resistance. [10,11]

Additionally, a grading method using both the resistive and capacitive mechanism can be employed for certain applications to achieve a more optimal grading.

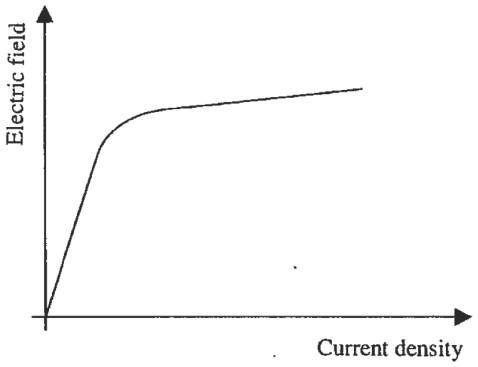

Figure 3: Schematic characteristic for a coating with field strength independent resistance. [4]

The determination of the grading mechanism is performed by comparing the values of $\sigma(E,T)$ and $\varepsilon(E,T)\omega$, where E is the electric field strength and T is the temperature.

For resistive field grading, the resistive component of the current is dominating, and the value of σ is thereby largest. If the current is dominated by the capacitive component, the value of $\varepsilon\omega$ is larger than σ and the system is capacitive graded. [12,13]

To illustrate how to the field develops along the cable length, an equivalent circuit is made. The cable's surface is divided into small, conductive rings around the cable as symbolized with black dots in Figure 4. Capacitance K is value between the rings while C is the value between the rings and the conductor. It can be shown that the maximum field strength will increase with the ratio $\sqrt{\frac{C}{K}}$. [4]

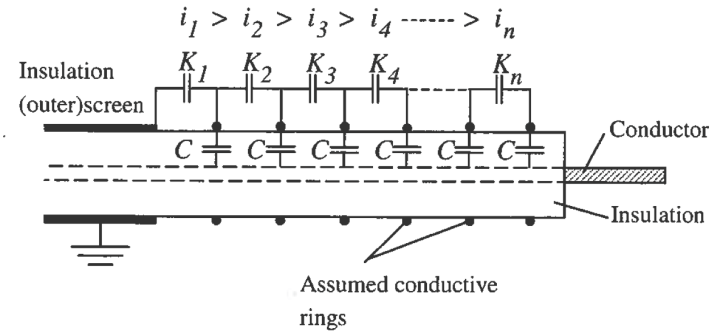

Figure 4: Approximate circuit equivalent in order to illustrate field system along the end of the cable. [4]

In order to keep the magnitude of the longitudinal field stress below critical values, the value of C should be decreased or K increased. However, the value of C cannot easily be changed as it is given by the potential between the semiconductor and the conductor. In order to reduce the maximum field strength, the value of K should rather be increased. Various techniques utilize this connection in order to improve the field distribution, e.g. resistive and refractive field control. [4]

Stress control tube

To achieve a satisfactory field distribution in a cable joint, it is common to apply a stress control tube (SCT). A frequently used type is heat-shrinkable tube, which can fit a large range of sizes and are shrink-heated onto the cable, to make a close fitting.

The heat-shrinkable SCT is made of semi-crystalline polymers compounded with additives making it possible to shrink. The material is made with cross-linking while it is in its original shape, which is the shape the material will remember. After a cross-linking, the material is heated above its crystalline melting temperature and expanded to a larger size and then cooled down in that position. When the tube is applied to a cable, it will remember its original shape when heated and form a tight fit to the cable section. [14]

The heat-shrinkable polymers are often used in combination with hot-melt adhesives and have field grading as nonlinear resistive, refractive or resistive-refractive [15].

Linear resistive grading is conversely rarely used. The field distribution for such materials is frequency dependent, and thus hard to give an acceptable field distribution both at impulse and operation voltage without high losses. A high conductivity is necessary in such cases and a consequence of this is that it creates high losses. To avoid this, non-linear material might be more suitable. By using such a material, the field grading can be efficient during both conditions. [11]

For resistive field grading a resistive coat are applied. Capacitance K will then be in parallel with the resistance R, giving an equivalent impedance. This is illustrated in Figure 5.

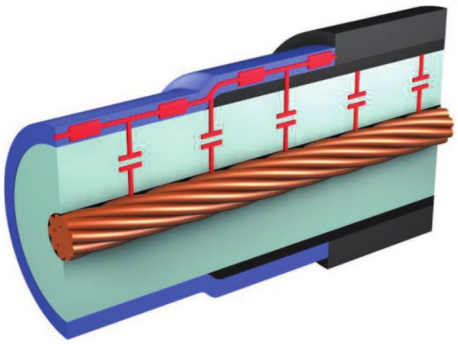

Figure 5. Equivalent circuit of an impedance stress control material (dark blue layer) applied to the cable. [10]

Resistive grading reduces the field enhancement by bringing a critical high field region to a conductive state. This will make the space charge within the tube change forms, and create a counter field reducing the enhancement. [10]

In addition, a non-linear resistive field grading material has a conductivity that is field dependent, $\sigma(E)$. This gives that it typically changes from a low to a high conductive value in narrow electric field region. Based on this, the material must have a reversibly change from highly conductive to resistive in order to have low losses. [10]

The highly conductive state provides a greater part of the current passing through the tube, increasing the resistive losses. If these losses exceed the dissipated energy to the environment, an overheating can be the result.

2.2 Basic electrostatic theory

2.2.1 Basic electrostatic

The electric field between two points can be expressed as

$$\boldsymbol{E} = -\nabla U \qquad \text{Eq. 2.1}$$

where **E** is the electric field and U the potential difference between the electrodes. By using Gauss's law, the relation between the electric field and charge q can be found. This can further be used to find the relation between the electric field and the capacitance. For a parallel plate capacitor this can be written as

$$C = \frac{Q}{U} = \varepsilon_r \varepsilon_0 \frac{A}{d} = \varepsilon_r \mathrm{C}_0 \qquad \text{Eq. 2.2}$$

where total charge is Q, area of the electrodes is A and distance between them is d. C_0 is then the geometrical vacuum capacitance of the object, ε_0 is the vacuum permittivity and ε_r is the relative permittivity.

For a homogeneous electric field in vacuum the dielectric displacement field becomes

$$D_0 = \frac{Q_0}{A} = \frac{C_0\, U}{A} = \varepsilon_0 E \qquad \text{Eq. 2.3}$$

2.2.2 Dielectric polarisation

A purely dielectric medium consists only of bounded electric charges. These are randomly oriented when no electric field is applied. When the dielectric medium is exposed to an electric field, these dipoles will start aligning themselves in the direction of the field. This is called polarisation and can be divided into four different types:

1. Electronic polarization
   The electrons in the orbit of an atom will be distorted when exposed to an electric field, giving a higher concentration of electrons at one side of the atom. The distortion results in a temporarily dipole, which is extremely rapid and proportional to the applied field. [5]

2. Ionic polarization
   Molecules consisting of negative and positive ions in a symmetrical array are not dipoles. When subjected to an electric field the negative and positive ions are pulled in different direction giving a temporarily dipole, which vanish when the electric field disappears. [5]

3. Orientation polarization
   Molecules that are permanent dipoles, e.g. water, have random direction when not exposed to an electric field. The effect of an applied field gives the permanent dipoles to line up in the same direction of the field. [5]

4. Interface polarization
   In dielectric materials there exist areas where the atoms, molecules and ions are not ideal arranged, in addition to impurities and free electrons. When an electric field is applied to the material, electrons start moving towards these areas. This will create a local electric field. [5]

2.2.3 Time dependent polarisation

The alignment of the dipoles in a dielectric medium is time dependent. Immediately after an electric field is applied the two first mechanisms, electronic and ionic polarisation, will happen momentary. The two last mechanisms, orientation and interface polarisation, are time dependent and will use some time to align themselves with the field. These two is commonly denoted as relaxation mechanism.

If a DC voltage is applied to a parallel plate condenser with dielectric insulation medium, all the dipoles will align themselves in the same direction. This results in a reduction of the net charge between the plates. The reduction is due to

the cancellation by the adjacent dipole and gives a lower voltage potential difference between the electrodes. The phenomenon is illustrated in Figure 6.

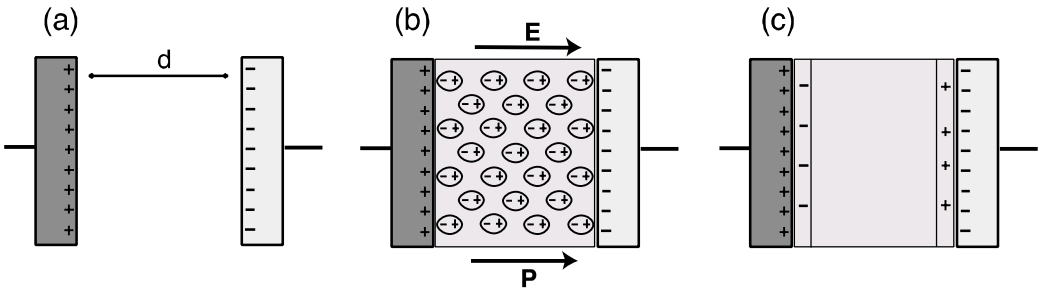

Figure 6: Parallel plate condenser. [16]
a) with vacuum. b) with dielectric medium.
c) Resulting net free charge on the surface of the plates when having a dielectric medium.

When the vacuum is replaced with a dielectric material, the dielectric displacement field will increase with the polarisation $\boldsymbol{P}(t)$

$$\boldsymbol{D}(t) = \varepsilon_0 \boldsymbol{E}(t) + \boldsymbol{P}(t) = \varepsilon_0(1 + \chi)\boldsymbol{E}(t) \qquad \text{Eq. 2.4}$$

where χ is the electric susceptibility of the dielectric material.

An equivalent circuit can be established based on the mechanisms present in a dielectric medium when a step voltage is applied. The current flowing through the dielectric can be divided into the following three contributions: conduction, momentary polarisation, and relaxation polarisation. These have each a different time constants, and the relation is used in the establishment of the circuit illustrated in Figure 7. The current i(t) indicated in the figure will then be the same as the current measured during an application of a DC step voltage.

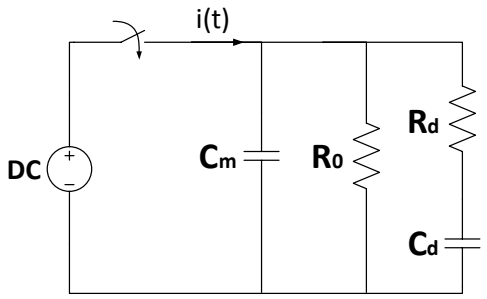

Figure 7: Equivalent circuit of a dielectric medium with conduction, momentary polarisation and relaxation mechanism.

Each of the components can be related to one of the three contributions to the current. Conduction is modelled with a resistance R_o and gives the stationary part of the current. This component will arise if the dielectric material is significantly conductive and is related to the materials conductivity σ.

Momentary polarisation gives a high current-spike immediately after applying a step voltage, and is modelled as a condenser C_m.

Relaxation polarisation is slow process and very temperature dependent and is modelled as a RC-unit with R_d and C_d. The mechanism will then have a time-constant τ equal for both polarisation and depolarisation state. [5]

The relation of the current through a dielectric medium is given in the following equations.

$$\mathbf{i}(t) = \left(\sigma_0 \, \boldsymbol{E}(t) + \frac{d\boldsymbol{D}(t)}{dt}\right)A = \left(\sigma_0 \, \boldsymbol{E}(t) + \frac{d(\varepsilon_0 \boldsymbol{E} + \boldsymbol{P})}{dt}\right)A \qquad \text{Eq. 2.5}$$

$$i(t) = \left(J_\delta(t) + \frac{P_d(\infty)}{\tau} \cdot e^{-\frac{t}{\tau}} + \sigma_0 \, E(t)\right)A \qquad \text{Eq. 2.6}$$

Eq. 2.6 shows that the current is a summation of the momentary polarisation, the relaxation polarisation and the materials conduction ability.

J_δ is the current density of the momentary polarisation given as a high current-spike immediately after applying a step voltage.

P_d presents the relaxation mechanism where its value initially high, but starts decreasing as the dipoles align themselves with the field. How fast this occurs is dependent on the time constant τ.

When both the momentary and relaxation mechanism has decayed, the current will stabilize at the conductive current. This current is dependent on the material's ability to conduct a current and is proportional with the conductivity. The shape of the current is illustrated in Figure 8.

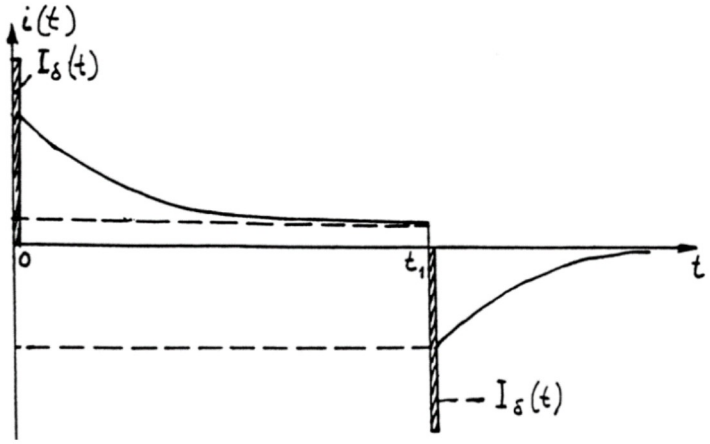

Figure 8. The current's shape for both polarisation and depolarisation time period. [5]

2.2.4 Frequency

Since dielectric relaxation is a slow mechanism, it will cause a contribution to the dielectric loss as well as cause a relative permittivity that varies with frequency, $\varepsilon_r(f)$.

When the dielectric medium is subjected to an AC voltage, the electric field will be alternating and the dipoles will try to follow the polarity of the voltage. How fast the electric field changes direction is proportional to the frequency.

If the dielectric is subjected to a low frequency ($\omega\tau \ll 1$), the dipoles will without difficulty manage to follow the electric field. However, when the frequency is increased, the dipoles will struggle to keep up with the alternating field. This will create a phase shift between alignment of the dipole and the field. When the frequency gets sufficiently high, $\omega\tau \gg 1$, the dipoles will no longer be able to follow. The result of an increasing frequency is a reduction in polarisation hence a reduction in relative permittivity. [5]

The phase shift created will cause the electrical flux density $\mathbf{D}$ to lag the applied electric field with an angle δ. Using this relation, the relative permittivity can be divided into a real (ε_r') and imaginary (ε_r'') part where both are functions of the frequency. The real part is commonly known as dielectric constant. The imaginary part is known as the dielectric loss factor, and represents the phase shift causing losses.

When assuming that the conductivity, σ, is zero, the relative permittivity, ε_r, can be expressed as

$$\varepsilon_r(\omega) = \frac{D}{\varepsilon_0 E} \cdot e^{-j\delta} = |\varepsilon_r| e^{-j\delta} = \varepsilon_r' - j\varepsilon_r'' \qquad \text{Eq. 2.7}$$

where ε_r describes how the capacitance C increases with regards to C_0.

At very low and very high frequencies, it can be assumed that the dielectric loss factor can be neglected, $\varepsilon_r'' \approx 0$ [5]. In such cases the Eq. 2.7 can then be expressed as

$$\varepsilon_r(\omega) = \varepsilon_r' - j\varepsilon_r'' \approx \varepsilon_r' \qquad \text{Eq. 2.8}$$

The relation of the real and imaginary permittivity is illustrated in Figure 9. At high and low frequencies the imaginary part is approximately zero and the maximum value appears when $\omega\tau_d = 1$, i.e. at frequency f_d with $\tau_d = R_d C_d$.

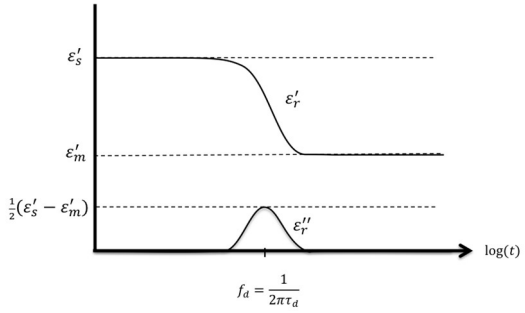

Figure 9: Real and imaginary part of the permittivity as a function of frequency.

The ratio between ε_r'' and ε_r' is denoted as the dielectric loss tangent, $\tan\delta$. This is the most commonly used parameter to characterize an insulation material when considering the dielectric loss [5].

$$\tan\delta\,(\omega) = \frac{\varepsilon_r''(\omega)}{\varepsilon_r'(\omega)} \qquad \text{Eq. 2.9}$$

For dielectric materials the parts of the relative permittivity can be considered to be $\varepsilon_r'' \geq 0$ and $\varepsilon_r' \gg \varepsilon_r''$. The dielectric constant and dielectric loss factor are dependent on the frequency, material homogeneity, anisotropy, moisture and temperature. [17]

As the temperature increases, the dipoles respond faster to frequency change thus giving a decrease in the relaxation time constant τ.

In a semiconductor, the conductivity is dependent of two different factors: the concentration of free charge carriers and their mobility. The charge carriers are formed by thermal activation and mobility increases with temperature, which provides a temperature dependency by both factors. The conductivity will experience an increase when the temperature is raised.

If the object is affected by humidity, water molecules might give an additional contribution to the charge carriers. For a joint without a watertight design, the conductivity can have a significant increase and be dependent of the electric field. [3,18]

Dielectric losses

When measuring the losses during application of an AC voltage, losses can no longer be divided into dielectric and conductivity parts when measuring. The dielectric loss tangent, $\tan\delta$, is therefore commonly used for express the total losses and characterization of the insulation system. [5]

$$P_{AC} = \omega \varepsilon_r' \varepsilon_0 \tan\delta E^2 \qquad \text{Eq. 2.10}$$

The total loss, P, within a system depends upon the electrical stress (E), frequency (ω), permittivity (ε) and the dielectric loss tangent

Due to the presence of both dielectric and conductivity losses, the total loss can be denoted as

$$P_{tot} = (\omega \varepsilon_r' \varepsilon_0 \tan\delta + \sigma) E^2 \qquad \text{Eq. 2.11}$$

As the losses are difficult to separate, a new expression is made for $\tan\delta$ as a function of both the dielectric and conductive losses.

$$\tan\delta = \tan\delta_1 + \frac{\sigma}{\omega\varepsilon'\varepsilon_0} = \frac{\varepsilon_r''}{\varepsilon_r'} + \frac{\sigma}{\omega\varepsilon'\varepsilon_0} \qquad \text{Eq. 2.12}$$

When the conductivity is included, the new expression for dielectric loss tangent will be inverse proportional with the frequency, $\omega \to 0$ provides that $\tan\delta \to \infty$.

In most cases, the relation $|\varepsilon_r'| \gg |\varepsilon_r''|$ will apply. This provides a good approximation to use $\varepsilon_r' \approx \varepsilon_r$. Based on this, the dielectric loss tangent can be simplified to

$$\tan\delta \approx \frac{\sigma}{\omega\varepsilon'\varepsilon_0} \qquad \text{Eq. 2.13}$$

When modelling the dielectric losses, a resistor can be represented in either parallel or series with an ideal and lossless capacitance. A cable is often modelled as a capacitor due to its capacitive connection between the conductor and semiconductor. In addition, the parallel model commonly represents the cable system [5].

The lossless capacitance C is therefore placed in parallel with a voltage dependent resistance R that represents the heat generated due to dielectric losses in the capacitor. The current will then be divided into a current I_C and I_R as shown in Figure 10.

The current I_R is in phase with the applied voltage, while I_C has a 90° phase shift. The resistive and capacitive current provides the resultant current I (Figure 11). The angle δ represents the displacement of the current I from I_C, where the capacitor have no losses. Additionally, the amplitude of I_R is much less than the one for I_C.

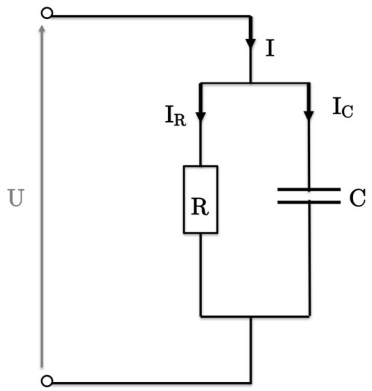

Figure 10: Equivalent circuit for parallel circuit.

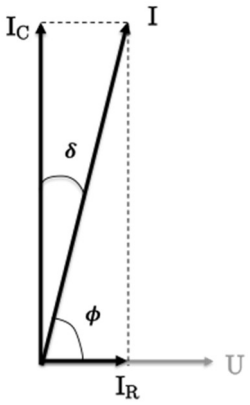

Figure 11: Phasor diagram for parallel circuit.

Using the geometric relation from the figure, the value of tan δ can be expressed as the ratio of the resistive and capacitive current.

$$\tan\delta = \frac{I_R}{I_C} = \frac{1}{\omega RC} \qquad \text{Eq. 2.14}$$

2.3 Non-destructive diagnostic methods

In order to perform condition assessment on cable accessorises, several methods are based on measurement of the dielectric response [19]. Dielectric response analysis is to be performed in either the time or the frequency domain, with respectively DC or AC voltages.

Time domain analysis is used to measure of the current response or return voltage as a function of time when either applying a step voltage or removing the voltage [20].

During frequency domain measurements, the test object is subjected to an AC voltage at a specified frequency [21]. The quantities measured are the dielectric loss tangent, changes in capacitance and the dielectric loss factor as a function of frequency.

2.3.1 Time domain analysis

Polarisation and depolarisation current measurement can be used to investigate the condition of the insulation. An equivalent circuit (Figure 12) of the test setup includes a DC source and a switch that changes from polarisation to depolarisation state.

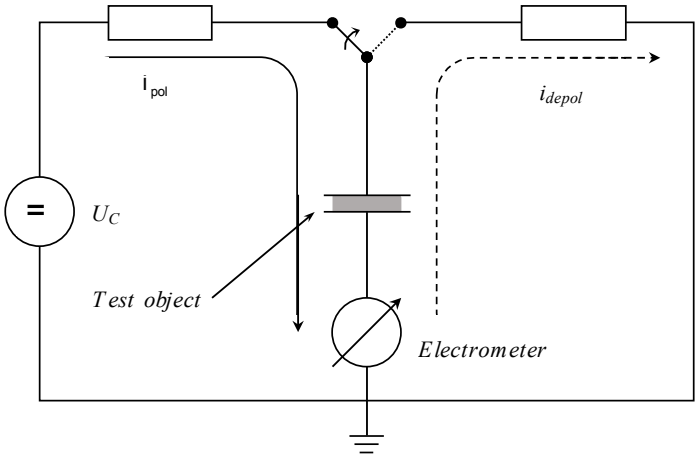

Figure 12: Equivalent circuit for time domain measurements.

The test object is subjected to step-voltage of U_0 for a time period t_{pol}. The response of the current will immediately have a spike, but strongly decrease before reaching a steady-state value.

After time period t_{pol}, the circuit is short-circuited to earth. A depolarisation current will flow as the dipoles align back to their original position. The current response is illustrated in Figure 13. [22]

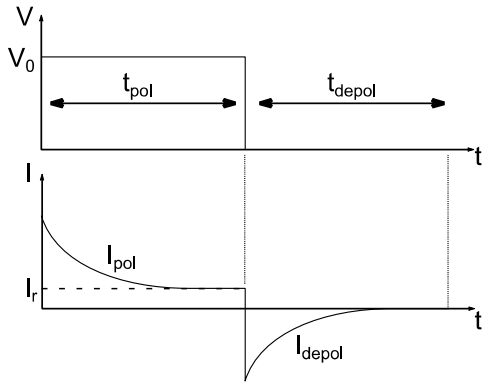

Figure 13: Polarisation and depolarisation current as a function of time. [18]

The polarisation and depolarisation current can expressed as

$$I_p(t) = C_0 U_0 \left[\frac{\sigma}{\varepsilon_0} + f(t)\right] \qquad \text{Eq. 2.15}$$

$$I_d(t) = C_0 U_0 \left[f(t) - f(t + t_c)\right] \qquad \text{Eq. 2.16}$$

where $f(t)$ is the dielectric response function of the test object. If the charging time of the test object is sufficiently long, the value of $f(t + t_c)$ could be disregarded and set to zero.

By combining Eq. 2.15 and Eq. 2.16, an approximated equation for the conductivity of the object can be found

$$\sigma \approx \frac{\varepsilon_o}{C_0\, U_0}\left[I_p(t) - I_d(t)\right] \qquad \text{Eq. 2.17}$$

2.3.2 Frequency domain analysis

Non-destructive methods when applying a sinusoidal voltage have been developed as a diagnostics method for cable systems [23].

Dielectric response measurements can be used as a measurement technique to determine the dielectric properties of the material that can be used for analysis of the dielectric material. The method used is dielectric spectroscopy, where measurements of the capacitance and the loss are given as a function of the frequency.

When applying a sinusoidal voltage to the test object, a sinusoidal current will start to flow though the object. Measurement of both the voltage and current enables calculation of the impedance. Furthermore, the impedance can be used to find several parameters that can be used for the analysis of the dielectric. Figure 14 shows the equivalent circuit used during dielectric spectroscopy measurements.

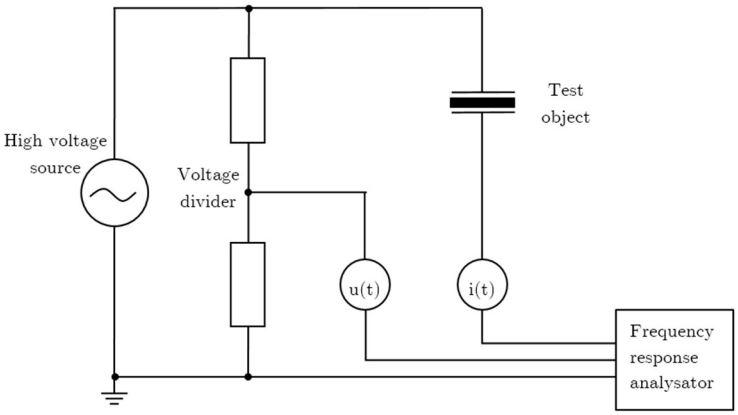

Figure 14: Principle for measuring dielectric response in frequency domain. Object is subjected to a high voltage source. The current and voltage is measured with amplitude and angle. Parameters can be calculated with these values.

For diagnostic purposes, several relevant dielectric parameters are established and are summarized in Table 1 [23,24].

Table 1: Diagnostic parameters

Parameter	Description
$\varepsilon'(\omega)$	Real part of the relative permittivity
$\Delta\varepsilon'(\omega)$	Changes in the real permittivity part
$\varepsilon''(\omega)$	Imaginary part of the relative permittivity (Dielectric loss factor)
$\tan\delta$	Dielectric loss tangent
$\Delta\,(\Delta\,\varepsilon'(\omega))$	Change in the real part of the permittivity with voltage
$\Delta\,\varepsilon''(\omega)$	Changes in the dielectric loss factor with voltage
$\Delta\,\tan\delta(\omega)$	Changes in the dielectric loss tangent

Active power losses in a dielectric medium, while subjected to an AC voltage (Eq. 2.18), is a function of both the conductivity and the dielectric loss factor.

$$p = p_{AC} + p_{DC} = \omega\,\varepsilon_r''\varepsilon_0 E^2 + \sigma E^2 \qquad \text{Eq. 2.18}$$

In order to be able to distinguish the losses, measurements over a large range of frequencies might be necessary. At low frequencies, the DC losses will be the dominating making it possible to provide a sufficient estimate of the conductivity. In most case, the relation $|\varepsilon_r'| \gg |\varepsilon_r''|$ will apply, returning $\varepsilon_r' \approx \varepsilon_r$ as a valid approximation.

The measurement executed on the test object can be performed with an Insulation Diagnostic System. Several measurements are performed on a suitable frequency range and for several voltages. This will provide a more comprehensive result where both frequency and voltage dependence can be determined.

2.3.3 Relation between time and frequency analysis

For a material responding linearly, i.e. independent of the applied voltage, time domain and frequency domain can be mathematically related. They are the Fourier transformation of one another [22,25]:

$$\chi'(\omega) = \int_0^\infty f(t) \cos \omega t \, dt \qquad \text{Eq. 2.19}$$

$$\chi''(\omega) = \int_0^\infty f(t) \sin \omega t \, dt \qquad \text{Eq. 2.20}$$

and

$$f(t) = \frac{2}{\pi} \int_0^\infty \chi'(\omega) \cos(\omega t) \, d\omega = \frac{2}{\pi} \int_0^\infty \chi''(\omega) \sin(\omega t) \, d\omega \qquad \text{Eq. 2.21}$$

The dielectric response function $f(t)$ is related to the polarisation mechanism in time domain. The function is associated to the change in current with time and is therefore a real value.

For frequency domain, the function has to be defined by a real and imaginary component $\chi'(\omega)$ and $-j\chi''(\omega)$. The variation is both a function of the phase and quadrature with respect to the driving harmonic signal [25].

The relation can be written as:

$$\chi(\omega) = \chi'(\omega) - \mathrm{j}\,\chi''(\omega) = \int_0^\infty f(t)\, \mathrm{e}^{-\mathrm{j}\omega t} \, dt \qquad \text{Eq. 2.22}$$

The response function will be different for each dielectric material and change differently depending on the time period for the material that is studied. Different types of dielectric response function are illustrated in Figure 15.

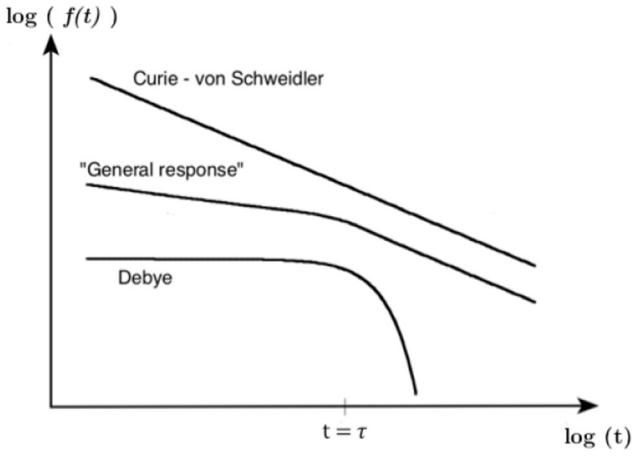

Figure 15: Different types of dielectric response function [26]

The most common relation is Debye and is a sufficient approximation for liquids. However, it is not typical for solid materials [22].

Curie-von Schweidler is more common when modelling a solid dielectric and will be valid for a wide range of different materials and time domains. The dielectric response function in a Curie-von Schweidler model is defined as: [26]

$$f(t) = A\, t^{-n} \qquad \text{Eq. 2.23}$$

The Hamon approximation is the Curie-von Schweidler model for a limited range of n. Using $0.3 < n < 1.2$, have been found to fit the measured current with this approximation quite well.

For a XLPE cable, the depolarisation current will typically be time dependent according to the Hamon approximation. This relation yields a loss factor expressed as [22,27]

$$\chi''(\omega) \approx \frac{I_d(t) \cdot t}{2\pi \cdot 0.1\, U_0 C_0} \qquad \text{Eq. 2.24}$$

A new expression for the loss tangent can be derived when combining the result inn Eq. 2.21 with Eq. 2.25.

$$\varepsilon''(\omega) \approx \frac{\sigma}{\omega \varepsilon_r} + \chi''(\omega) \qquad \text{Eq. 2.25}$$

$$\tan\delta\ (\omega) = \frac{\varepsilon_r''(\omega)}{\varepsilon_r'(\omega)} \approx \frac{I_d(t) \cdot t}{2\pi\ \varepsilon_r \cdot 0.1\ U_0 C_0} + \frac{\sigma}{\omega \varepsilon_0 \varepsilon_r} \qquad \text{Eq. 2.26}$$

2.4 Material characteristic analysis

2.4.1 Diffusion

Materials have different degrees of porosity. A porous material consists of pores, voids and cracks that make it possible for liquids and gasses to be accumulated. In order for the molecules to be transported within the material, this free volume has to be connected into channels. The degree of which the material allows a molecular transportation is called permeability.

If a material is exposed to e.g. water, its ability to absorb the water from the surroundings can be determined by investigating the permeability coefficient, P_e. From Eq. 2.1, the coefficient is defined as the product of the diffusion coefficient D, and solubility coefficient S.

$$P_e = D \cdot S \qquad \text{Eq. 2.27}$$

The diffusion coefficient gives the kinetic driven absorption where the molecules are transported within the material. The solubility coefficient is the thermodynamically component presenting the amount of molecules the material can absorb under defined conditions [28].

If a material is immersed in water, it is reasonable to assume that its surface reaches saturation immediately [28]. The water uptake by the material will therefore depend on the diffusion of water from the surface into the material. After a time period, the absorption will reach equilibrium given by the diffusion behaviour and the materials dimension.

The diffusion behaviour, or transport mechanism, can follow three different cases dependent on the relative mobility of the penetrant and polymer. [29]

1. Fickian diffusion, n = 0.5.
2. Non-Fickian diffusion, n=1.0.
3. Anomalous diffusion, $0.5 < n < 1.0$.

A common practice to distinguish the different diffusion behaviour is to adjust the sorption results by the use of Eq. 2.28. The value of n can then be found and used for determination of the transport mechanism. [21,29]

$$\frac{M_t}{M_\infty} = kt^n \qquad \text{Eq. 2.28}$$

where M_t is the mass uptake at time t, M_∞ is the mass uptake when equilibrium is reached, k is a constant and n is given by the transport mechanism.

For an experimental determination of the diffusion, a method called *Mass Uptake Measurement* can be performed [28,30]. The method provides the material's gained moisture weight in percentage as a function of time, M(t).

$$M(t) = \frac{m_{moist\ material} - m_{dry\ material}}{m_{dry\ material}}\ 100\% \qquad \text{Eq. 2.29}$$

The time dependent mass uptake can be approximated to Eq. 2.30 if the three following conditions are satisfied. Firstly, the situation can be regarded as one-dimensional with the edge effect neglected. Secondly, the material initially has a uniform temperature and moisture distribution inside. Last, the moisture and temperature in the environment is constant. [30]

This yields the moisture content in the material as a function of the maximum moisture content, M_m, and the initial moisture content, M_i.

$$M(t) = G\,(M_m - M_i) + M_i \qquad \text{Eq. 2.30}$$

The time dependent parameter G can then be approximated to

$$G(t) = \frac{M(t) - M_i}{M_m - M_i} \approx 1 - exp\left[-7.3 \cdot \left(\frac{D_x \cdot t}{s^2}\right)^{0.75}\right] \qquad \text{Eq. 2.31}$$

Where D_x is the diffusion coefficient in the one-dimensional situation, and s is related to the thickness of the medium. If the material is exposed at both sides, s becomes equal to the thickness. If only one side of the material is exposed, s become equal to twice the thickness.

The permeability coefficient of the gas through the polymer is dependent of several factors: The polymer nature, the gas, pressure and temperature will influence its value when changed [28,29]. At a given pressure, an increase in the temperature will increase the free volume of the material. As the free volume

increase, the materials ability to absorb water increases, as well as the permeability coefficient.

Another factor that can give an altered characteristic of moisture absorption is filler particles. When a material contains filler particles, the diffusion behaviour might differ from the Fickian diffusion.

The solubility of the filler particles can have solubility different from the polymer, resulting in two-stage diffusion. First, the diffusion is dominated by the polymer's sorption. Then the filler particles in the polymer will contribute to the sorption. This can give two different diffusion coefficients for the material.

Whether the total absorption will increase or decrease is dependent on the filler particles. [28]

2.4.2 Differential scanning calorimetry

Differential scanning calorimetry (DSC) is a technique used for investigation of the thermal transitions of a polymer. The sample can be heated, cooled or held at constant temperature, and its response is monitored.

The level of heat required to achieve a constant temperature increase is dependent of the specimen. When reaching the transition temperature, the material can both absorb and release heat, changing the required heat delivered from the gauge. The changes are monitored and can later be used for analysis of the test specimen.

The measurement is performed as a comparison of the test specimen and a reference sample. A small piece of specimen is placed in in a crucible, while an empty crucible is used as a reference. As the temperature increases, the two samples might react differently. For the crucible containing a test specimen, a non-uniform heat flow might be necessary for achieving the same increase in temperature as the reference.

The experiment is performed under an atmosphere of nitrogen gas. The nitrogen gas will provide a dry environment as the measurement is executed. In addition, the gas flow can provide a better heat transfer that contributes to a faster response time.

Figure 16 illustrates how the heat flow to the test specimen might change when the temperature is increased. When reaching a transition temperature, the

material can experience phase changes, glass transitions, melts or curing. The type of transition can be determined by analysis of the shape of the curve. The response could be either exothermic (delivering energy) or endothermic (consuming energy).

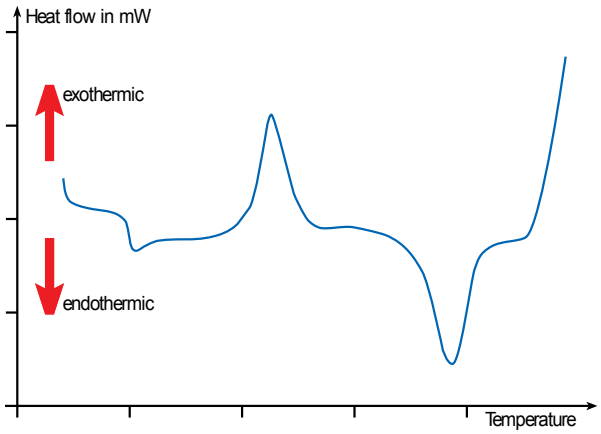

Figure 16: Typical curve received from the DSC measurement. [31]

Chapter 3

3 Method

3.1 Diffusion

Dielectric response measurements are to be performed with both temperature and humidity as variable parameters. As the humidity is introduced, a better knowledge of the SCT's ability to diffuse water is required.

Measurements performed on pieces of SCT can provide saturation curves, which further can be used to conditioning the test object to a desired humidity level.

If the level is selected to be >90 % of the maximum water content, this will provide a good criterion for to evaluation, as the object is entirely wet. By comparing the measurements on an entirely wet object to that of a dry object, the effect of humidity may be determined.

For examination of the diffusion mechanism, *Water Uptake Measurement* is performed on pieces of SCT. The essence behind the method is to measure the relative water uptake as a function of time. The result can then be presented as a curve with relative mass uptake versus time, and can be used to find the diffusion coefficient D_x.

By the use of Eq. 2.31, these two equations can be used to make two distinct curves. The first curve is made from the measured quantities giving $G_{measured}$, while $G_{calculated}$ is made for a defined D_x, shown in Eq. 3.1 and Eq. 3.2.

$$G_{measured}(t) = \frac{M(t) - M_i}{M_m - M_i} \qquad \text{Eq. 3.1}$$

$$G_{calculated}(t) = 1 - exp\left[-7.3 \cdot \left(\frac{D_x \cdot t}{s^2}\right)^{0.75}\right] \qquad \text{Eq. 3.2}$$

The value of D_x is then changed with the purpose of achieving $G_{calculated}$ to be a good approximation to $G_{measured}$. The value of D_x, which gives the best approximation is then be defined as the SCT's diffusion coefficient. As the value of D_x is determined, new curves can be made with different value of the geometric constant *s*, e.g. whether the situation is one or two-sided.

In order to make a curve to illustrate the water uptake in a SCT shrunk on a PTFE cylinder during conditioning, the value of s is set to 2h as the water uptake is limited to be one-sided.

Water uptake measurements

The diffusion characteristics were investigated at three different temperatures, 30, 60 and 90 ℃, in addition to three different degrees of shrinking

i) Not shrunk (Virgin)
ii) Partially shrunk to fit the PTFE rods
iii) Fully shrunk to its minimum size

As a result, it is possible to examine how the water uptake changes with both variations in the temperature and the degrees of shrinking.

The measurement required preparation in advance of the execution. Three identical pieces with length 100 mm was shrunk to the three different degrees. As the measurement device, Mettler Toledo UMX2, is highly sensitive, the weight of each pieces was required to be below 2 grams.

The pieces of SCT were cut into 16 smaller samples with an individual weight around 1.5 grams. Figure 82 illustrates the preferable geometry of the test specimen. The size of *n* and *l* should be much larger than *h*, resulting in a dominating diffusion through the *nl* –surface. The diffusion is then considered to have one-dimensional conditions, $D(t) = D_x(t)$. [30]

The samples were thus cut in such a way to achieve smooth surface on the edges, and therefore avoid roughness where water droplets can attach easier.

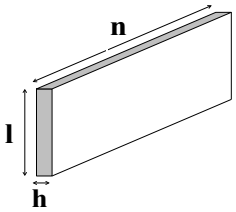

Figure 17: Geometry of test specimen.

Afterwards, the pieces were placed in a vacuum drying oven at 70 ℃ for one week in order to obtain dry-weight. Prior to the measurement, the temperature in the vacuum drying oven was decreased to 25 ℃, giving a sample temperature approximately equal to the room temperature.

The sample's initial (dry) weight, M_i, was measured immediately after removal from the vacuum drying oven, avoiding interaction with the surrounding. Afterwards, the sample is immersed in distillate water, which was preheated to the experimental temperature.

The sample should be kept immersed in water with a limited time in contact with the surroundings to avoid interactions influencing the experiment.

Continuously measurements of the sample are carried out with the equipment illustrated in Figure 18. A computer is connected to the measuring device, Mettler Toledo UMX2, where the date, time and weight automatically are stored in Excel.

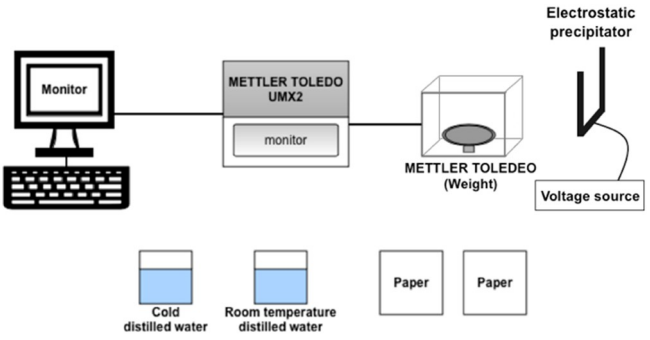

Figure 18: Equipment used when performing Mass Uptake Measurement. A computer connected to the measurement instrument Mettler Toledo UMX2. An electrostatic precipitator removes the surface charge.

Cold distillate water is used in order to remove convection currents and lock the water content in the sample before weight measurement. Placing the object in room temperate water gives the same basis for all measurements.

Paper sheets are used in order to remove the surface water, ensuring that the weight increase is due to the diffusion. Before placing the sample on the weight, it is moved through an electrostatic precipitator removing the surface charge. The measurement instrument sends the information to Excel, while the sample is placed back in its container for continuous exposure to water.

The preparation and measurement procedure used in for experiment is described in more detail and can be found in Appendix A1.

3.2 Differential scanning calorimetry

Dielectric response measurements are to be performed at temperatures from 40 ℃up to 150 ℃. In order to be able to compare measurement at different temperatures, the material should not experience any changes within that temperature range.

DSC is used for investigation of the thermal transition of the SCT for a selected temperature interval. The stress control tube thereby checked for thermal transitions giving changes in the material. The measuring device used for the examination was Mettler Toledo High-Pressure Differential Scanning Calorimetry with nitrogen gas.

The specimen was prepared and placed in a crucible pan, while the reference was kept empty. Both of the crucibles pans were placed in the DSC-device, a temperature program was selected and started. During the measurement the crucibles was kept in an atmosphere consisted of nitrogen gas giving a better heat transfer.

The temperature program was selected as the temperature interval from 20 ℃ to 200 ℃. The temperature program with a length of 97 minutes, are shown in Figure 19.

The temperature program starts with a temperature stabilization at 20 ℃. It is then linearly increased up to 200 ℃, where it is kept for a small period before decreasing linearly back to its starting point.

This program is executed twice in a row. The two parallels are identical, causing period 2 and 6 in Figure 19 to be equal.

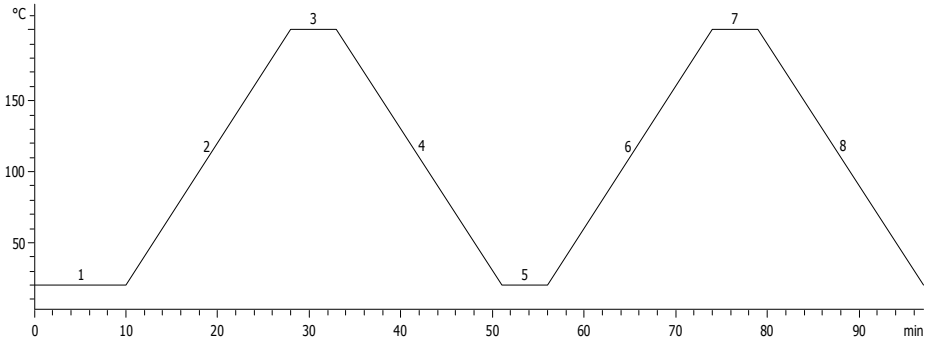

Figure 19: Temperature program for DSC measurement.

Table 2: Temperature program used for the differential scanning calorimetry.

Interval	Start temperature	End temperature	Duration	Slope
1 | 5	20 °C	20 °C	10 min	0 °C/min
2 | 6	20 °C	200 °C	20 min	10 °C/min
3 | 7	200 °C	200 °C	5 min	0 °C/min
4 | 8	200 °C	20 °C	20 min	-10 °C/min

The aim of the experiment is thus to examine the changes as the temperature increases to 200 °C. For this reason, the analysis is limited to concern only interval 2 and 6.

Measurement procedure

DSC measurement was to be performed at each of the three different degrees of shrinking. Pieces of stress control tube is shrunk into the three degrees before they are cut into smaller pieces and placed in a vacuum drying oven. The samples were dried at 70 °C for a week in prior to the measurement.

As the volume of the crucible pan is only 40 µL, the SCT had to be cut into smaller test samples to fit into the crucibles. In order to avoid temperature gradients over the sample, the height h should be kept small in addition to be kept uniform over its area (Figure 20).

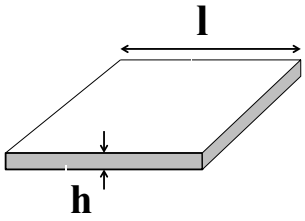

Figure 20: Illustration of the test samples used for DSC measurement.

A more detailed description of the preparation procedure for the test sample is found in Appendix B2.

Analysis of measured data

The measurement results in a heat flow curve, which presents the required power from the heat pan in order to follow the temperature program. The curve can be analysed by the usage of software program STARe Excellent.

The purpose of the DSC measurement is to determine if there is an occurrence of transition phases within the specified temperature range. Analysis is reduced to find the onset-, minimum- and maximum temperature.

Onset is defined as the temperature in the beginning of a transition change, i.e. the knee point where the curve has a significant change from the baseline.

Minimum temperature is where the curve has its lowest demand for heat transfer, yielding the melting peak. Maximum temperature describes the point where heat flow required is back to its baseline where it is approximately uniform.

3.3 Dielectric response measurement

Dielectric response measurements were to be performed on a commercially available heat-shrink stress control tube installed on a PTFE rod. These measurements were performed with purpose to characterize the electrical properties of the stress control tube when changing the temperature and humidity level.

3.3.1 Test object

The test object used in this study is a simple cylinder with metal electrodes and insulation material made of polytetrafluoroethylene (PTFE).

To achieve higher electric field strengths using the same voltage source, two different dimensions of PTFE was used. The largest object had an insulation dimension of 100 mm and is referred to as Object L whilst Object S is the shorter object with an insulation length of 20 mm.

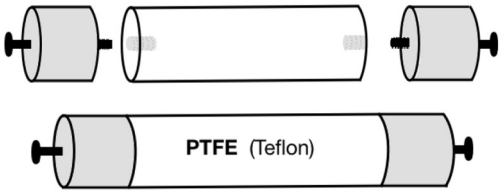

Figure 21: Cylinder consisting of metal electrodes assembled together with a PTFE rod.

In order to consider the properties of a stress control tube, the cylinder was chosen to be made of PTFE. By the reason that it has extremely good electrical properties; the value of tan δ, for all frequencies, is one of the lowest known for solid insulation and the material has a dielectric constant as low as 2 [5].

The cylinder had an outer diameter of 25 mm before installing the SCT, and 29 mm after installation of the SCT. The diameter of the tube is within the recommended range when installing the stress control tube in a real joint. [1]

The stress control tube to be characterized is Raychem JSCR 42/16. Previous experiments on this tube indicate that the conductivity has a non-linear field dependence. [32]

When installing the tube on the PTFE rod, some caution must be taken into account. In order to avoid impurities at the interface between the insulation and the tube, the test object should be properly cleaned before application.

When shrinking the tube, the heating should start at the rod's midpoint and performed outward toward each end separately. This will avoid that voids filled with air are trapped beneath the tube, resulting in reduced breakdown strength. The finished test object is illustrated in Figure 22.

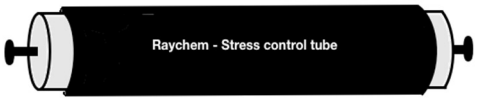

Figure 22. Cylinder consisting of PTFE rod, two metal electrodes and heat shrink stress control tube.

Before placing the test object in the experimental circuit, the following adjustment was performed as shown in Figure 23:

Corona rings (1) were attached in both ends, in order to avoid corona discharge. A PTFE ring (2), is attached at one end of the object to avoid that the measuring electrode is connected to the grounded corona-ring. Metallic clams (5) were used on both electrodes to ensure good electric contact between the electrode and stress control tube. This will provide a better and more uniform contact as the temperature increases.

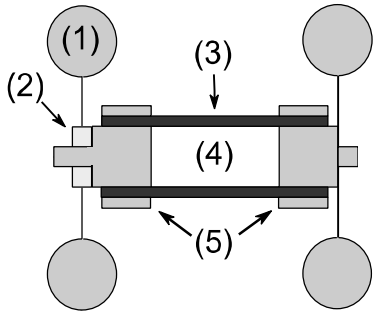

Figure 23. Illustration of test object; (1) Corona rings, (2) PTFE ring insulating the measuring electrode from the grounded corona ring, (3) stress control tube, (4) PTFE rod, and (5) metallic clamps. [1]

3.3.2 Dielectric spectroscopy

Measurements of dielectric response, dielectric spectroscopy, performed using an Insulation Diagnostic System, IDA 200 [33]. IDA 200 utilizes low voltages, up to 200 $V_{peak,}$ with a frequency range of 0.1 mHz to 1 kHz.

To achieve higher voltages, an external voltage unit is added providing an output voltage up to 30 kV_{peak}. This will however limit the upper limit of the frequency range to 100 Hz.

IDA 200 can measure capacitance ranging from 10 pF to 100 mF. Dielectric loss tangent is within the range of 0 – 10 when the accuracy of the capacitance is retained, otherwise, the value can be higher. [34]

The measurement inaccuracies for IDA 200 are given in Figure 24 as a function of the sample capacitance and the measurement frequency.

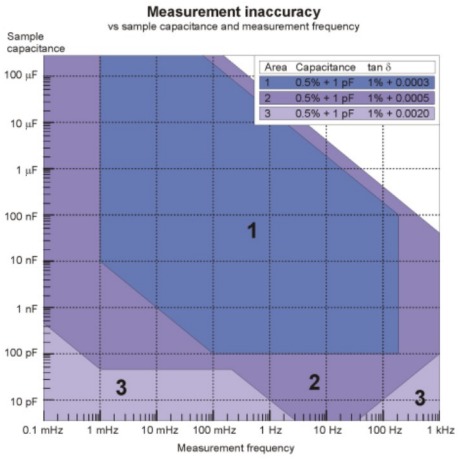

Figure 24. Measurement inaccuracies for IDA 200 at different values of capacitance and dielectric loss tangent. [34]

IDA 200 produces a sinusoidal voltage with different frequencies, which produce a current though the sample, illustrated in Figure 25. Both the current and voltage is measured with amplitude and angle, and enables the impedance Z to be calculated. This could be used in order to determine the different diagnostic parameters (Table 1).

The impedance can be presented directly with rectangular or polar form, or by using different impedance models. The four different models are

1. RC circuit in series or parallel. (R and C)
2. Complex C (C' , C'' and $\Delta C'$)
3. Dielectric (ε', ε'', $\Delta\varepsilon'$ and $\tan\delta$)
4. Resistive (ε, ρ and σ)

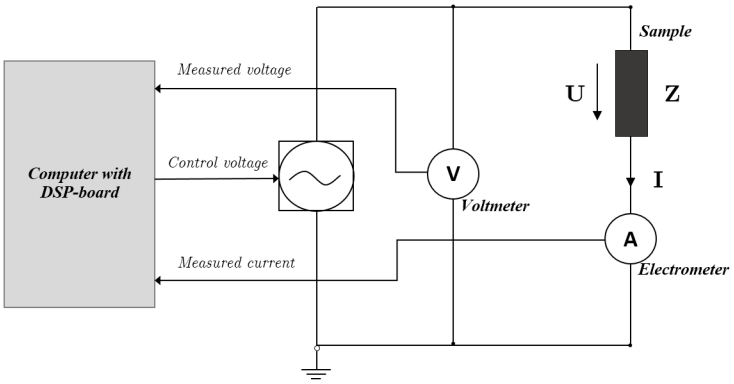

Figure 25. Measurement of electrical impedance. [33]

This thesis will use the complex and dielectric model, to examine the dielectric loss tangents and complex capacitances. Analysis of these parameters is performed with regard to the change in voltage, frequency, temperature and humidity. These parameters can further be used for calculation of the stress control tube's conductivity.

The measured complex capacitance can be related to the complex permittivity by:

$$C = C_0\,\varepsilon' = C_0\,(\varepsilon' - j\varepsilon'') = C' - jC'' \qquad \text{Eq. 3.3}$$

Dielectric spectroscopy can be performed with a grounded or ungrounded specimen, in addition to either with or without a guard. The two different connection diagrams are shown in Figure 26 and Figure 27.

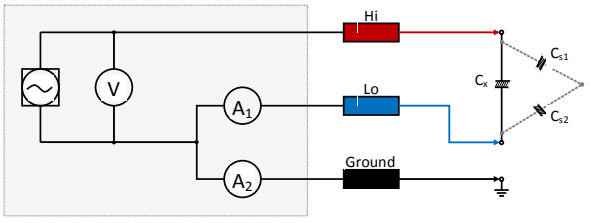

Figure 26. Connection diagram for Ungrounded Specimen Test (UST).

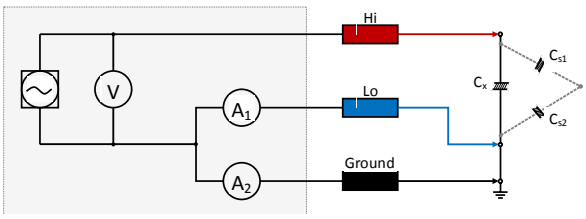

Figure 27. Connection diagram for Grounded Specimen Test (GST).

This experiment will perform measurement with the connection illustrated in Figure 26, i.e. ungrounded specimen without a guard. The test object from Figure 23 is placed within a heating cabinet, which provide a stable temperature during measurement. The final experimental setup is shown in Figure 28.

IDA 200 is connected to an external high voltage unit (HVU) and further to a termination box. Two separate connections, referred to as "Hi" and "Lo", are connected between the termination box and the specimen.

"Hi" is connected to the high voltage electrode of the test object by the high-voltage supply. Corona rings are attached at the connection point in order to avoid corona discharges. "Lo" is connected to the opposite electrode, which is separated from the grounded corona ring.

Due to large temperatures inside the heating cabinet, both the measuring- and high voltage cable had to be rated for temperatures above 150 °C.

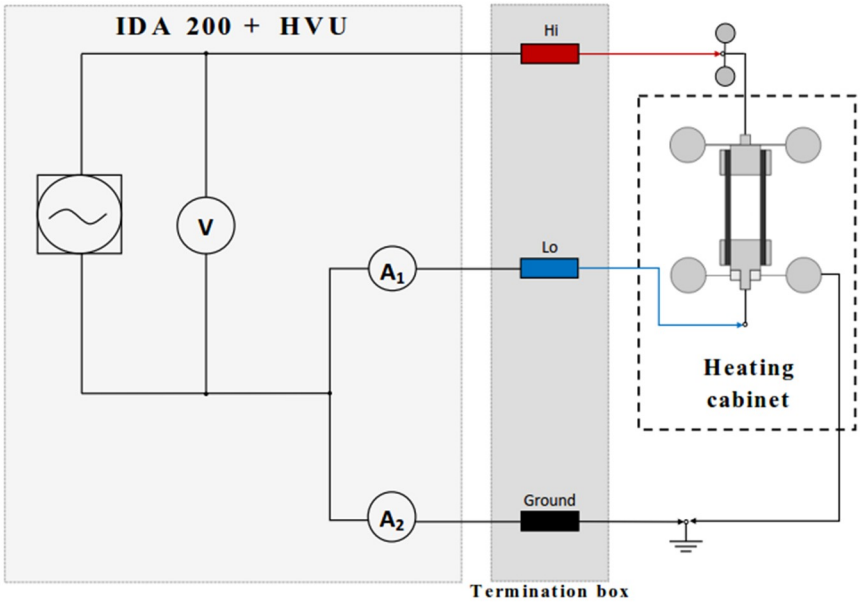

Figure 28. Measurement diagram for the experiment using UST without a guard.

Measurement procedure

Voltages used for the experiment are chosen with the intention to have comparable values with time domain dielectric response measurements [1] performed on the same test objects.

As the time domain analyses are using a DC source, the voltage levels used in this experiment is defined as peak values. The voltage applied to the Object S and Object L differs. Higher voltages are used for Object S in order to achieve a higher electric field strength. The maximum field strength applied to Object S is 1.0 kV/mm, i.e. 20 kV_{peak}. This is below the DC breakdown strength of the test object, which is 1.25 kV/mm [1,32].

In addition, voltages are selected with the purpose of achieving the same applied electric field strength of Object L and Object S.

The electric field strength for the applied voltage is listed in Table 3.

Table 3. Electric field strength in [kV_{peak}/mm] for the applied voltages.

Voltage	0.5 kV_{peak}	1.0 kV_{peak}	2.5 kV_{peak}	5.0 kV_{peak}	10.0 kV_{peak}	12.5 kV_{peak}	15.0 kV_{peak}	20.0 kV_{peak}
Object S [20mm]	0.025	0.05	0.125	0.25	0.50	0.625	0.75	1.0
Object L [100mm]	0.005	0.01	0.025	0.05	0.10	-	-	-

The voltage and frequency applied to Object S and Object L are listed in Table 4 and Table 5. The measuring sequence will start at the lowest voltage and perform measurement for two periods at each frequency to provide a more accurate result. The frequency is decreased from 100 Hz to 1 mHz.

Measurements performed at 50 Hz and 100 Hz (2x50 Hz) can be influenced by external sources with power frequency of 50 Hz. Measurements are therefore performed at 49.8 and 98.4 Hz in order to limit such influence. After application of the highest voltage level, the voltage is decreased to 1.0 kV_{peak}.

Table 4. Measurement program for Object S.

Voltage [kV_{peak}]	0.5	1.0	2.5	5.0	10.0	12.5	15.0	20.0	1.0	
Frequency [Hz]	98.4	49.8	20	10	5	2	1	0.5	0.2	0.1	0.01	0.001

Table 5. Measurement program for Object L.

Voltage [kV_{peak}]	0.5		1.0		2.5		5.0		10.0		1.0	
Frequency [Hz]	98.4	49.8	20	10	5	2	1	0.5	0.2	0.1	0.01	0.001

Temperature

Measurements is to be performed at three different temperatures: 40 °C, 90 °C (rated temperature) and 150 °C (temperature during failure). The sequence of the measurements is to be 40 °C, 90 °C, 150 °C and then repeated at 40 °C.

This measurement is to examine whether the measurement has changed the electrical properties after a high voltage application. Such change can be caused by an anomalous (hysteresis) effect or desorption of volatiles during application of high temperatures.

Humidity

In order to increase the water content within the stress control tube the test object is immersed in distillate water at 90 °C. The object is kept at these conditions for 39 days. Preparation of the test object is required before performing dielectric response measurement.

The test object was immediately placed in circulating cold water (4 °C) for 5 minutes, in order to quickly cool the object and lock the water inside the tube. The sample was paper-dried to remove water on the object's surface. Layers of plastic foil applied tight to avoid air bubbles form between the layers, and last, insulation tape was applied to cover the plastic foil.

This application was performed in order to avoid the moisture to diffuse out of the test object during the measurement.

Conditioning of the test object

The test object was pre-conditioned in a vacuum drying oven at 70 °C for three days. After three days, the test object is connected to the experimental setup. In order for the test object to achieve a stable temperature, the object was temperature conditioned for about one hour before performing measurements.

3.4 Measurement sequence

The measurement sequence for this thesis is:

1. Diffusion measurements

   Measurement on three degrees of shrinkage of the stress control tube, at 30 °C, 60 °C and 90 °C.

2. Differential scanning calorimetry

   Measurement of three degrees of shrinkage of the stress control tube.

3. Dielectric response measurements
   - i. Measurement 40 °C – 90 °C – 150 °C – 40 °C
   - ii. Measurements at temperatures results found by differential scanning calorimetry.

   Measurements described in i. and ii. are performed for both Object S and Object L.

   - iii. PTFE rod (100 mm) without application of a stress control tube at 40, 90 and 150 °C.
   - iv. Object S2 at 20 °C before placed in distillate water.
   - v. Object S1 with plastic foil and insulating tape.
   - vi. Object S2 in wet condition with plastic foil and insulating tape at 20 °C.
   - vii. Dissection of Object S2 after measurements.

Chapter 4

4 Results

4.1 Diffusion

Water uptake measurements were performed according to the description in chapter 3. Small pieces of stress control tube, holding three different degrees of shrinkage, were examined. The purpose of the experiment was to determine their water uptake characteristic as a function of both degree of shrinkage and temperature.

Test measurements were first performed on three objects for determination of a suitable measurement sequence. As water uptake is most rapid in the beginning, measurements were performed more frequently the first hours. Measurements indicate that the stress control tube has a slow water uptake. On this basis, the measurement sequence was performed less frequently after the first two hours.

At each measurement, the test sample's weight in addition to the time and date was noted. Eq. 2.29 can then be used to find the material's gained moisture as a percentage of the dry weight, which is plotted as a function of time.

Figures made from the measurement indicate that the stress control tube keeps absorbing water, and the test samples do not reach saturation during this experiment.

In addition, the measurements show signs on having two stages of diffusion. A steeper slope is visible in the beginning, and after a period, the water uptake curve shifts towards a new and linear slope. This seems to be applicable for measurements performed at 90 ℃ and 60 ℃, but also in some extent for the measurement at 30 ℃.

4.1.1 Water absorption affected by the degree of shrinkage

Analyses performed at samples kept at the same temperature shows that the water uptake by the stress control tube is dependent on the degree of shrinkage. When the shrinking increases, water uptake by the tube decreases.

A virgin stress control tube has the highest water uptake, while the fully shrunk tube has the lowest. For a partially shrunk stress control tube, the water uptake will lie in between the value for virgin and fully shrunk stress control tube.

After closer examination, partially shrunk samples appear to be unevenly shrunk. A 10 cm tube was shrunken on a PTFE rod, and cut into 16 samples. Comparison of those samples shows that some have areas with higher degree of shrinkage, while other have lower. This variation provides curves of the water uptake that differs.

For both samples of virgin and fully shrunk SCT, the thickness of the tube is uniform over its whole area. This provides a water uptake by the samples to be approximately the same for the given degree of shrinkage.

Water uptake at 30 °C

Figure 29 show the water concentration in percentage of the total weight as a function of days for the different degrees of shrinkage.

Water uptake for samples at 30 °C indicates that none of the samples has reached saturation after 100 days. The water uptake seems to rather be increasing, than stagnate.

After reaching 100 days, the water concentration weight can be found to be 1.15 % (virgin), 0.89 % (partially shrunk) and 0.82 % (fully shrunk).

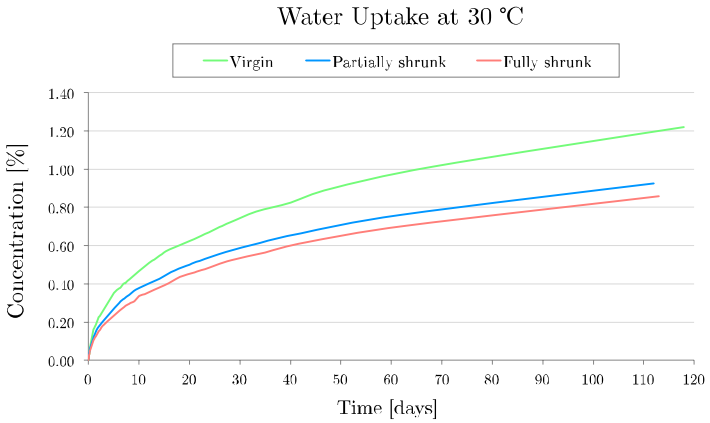

Figure 29. Water content at 30 °C, given as percentage of the total mass. One sample of each degree of shrinkage is shown in the figure.

Water uptake at 60 °C

Measurements on samples held at 60 °C, provides three curves having similar shape. Water uptake by the stress control tubes will still not reach saturation.

After being immersed in water for 95 days, the water concentration in the tube will be 3 % for virgin SCT, 2.4 % for partially shrunk SCT and 1.95 % for fully shrunk SCT.

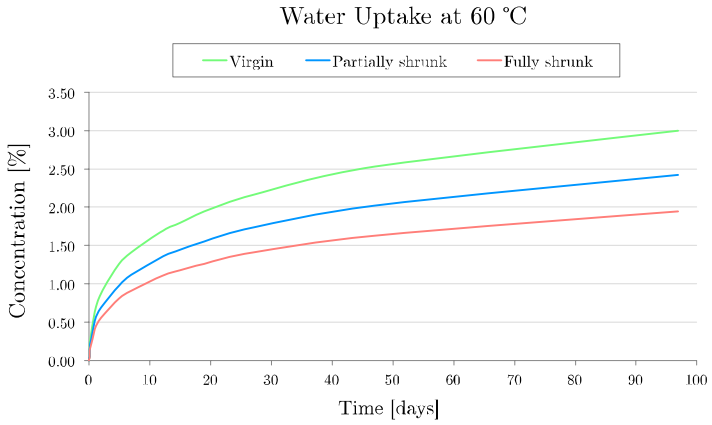

Figure 30. Water content at 60 °C, given as percentage of the total mass. One sample of each degree of shrinkage is shown in the figure.

Water uptake at 90 °C

Test samples kept at 90 °C provides the highest water uptake by the stress control tube. Still, there is no sign of saturation in the test samples, but rather a linearly increase.

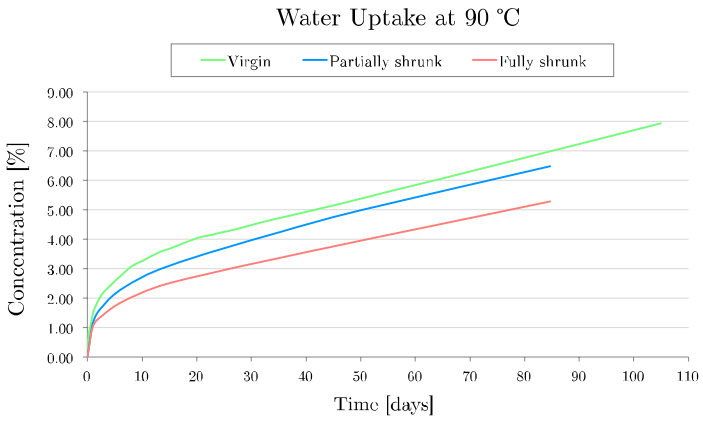

Figure 31. Water content at 90 °C, given as percentage of the total mass. One sample of each degree of shrinkage is shown in the figure.

The water uptake by the stress control tubes seems to have two different phases of diffusion. The first phase follows a typical saturation curve, while the second phase has a water uptake following an approximate linear increase.

The daily increase in water uptake during second phase will almost be identical for the three samples. The slope of the curve can be graphically found as shown in Figure 32. The increase is given as the percentage increase per day.

Values of the increase in water uptake can thereby be found to be 0.046 %/day (virgin), 0.045 %/day (partially shrunk) and 0.040 %/day (fully shrunk).

Because the water uptake has two phases, the diffusion coefficient D_x is difficult to determine by use of

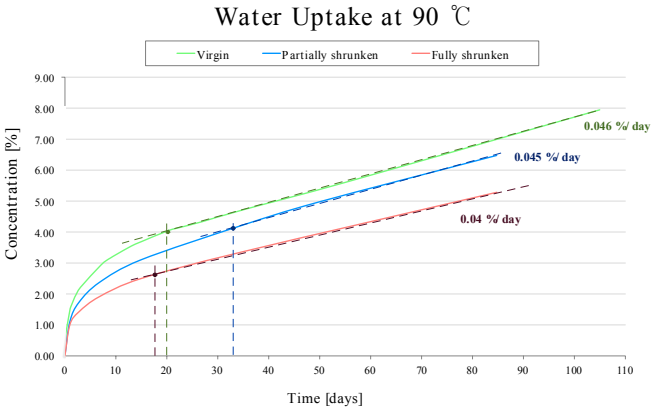

Figure 32. Graphically determination of the water increase per day.

equation for $G_{measured}$ and $G_{calculated}$ (Eq. 3.1 and Eq. 3.2). Using the formulas will not provide a good curve fitting.

Due to the unknown value of the diffusion coefficient, the water content in the test object used for dielectric response measurement cannot be mathematically calculated. An approximated value of the water content is found graphically instead.

4.1.2 Water absorption affected by temperature

Results show that the water uptake increases with temperature. The slope of the water uptake is also highest at 90 °C, presenting the highest increase in concentration.

Figure 33 gives water uptake curves for partially shrunk stress control tube at the three temperatures. At each temperature, two test samples are used and thus providing two different curves. The two curves indicate that the samples have different water uptake, as the concentration differs through the whole experiment.

After closer examination, the stress control tube is found to be unevenly shrunk, giving different thickness of the samples. The sample with the highest degree of shrinking, i.e. the thickest, have the lowest water uptake.

For virgin and fully shrunk stress control tube, the water uptake is approximately identical for both measurement. Figures illustrating this are found in Appendix A2.

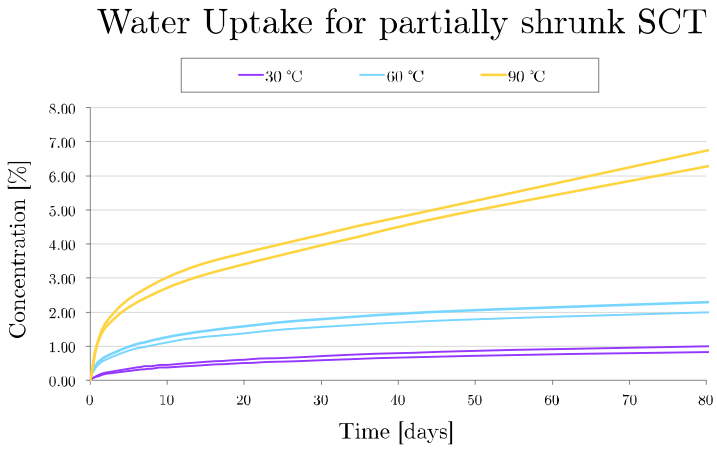

Figure 33. Water uptake for partially shrunk stress control tube at 30, 60 and 90 °C. Results from two test samples at each temperature are shown.

The curves for water uptake at 30 and 60 ℃ seems to have reached their maximum water content, however, this is not the case. A small increase in water uptake at 30 ℃ and 60 ℃ is visible in respectively Figure 29 and Figure 30.

Water content for six different partially shrunk test samples after 80 days, is listed in Table 6. The water uptake at 90 ℃ is approximately three times higher than for 60 ℃ and approximately seven times higher than samples at 30 ℃.

Table 6. Water content for six test samples of partially shrunk SCT after being immersed for 80 days.

Temperatur e	Sample 1	Sample 2
30 ℃	6.75 %	6.28 %
60 ℃	2.29 %	2.00 %
90 ℃	1.00 %	0.82 %

4.2 Differential scanning calorimetry

Differential scanning calorimetry was used for examination of phase transitions within the temperature interval used for dielectric response measurements.

Three measurements were performed for each degree of shrinkage. This provides a possibility to check for insignificant measurements.

Results from DSC show that the stress control tube experiences an endothermic phase transition, which is independent of the degree of shrinkage. A large dip in the curve indicates that the sample requires less heat power in order to follow the temperature program.

The endothermic melting point is analysed in order to find the onset, minimum and maximum temperature. These temperatures are illustrated in Figure 34.

Onset temperature describes where the stress control material starts to experience changes. Minimum temperature is the temperature when the material has its melting peak. Maximum temperature appears when the heat flow required is reduced and approximately uniform.

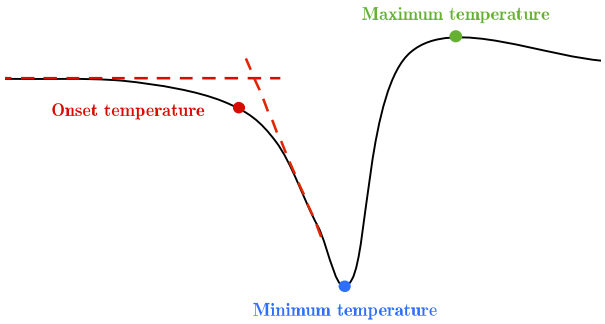

Figure 34. Illustration of the temperatures found for the endothermic melting transition.

4.2.1 Virgin

The results from DSC analysis of the endothermic melting peak are listed in Table 7. The results indicate that the onset temperature of the melting transition occurs at a temperature slightly above the rated temperature for XLPE cables (90 ℃).

Mean value of the onset temperature for a virgin stress control tube is found to be 93 ℃. Mean value of the minimum temperature is 104.8 ℃ and for maximum temperature 118.3 ℃.

Table 7. DSC analysis of maximum endothermic phase transition for a virgin stress control tube.

	Measurement 1		**Measurement 2**		**Measurement 3**		Mean value
	First run	Second run	First run	Second run	First run	Second run	
Onset	96.6 ℃	90.1 ℃	94.4 ℃	90.6 ℃	94.8 ℃	91.9 ℃	93.0 ℃
Minimum	103.1 ℃	105.5 ℃	104.4 ℃	105.6 ℃	103.4 ℃	106.9 ℃	104.8 ℃
Maximum	118.4 ℃	119.1 ℃	114.1 ℃	119.8 ℃	117.0 ℃	121.2℃	118.3 ℃

Figure 35 shows the curves for DSC measurement 2. The blue curve presents the first run, which has a local endothermic peak at 80 ℃. During the second run (red curve), this local peak disappears and less power is required from the samples to follow the temperature program.

Figures for the first and third measurement can be found in Appendix B2. Both have similar curves as for the second measurement, with a local peak at approximately 80 ℃. The first measurement shows a more unstable power consumption, with both endothermic and exothermic peaks.

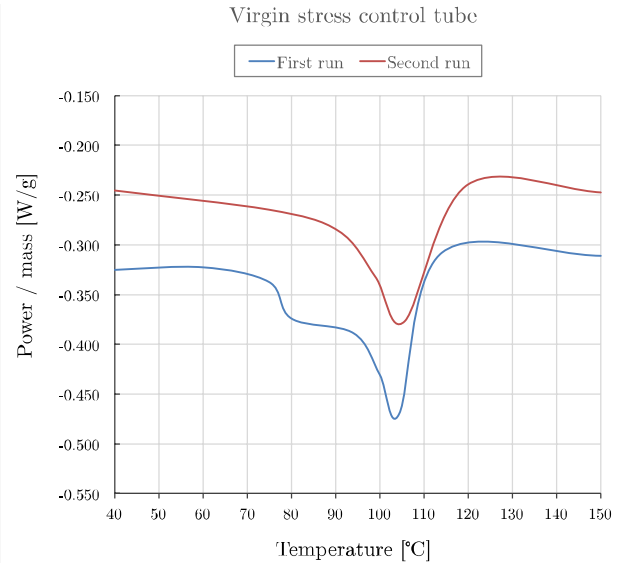

Figure 35. DSC measurement on a sample of virgin stress control tube.

4.2.2 Partially shrunk

Table 8 gives the results after DSC measurement on a partially shrunk stress control tube.

As for virgin stress control tube, the mean onset temperature is slightly above the rated temperature for XLPE cables. However, the onset values are found to be both above and below 90 °C, which is the temperature range XLPE cables holds during service.

Table 8: DSC analysis of maximum endothermic phase transition for partially shrunk stress control tube.

	Measurement 1		**Measurement 2**		**Measurement 3**		Mean value
	First run	Second run	First run	Second run	First run	Second run	
Onset	92.0 °C	83.3 °C	96.7 °C	89.5 °C	93.9 °C	90.4 °C	91.0 °C
Minimum	103.9 °C	103.4 °C	104.1 °C	104.0 °C	103.2 °C	103.3 °C	103.7 °C
Maximum	114.7 °C	112.7 °C	114.7 °C	113.2 °C	114.6 °C	112.7 °C	113.8 °C

Mean value for the minimum temperature is found to be 103.8 ℃, while the maximum temperature's mean value is 113.8 ℃. During the first run, the onset temperature is slightly higher than the second run, with respectively 94.2 ℃ and 87.7 ℃.

Figure 35 shows the curves for the first DSC measurement. The blue curve presents the first run, and the second run is represented by the red curve.

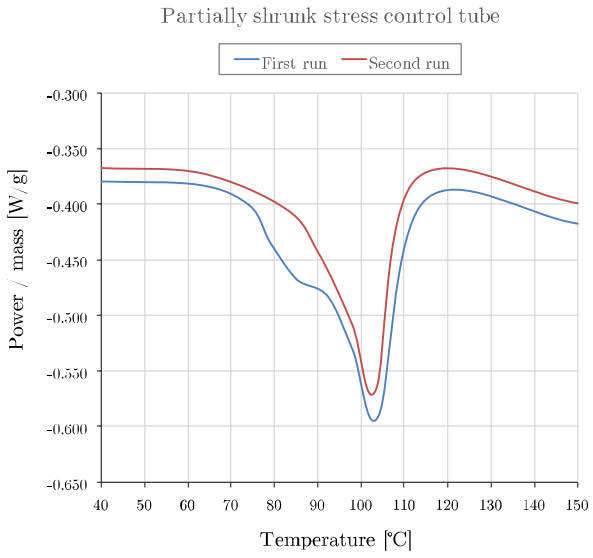

Figure 36. DSC measurement for a partially shrunk stress control tube sample.

The partially shrunk sample has, in similar to a virgin sample, a local endothermic peak at approximately 80 ℃. This local peak disappeared during the second run, and also here the sample requires less power to follow the temperature program.

Figures for the second and third measurement can be found in Appendix B2.

4.2.3 Fully shrunk

Table 8 gives the results after DSC measurement on a fully shrunk stress control tube. The results are similar to the partially shrunk tube; however, the first run does not have a local peak. The curve for the first and second run is almost identical, except that the second run has a slightly smaller power consumption.

The mean values are similar to both virgin and partially shrunken, with onset temperature of 92 ℃, minimum temperature of 103.8 ℃ and maximum temperature of 114 ℃.

Figures for second and third measurement are found in Appendix B2.

Table 9. DSC analysis of maximum endothermic phase transition for fully shrunk stress control tube.

	Measurement 1		**Measurement 2**		**Measurement 3**		Mean value
	First run	Second run	First run	Second run	First run	Second run	
Onset	91.9 ℃	89.9 ℃	92.0 ℃	91.7 ℃	97.3 ℃	89.6 ℃	92.0 ℃
Minimum	103.0 ℃	103.2 ℃	105.0 ℃	104.7 ℃	103.6 ℃	103.3 ℃	103.8 ℃
Maximum	113.8 ℃	112.5 ℃	114.8 ℃	114.7 ℃	114.5 ℃	113.8 ℃	114.0 ℃

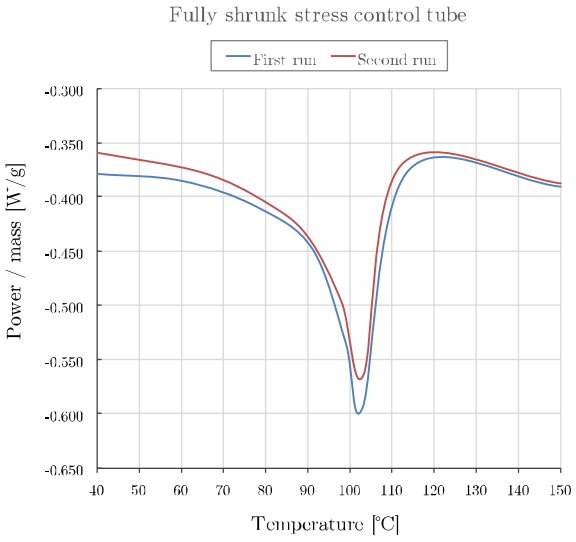

Figure 37. DSC measurement for a fully shrunk stress control tube sample.

4.2.4 Results from differential scanning calorimetry

DSC measurement for the three degrees of shrinkage are separated into first and second run, and then combined in Figure 38. The result show that both virgin and partially shrunk stress control tube experience a local peak at approximately 80 ℃, but such local peak are not visible for the fully shrunken. The local peak is therefore likely due to incomplete shrinking.

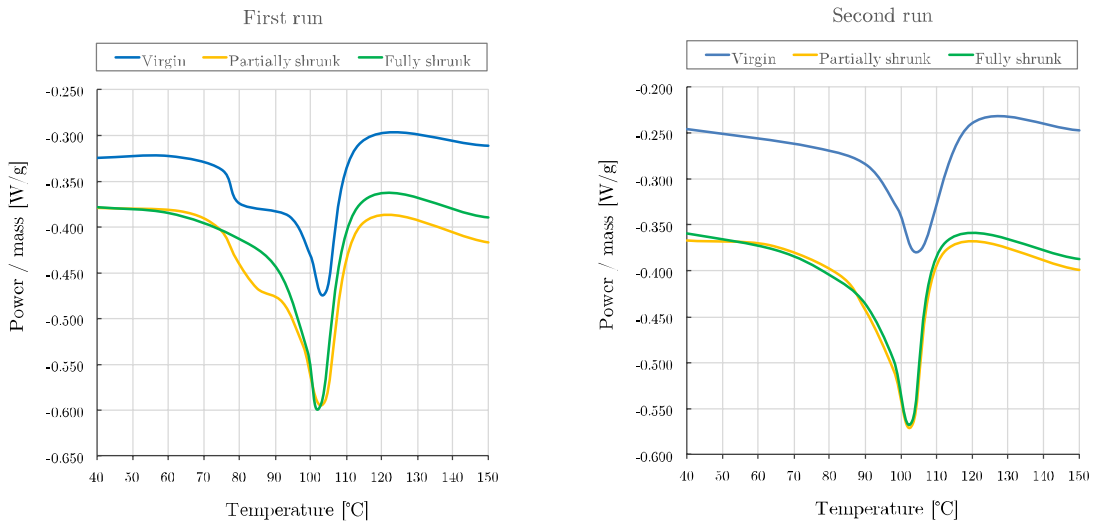

Figure 38. Curves from DSC measurement of the three degrees of shrinkage, divided intro first and second run.

The curves for partially and fully shrunk SCT are similar in both the first and second run, except for the local peak. Results from DSC measurement of the virgin sample show a smaller specific power consumption, and a smaller endothermic peak.

Results from DSC measurement show an endothermic peak within the temperature interval used for dielectric response measurement. Further analysis is to be performed in order to examine if this phase transition changes the electrical properties of the material.

The test object used in dielectric response measurement has a partially shrunken tube. Temperatures used for further investigations have been chosen to be 94 ℃, 104 ℃ and 114 ℃.

4.3 Dielectric spectroscopy

In order to determine the electrical properties of the stress control tube, dielectric response measurements was performed on test objects with different lengths. The parameters analysed is dielectric loss tangent and complex capacitance, which further can be used for calculation of the stress control tube's conductivity.

The main focus is to determine how the conductivity changes when changing the electric field strength, temperature, humidity level and if a phase transition will influence the value.

Conductivity is calculated at the lowest frequency that provides a sufficient accuracy, by use of Eq. 2.13. Conductivity obtained for Object S is further compared to conductivity found in time domain analysis in performed by SINTEF Energy Research on the same object [1].

4.3.1 PTFE rod without stress control tube

When performing dielectric response measurement on the test object, the aim is to determine the electrical properties of the stress control tube. Since the stress control tube is applied to a PTFE rod, they will form a parallel coupling as illustrated in Figure 39. The measured quantities are then given for the equivalent capacitance and not for the stress control tube alone.

Additional measurements were performed on a PTFE rod without a stress control tube applied. The object had the same length as Object L (100 mm). The purpose was to examine its influence on the measured quantities in the main experiment.

Results show that the values of dielectric loss tangent in the PTFE rod are smaller than 0.01 for all frequencies and temperatures. Comparing this result value with the one found in the main experiment, these will have a marginal contribution and can thereby be neglected.

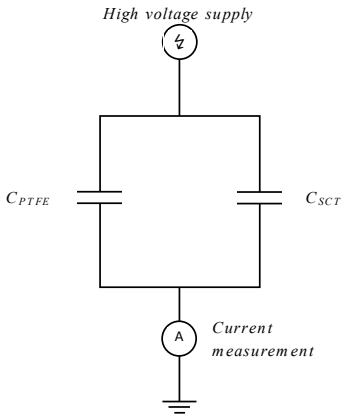

Figure 39. Equivalent circuit for measurement of the total capacitance in the test object.

The dielectric loss tangent for a PTFE rod is illustrated Figure 40. A large dispersion can be observed, but the losses have a minor change as the temperature increases.

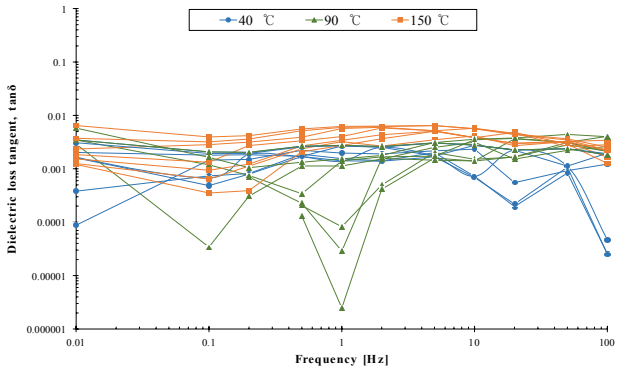

Figure 40. Dielectric loss tangent for a PTFE rod without a stress control tube.

Analysis of the complex permittivity ε' depicts that it has an approximately constant value of 5, with small variations from 4.8 to 5.2, for all measurements (Figure 41). It appears to be independent of frequency, voltage and partly temperature. Results from measurements show that an increase in temperature yields a slightly smaller value of ε'.

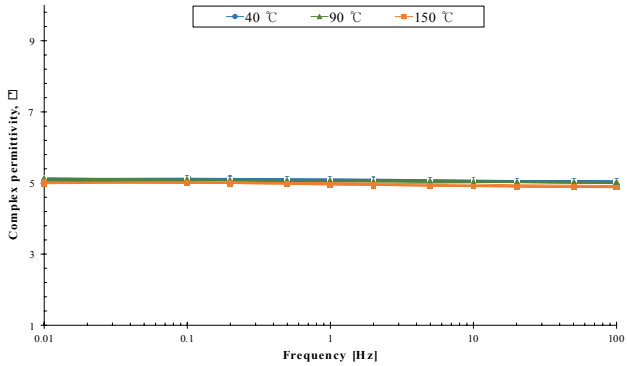

Figure 41. Complex permittivity, ε', for a PTFE rod a stress control tube.

Complex capacitances for the PTFE rod have a similar shape as found for dielectric loss tangent and complex permittivity. As C' is connected to ε' by the constant C_0, its value will be constant and independent of the frequency, electric field and temperature. Comparing this value to the ones measured at Object L, its influence can be assumed negligible (Figure 42).

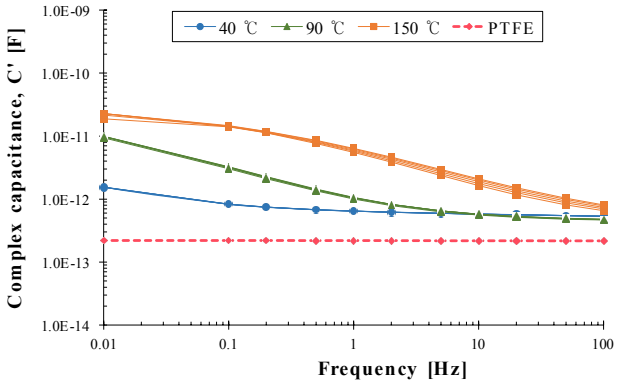

Figure 42. Real value of complex capacitance for Object L and PTFE rod.

The values of C'', has a large dispersion of values as found for $tan\,\delta$ and the curves will be similar as found in Figure 40. Its value is compared to the one measured on Object L (Figure 43) and is also assumed negligible.

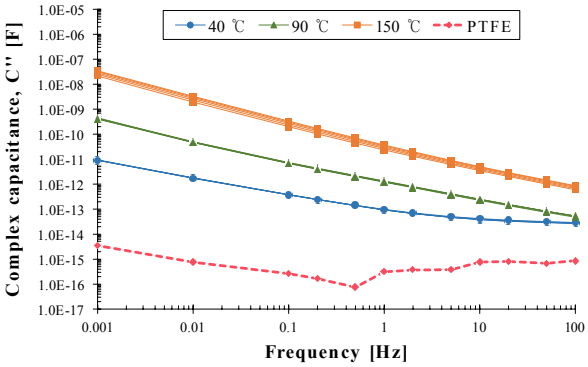

Figure 43. Imaginary value of complex capacitance for Object L and PTFE rod.

4.3.2 Measurement on Object L

Measurement on Object L provides analysis in the electric field range of 0.005–0.01 kV/mm. Dielectric response measurements were performed at frequencies from 100 Hz to 1 mHz.

However, when the temperature was increased to 90 ℃ and 150 ℃, the losses became substantial at the lowest frequencies. Losses at 1 mHz would then exceed range at where the measuring instrument, IDA 200, can detect precisely.

The result can be observed as large spread in measured values, where IDA 200 gives both positive and negative measurement results.

For that reason, analysis at these temperatures provides a restraint in the frequency range to be from 100 Hz to 10 mHz at the highest temperatures.

The results in this section will be presented as a function of the frequency. All measurements at different temperatures are combined into one figure that provides an opportunity to compare the effect of changes in the frequency, electric field and temperature. Electric field dependency for a parameter is detected where the curves at the same temperature have a deviation.

Curves with results from dielectric response measurement on Object L, is found in Appendix C1.

Dielectric loss tangent, $\tan\delta$

Values for the dielectric loss tangent for measurements on Object L are presented in Figure 44. Results show that the losses increases with temperature.

Furthermore, the dielectric loss tangent increases with decreasing frequency. The highest dielectric loss tangent is thus observed at 150 ℃, at the highest electric field and lowest frequency. At 10 mHz, $\tan\delta$ have gained a value above 100, which is above the measuring range of IDA 200. Inaccuracies can thereby be expected for both complex capacitance and the dielectric loss tangent.

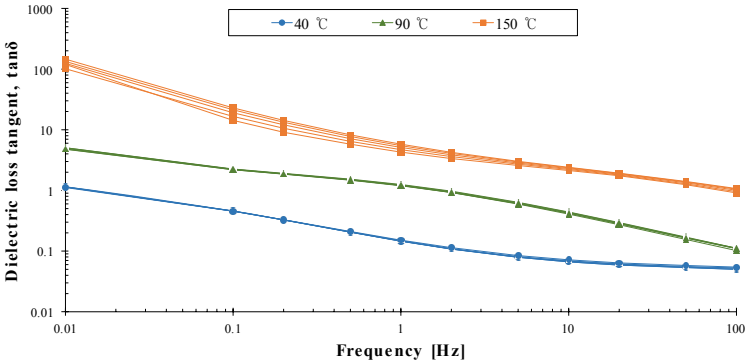

Figure 44. Dielectric loss tangent for measurement at Object L. All fields are included with a lower frequency limitation of 10 mHz.

The dielectric loss tangent for 40 ℃ and 90 ℃ has a significant lower value and will for both be below 10 at 10 mHz. However, as the frequency is decreased to 1 mHz, their value will be doubled.

For measurements at 150 ℃, a minor field dependence is observed for frequencies below 10 Hz and is illustrated in Figure 45.

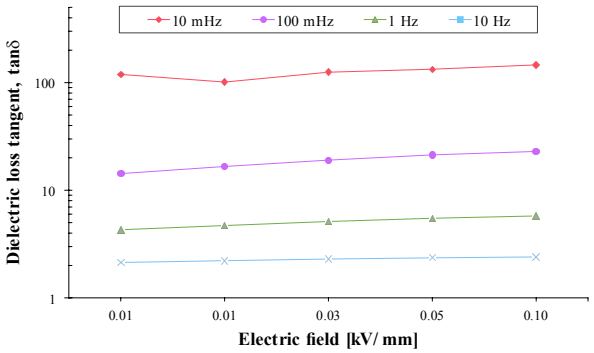

Figure 45. Dielectric loss tangent as a function of the electric field for 150 ℃.

Complex capacitance

The measured value of real value of complex capacitance C' is presented in Figure 46. At 100 Hz, all measurements have a value within the range of 0.5–0.7 pF. Measurements at 40 ℃ and 90 ℃ provide approximately the same value at frequencies above 5 Hz. As frequency is decreased below 5 Hz, the complex capacitance will start to increases for the test object at 90 ℃, while the value is within the same range for the object at 40 ℃.

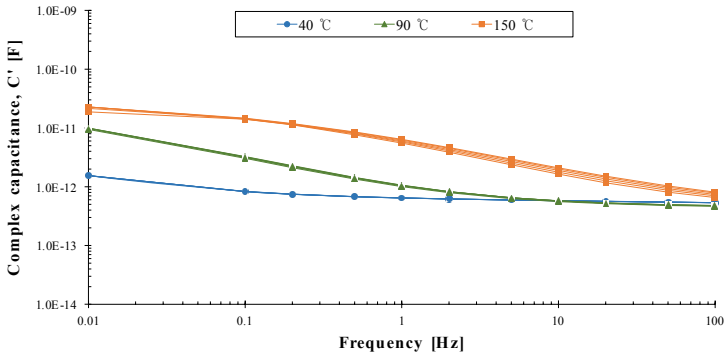

Figure 46. Real value of the complex capacitance, C', for Object L.

For measurement at 150 ℃, a minor electric field dependency is found at frequencies above 1 Hz. At 0.01 Hz, the result at 0.005 kV/mm deviates from measurement at higher electric fields.

The imaginary part of complex capacitance C'' is found to have an approximated linearly increasing in a log-log scale. This is observed for all temperatures. A minor field dependency is observed at 150 ℃, while both 40 ℃ and 90 ℃ is field independent.

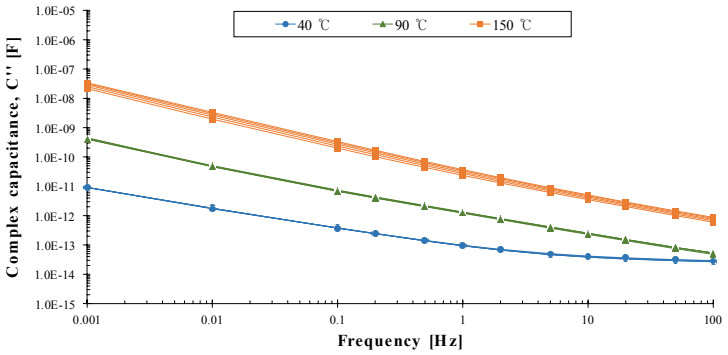

Figure 47. Imaginary value of the complex capacitance, C'', for Object L.

4.3.3 Measurement on Object S

As the length of the PTFE rod is decreased from 100 mm to 20 mm, higher electric field strengths are obtained during measurement on Object S. Measurements provide analysis of the material's electrical properties in the electric field range of 0.025 to 1.0 kV/mm with frequency varying from 100 Hz to 1 mHz.

As for measurement at Object L, the losses became substantial when the frequency is decreased to 1 mHz, and is specially observed for measurement at 150 ℃. Here, the losses exceeded the range where IDA 200 can detect accurately. The consequence is a large variety in the value of the dielectric loss tangent. This is especially true for the highest electric fields where the value is observed to be decreasing. This is can be seen in Figure 48.

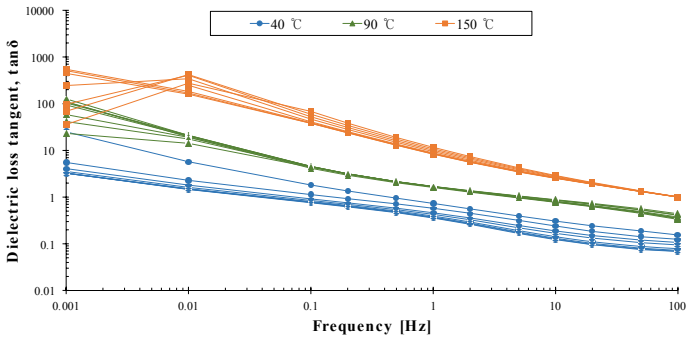

Figure 48. Dielectric loss tangent for Object S when including the entire frequency range from 1 mHz to 100 Hz.

During the first measurement at 40 ℃, observations made indicated that the current had a deformation as the frequency was decreased. In addition, large current peaks were noticed during application of the highest electric fields, i.e. 0.75 kV/mm and 1.0 kV/mm.

During the measurement at 0.75 kV/mm, i.e. 15 kV, the experiment experienced a malfunction at 20 Hz where IDA200 kept measuring for several hours without altering voltage or frequency. The measurement was stopped and new measurements were performed at 0.75, 1.0 and 0.05 kV/mm, i.e. 15, 20 and 1 kV.

Dielectric loss tangent, $\tan\delta$

When analysing of the results from the two measurements at 40 °C, a field dependence is observed. Figure 49 illustrates the dielectric loss tangent for both low electric fields, i.e. red curves, and the highest electric fields, i.e. blue curves.

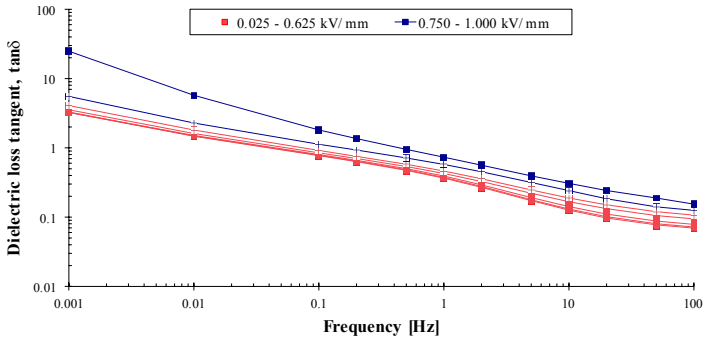

Figure 49. Dielectric loss tangent at 40 °C. Red curves illustrate the first measurement, while the blue presents the second measurement.

A field dependence is observed for the electric fields in the range from 0.5 – 1.0 kV/mm. This dependence will increase as the field increases and is illustrated in Figure 50.

Analysis of the dielectric loss tangent for measurement at 90 °C and 150 °C is performed by examination of the curves in Figure 48.

Observations made indicate that both have a field dependence at low frequencies. However, as the value exceeds the value of 10, the accuracy of the measurement at 1 mHz can be seen as insignificant.

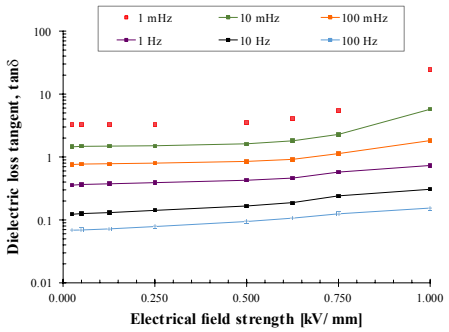

Figure 50. Dielectric loss tangent as a function of electric field strength.

For 90 °C, dielectric loss tangent will exceed the value of 10 at 10 mHz, while 0.5 Hz for measurements at 150 °C. At these frequencies, field dependency can be observed.

A minor field dependence is observed at 50 Hz and 100 Hz for measurements performed at 90 °C. This is likely due to measurements performed at their exact values. Measurement at these values can be influenced by external sources with power frequency of 50 Hz.

Complex capacitance

Results indicate that C' increases when the frequency is decreased. When examining results at 40 ℃, a minor field dependence is observed for measurement when applying the two highest electric field strengths. The deviation is most likely caused by the two separate measurements, where measurement at the two highest field strengths was delayed several hours.

For both 90 ℃ and 150 ℃, an electric field dependence is observed as for the dielectric loss tangent. When the dielectric loss tangent exceeds 10, the value of capacitance may not be retained. The field dependence is then likely caused by exceeding region where the measurement is given with good accuracy.

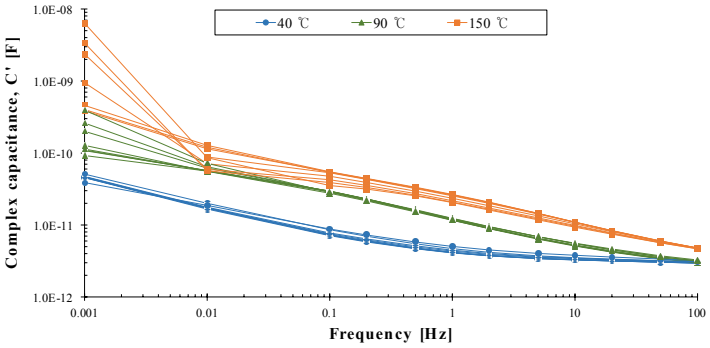

Figure 51. Complex capacitance C' from measurement at Object S

The imaginary value the complex capacitance C'' will, for all temperatures, increase when the frequency is decreased. At 90 ℃ and 150 ℃, the capacitance will be independent of the electric field. Measurement results at 40 ℃ imply a field dependence. This dependence is comparable to the one found for dielectric loss tangent, as the curves in Figure 48 and Figure 52 are similar.

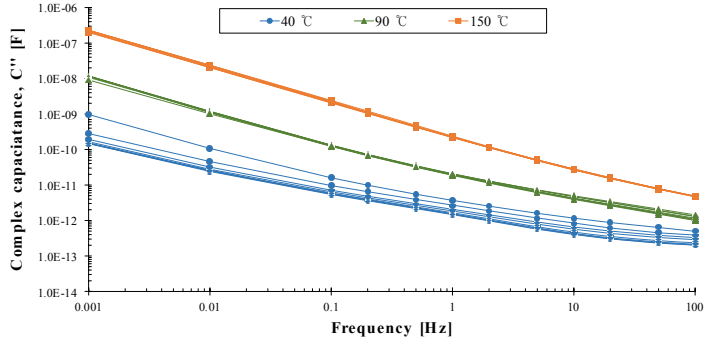

Figure 52. Complex capacitance C'' from measurements on Object S.

4.3.4 Comparison of measurement at 40 °C

Measurement on Object L

Two distinct measurement was performed at 40 °C, one before increasing the temperature to 150 °C and one after. A higher value is observed for the second measurement, i.e. after being subjected to higher temperatures. Field independence is found for both first and second run.

The difference between C' in the first and second run increases when decreasing the frequency (Figure 53). At the highest frequencies, values of the capacitances are both in the same range. When reaching the lowest frequencies, the capacitance in the second run have increased with one order of magnitude.

The value of the imaginary part C'' is found to be higher during the second run for all frequencies. The value is six times higher at 1 mHz, but only 1.15 times higher at 100 Hz.

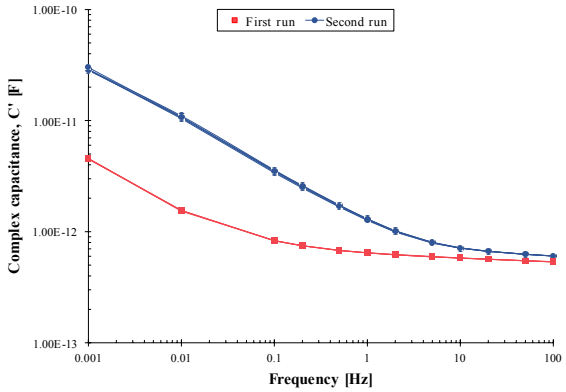

Figure 53. Real part of complex capacitance.

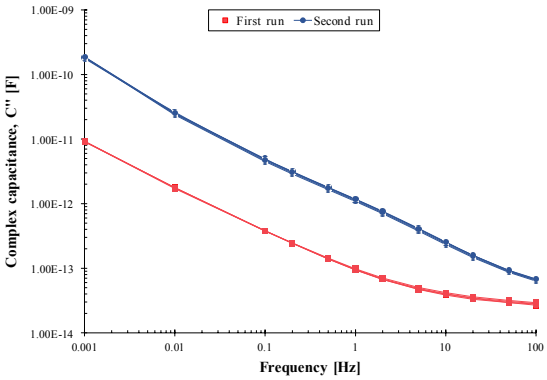

Figure 54. Imaginary part of the complex capacitance.

Values of the dielectric loss tangent are presented in Figure 55. Results show that the losses during the second run are higher than observed during the first run. The deviation changes over the frequency range, and the highest deviation is found around 1 Hz. Here the value is 6 times higher than found in the first run.

Figure 56 show the calculated conductivity for the whole frequency range. However, the material's conductivity will be most accurate if using values found at

the lowest frequency. Here, the losses in the object will dominated by the conductivity.

Results show that the conductivity increases after the test object has been subjected to high temperatures. At 1 mHz, the conductivity in the first run is found to be 33 pS/m. After being subjected to 150 ℃, the conductivity in the stress control tube increases to 680 pS/m.

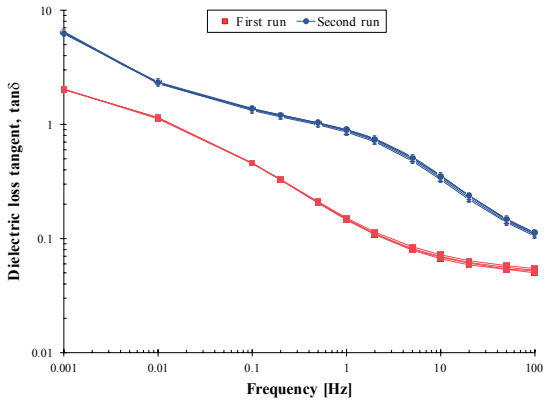

Figure 55. Dielectric loss tangent, for first and second measurement at 40 ℃.

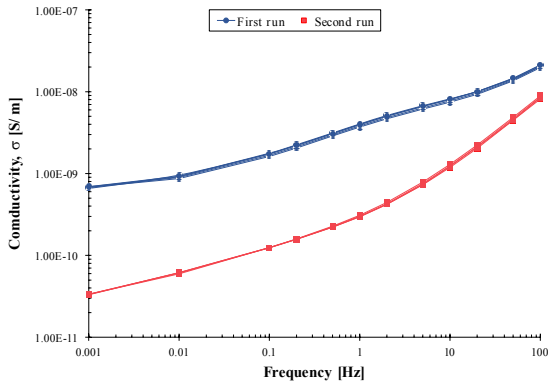

Figure 56. Conductivity, σ, for first and second measurement on Object L at 40 ℃.

Measurement on Object S

As for Object L, two distinct measurement was performed at 40 ℃, one before increasing the temperature to 150 ℃ and one afterwards. For the first measurement, the second run (0.625 and 1.0 kV/mm) provides higher values for the parameters. This is assumed to be caused by the two separate measurement and is disregarded in this analysis.

Comparison shows that the C' has a slightly higher value during the second measurement for frequencies below 2 Hz, while a lower value for frequencies above 5 Hz. In the range of 2 – 5 Hz, the value is approximately equal. The electric field dependence found during the first measurements is not present in the result from the second measurement. The imaginary part, C'', has a marginally larger value during the second measurement.

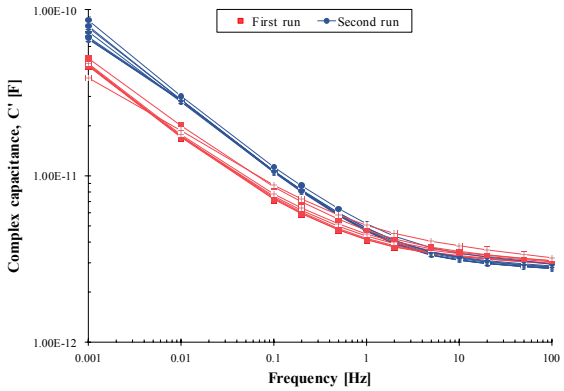

Figure 57. Real value of complex capacitance, C', for Object S at 40 °C.

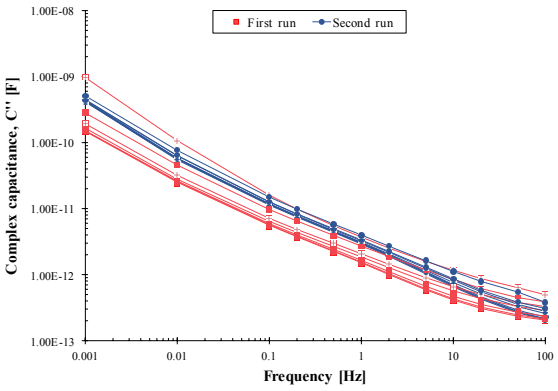

Figure 58. Imaginary part of the complex capacitance, C'', for Object S at 40 °C.

Figure 59 presents the dielectric loss tangent for the two measurements. The losses will have a minor increase in the second measurement for lowest frequencies. At frequencies higher than 10 Hz, the value of dielectric loss tangent will be in the same range.

The calculated conductivity is given by Figure 60 for the whole frequency range. The material's conductivity is determined at 1 mHz, and will be largest during the second run. The conductivity of the stress control tube will increases from 11 to 31 nS/m, after being subjected to 150 °C.

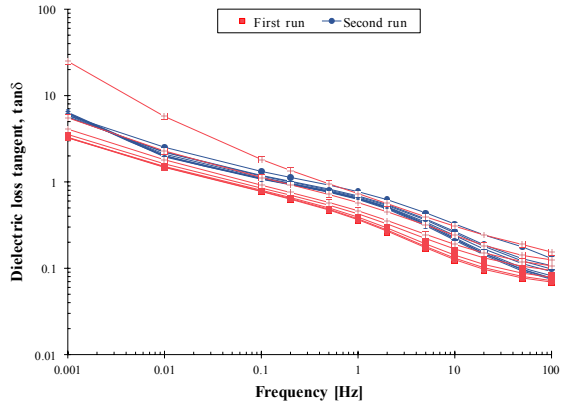

Figure 59. Dielectric loss tangent for Object S at 40 °C.

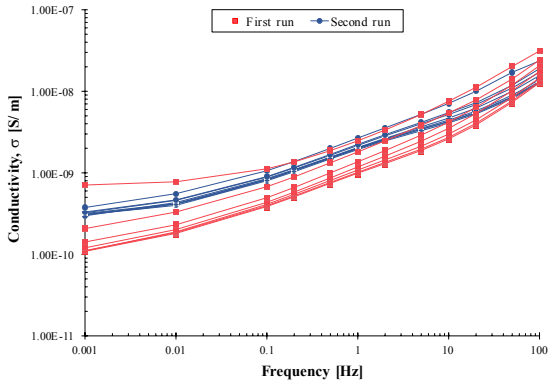

Figure 60. Conductivity, σ, for Object S at 40 °C.

4.3.5 Measurement at DSC temperatures

Result from DSC measurement on a partially shrunk sample of stress control tube show an endothermic melting peak at 104 ℃. DSC temperatures were found to be 94 ℃ (onset), 104 ℃ (melting peak) and 114 ℃ (after melting).

Dielectric response measurement was performed at these temperatures in order to examine if the phase transition in the material would change the electrical properties.

Measurement on Object L

Measurements are performed with electric field strength from 0.005–0.01 kV/mm. Dielectric response measurement was performed at frequencies from 100 Hz to 1 mHz.

Real part of the complex capacitance has approximately equal value, for all temperatures, at both 100 Hz and 1 mHz. The difference increases towards 0.5 Hz, while decreasing towards the ends (Figure 61).

For both the real and imaginary part, a minor electric field dependence is observed as the temperature increases. However, this dependency insignificant and is assumed neglected.

The imaginary part of the complex capacitance will for all temperatures increases with roughly the same rate, as the frequency is decreased.

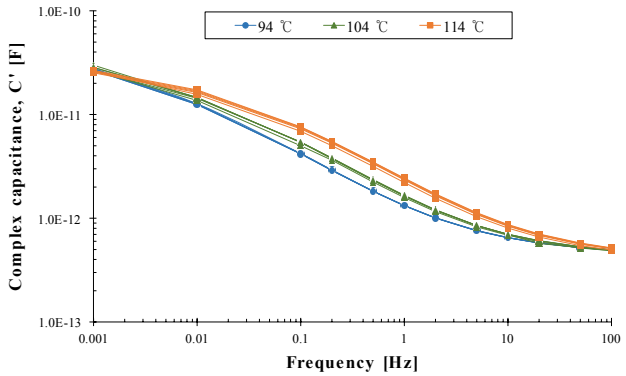

Figure 61. Real value of complex capacitance, C', at DSC temperatures.

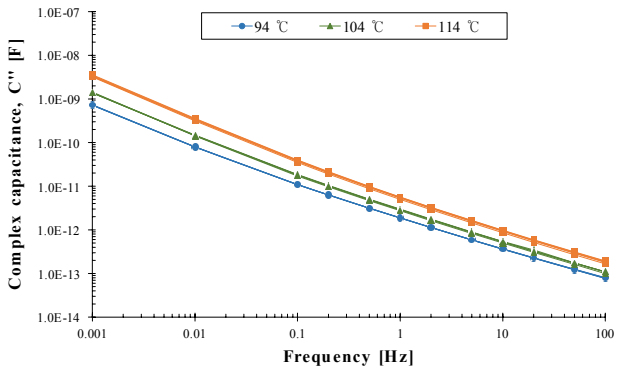

Figure 62. Imaginary part of the complex capacitance, C'', at DSC temperatures.

Dielectric loss tangent has a slight increase when increasing the temperature. All measurement has the same curved shape, and no field dependence is observed.

Calculation of the conductivity is performed and the result is presented in Figure 64. The material's conductivity is found at 1 mHz, is observed increasing when temperature is increased.

Field dependence is observed for measurement performed after melting transition of the material, i.e. at 114 ℃. The conductivity of the stress control tube is found increasing when the electric field strength is increased.

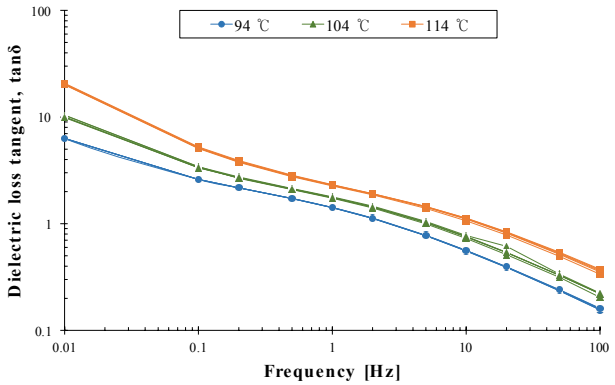

Figure 63. Dielectric loss tangent for Object L at DSC temperatures.

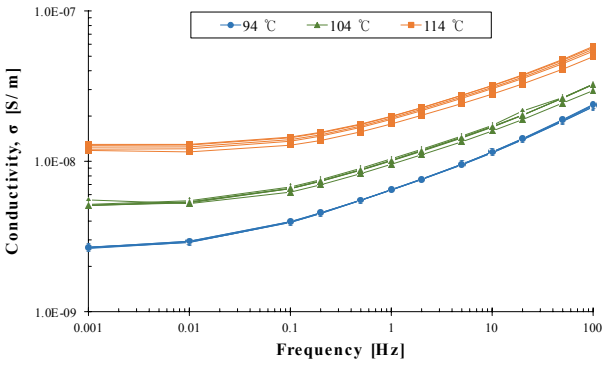

Figure 64. Calculated conductivity for Object L at DSC temperatures and all frequencies.

Measurements on Object S

Measurements on Object S is performed with electric field strength from 0.025 – 1.0 kV/mm with frequencies in the range of 100 Hz to 10 mHz. Frequency of 1 mHz was excluded, due to inaccuracies found when measuring at 40, 90 and 150 ℃.

Real part of the complex capacitance will increase when decreasing frequency or increasing the temperature. At 10 mHz, the value of the capacitance has a large spread as the accuracy is decreased. This is illustrated in Figure 65.

Field dependence is not observed for the measurements, however, a smaller value can be detected for the first measurement at 94 ℃.

The imaginary part of the conductivity will increase as frequency is decreased, and is observed for all temperatures. A minor field dependence is found at 50 Hz and 100 Hz, and is likely due to measurement at its exact value.

As observed for C', the first measurement at 94 ℃ have a slightly smaller value than found for higher electric fields. This might be caused by not reached a uniform temperature before dielectric measurement was performed.

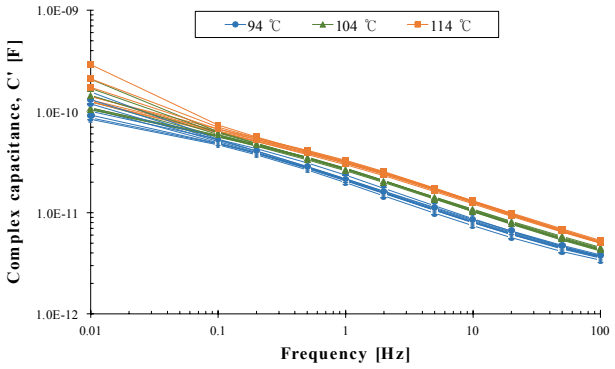

Figure 65. Real value of complex capacitance, C', at DSC temperatures.

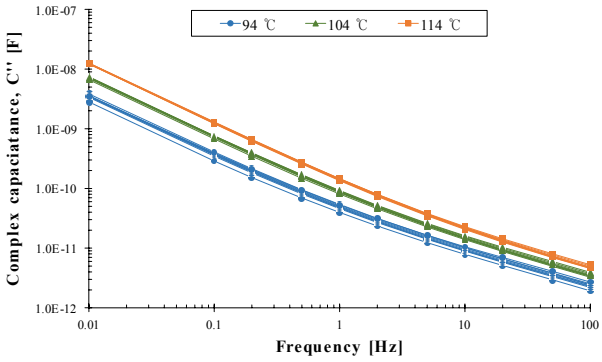

Figure 66. Imaginary part of the complex capacitance, C'', at DSC temperatures.

Observations presents that the dielectric loss tangent does not have a field dependency for frequencies below 100 mHz. When the frequency is decreased to 10 mHz, the values of $\tan\delta$ exceeds 10 and inaccuracy is observed. As for the complex capacitance, a lower value is observed for the first measurement at 94 °C.

An increase is observed in the conductivity of the stress control tube as temperature increases. However, the field dependency is observed with a minor increase when the temperature is decreased. This is opposite of what observed for Object L.

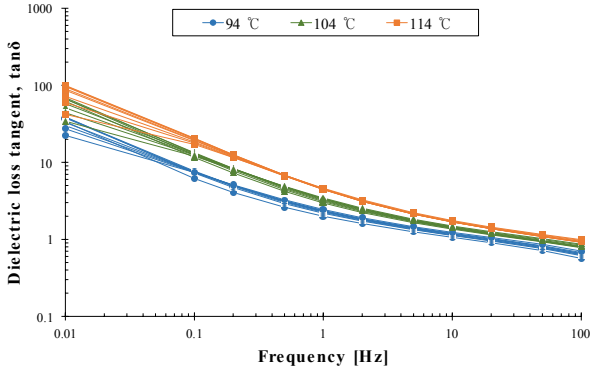

Figure 67. Dielectric loss tangent for Object L at DSC temperatures.

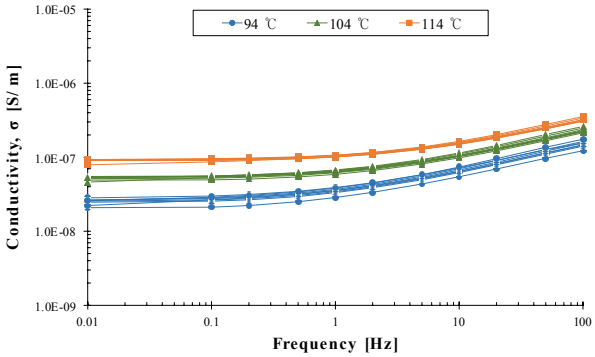

Figure 68. Calculated conductivity for Object L at DSC temperatures and all frequencies.

4.3.6 Conductivity

The conductivity of the test object can be calculated with the parameters found in dielectric spectroscopy measurements. The relationship between dielectric loss tangent, permittivity and conductivity is seen in Eq. 2.3, and can be rewritten as in Eq. 4.1.

$$\sigma \approx \tan\delta \cdot \omega\varepsilon'\varepsilon_0 \qquad \text{Eq. 4.1}$$

This equation is an approximation and will apply when the relation $|\varepsilon_r'| \gg |\varepsilon_r''|$ is fulfilled. At low frequencies, the losses in the test object will be dominated by the conductivity. Using this relation the conductivity of the stress control tube can be calculated when using $\tan\delta$ and ε' found at the lowest frequencies. A more detailed description for calculation of the conductivity can be found in Appendix D.

The value of PTFE's complex permittivity is in the calculations used as 2.1. During measurement of a PTFE rod, the complex permittivity was measured to have a value of 5. However, an increase from 2.1 to 5 will scarcely influence the result of the conductivity.

The percentage increase or decrease when changing relative permittivity from 2.1 to 5.0 is presented in Table 10. The prevalent change is observed for Object L with only a 2.85 % decrease when increasing the complex permittivity. Due to minor changes, this is considered as insignificant for this thesis.

Table 10. Percentage change in conductivity when increasing the complex permittivity from 2.1 to 5.0 in the calculations of conductivity.

	Object L	Object S
40 °C	-2.85 %	-1.64 %
90 °C	-0.83 %	-0.68 %
150 °C	+1.04 %	-0.72 %

Conductivity calculated for Object L

Calculation of the conductivity is performed for values obtained at 1 mHz. As the dielectric loss tangent can be assumed to have a good accuracy here.

Results show that the conductivity will increase linear with the temperature. The conductivity obtained at an electric field strength of 0.1 kV/mm is presented as a function of the temperature in Figure 69.

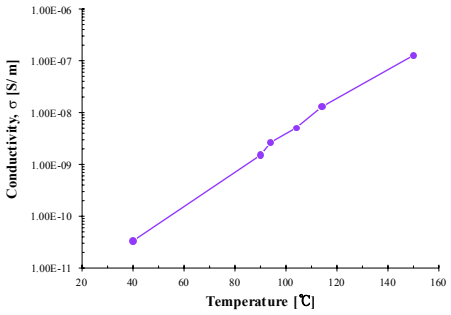

Figure 69. Conductivity obtained at an electric field strength of 0.1 kV/mm calculated at frequency of 1 mHz.

The transition phase at 94 ℃ – 114 ℃ does not indicate a change in the electrical properties of the material, as there is a linear increase in the conductivity.

From Figure 69, the conductivity is observed independent of the electric field in the field range from 0.005 kV/mm to 0.1 kV/mm.

A hysteresis effect is observed, as the conductivity has increased when performing the second measurement at 40 ℃. The conductivity will then be 20 times higher than during first measurement, however, only 2 timer less than the conductivity at 90 ℃.

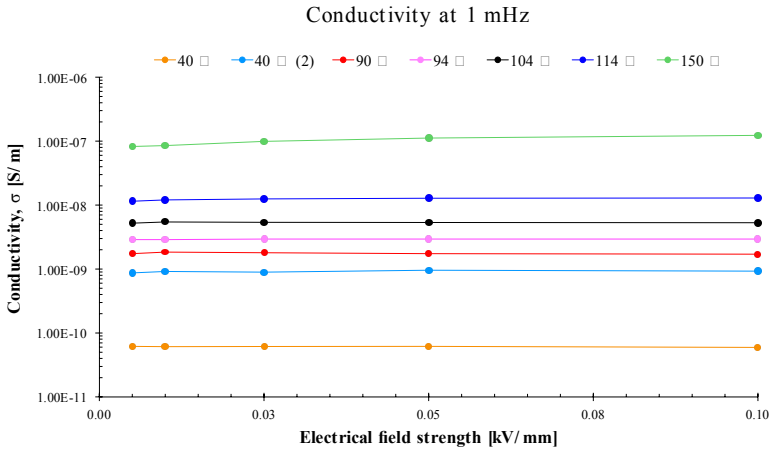

Figure 70. Conductivity calculated for Object L with values obtained at 1 mHz.

Conductivity calculated for Object S

The conductivity is calculated for values obtained at 10 mHz. Measurements at 1 mHz provided inaccurate values, while the accuracy is assumed to be good for the results gained at 10 mHz.

For Object L, i.e. low electric field strengths, the conductivity will increase linear with temperature. Figure 71 presents the conductivity obtained at an electric field strength of 1.0 kV/mm. The conductivity will no longer increase linearly with temperature.

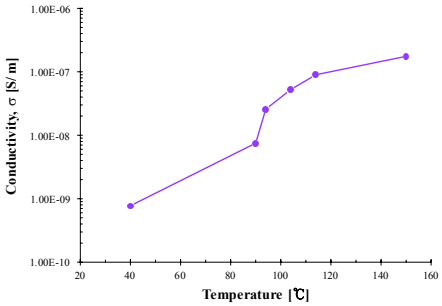

Figure 71. Conductivity obtained at an electric field strength of 0.1 kV/mm calculated at frequency of 1 mHz.

Observations made indicates that the transition phase at 94 ℃ – 114 ℃ will affect the conductivity. A larger increase discovered for the transition phase.

Figure 73 presents the conductivity for all temperatures as a function of the electric field applied. The figure indicates that the conductivity for Object S will be independent of the electric field for all measurements except the first measurement at 40 ℃. Here, a field dependence is observed for field strengths above 0.5 kV/mm.

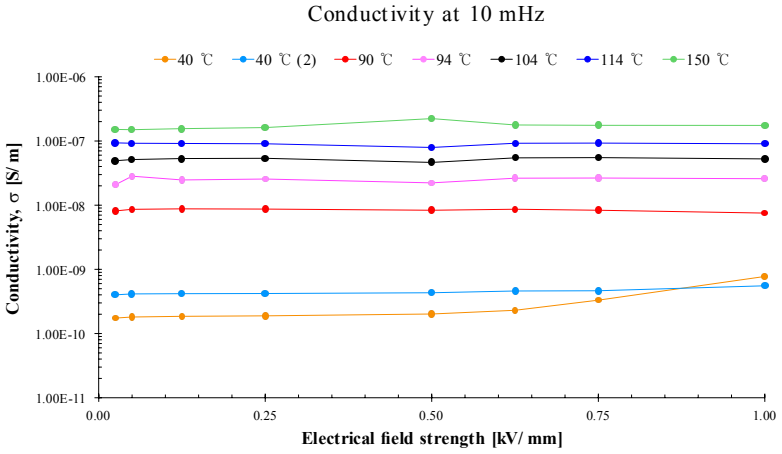

Figure 72. Conductivity calculated for Object S with values obtained at 10 mHz.

A hysteresis effect is also observed for Object S, with an increase in the conductivity after being exposed to 150 ℃. The conductivity will be 2.3 times larger during the second run, which is much smaller than found for Object L. A field dependence is observed for first measurement, which disappears during second measurement. This field dependence makes the conductivity at 1.0 kV/mm to have a higher value during the first than the second measurement.

Comparison of the conductivity from measurement in time domain and frequency domain

Time domain measurements on the object are performed in [1]. The same voltages are used in both measurements in order to make comparison possible.

Conductivity calculated from time domain (TD) measurements have a slightly smaller than the value calculated in frequency domain (FD). This is illustrated in Figure 73, where TD is presented with a dashed line and FD with a solid line.

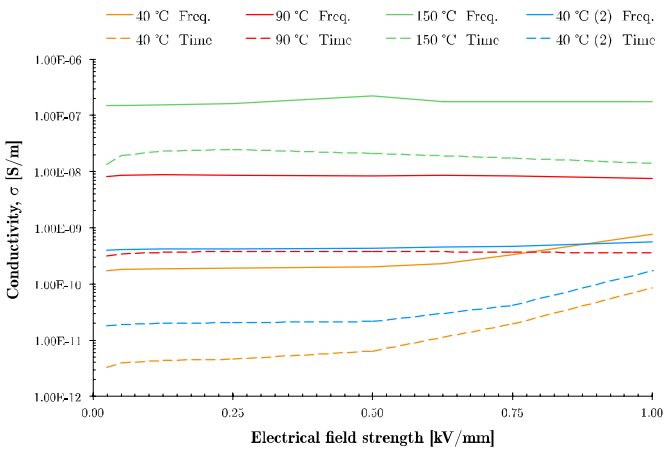

Figure 73. Conductivity as a function of the electric field strength for both frequency- and time domain analysis.

Both measurements at 40 ℃ (yellow lines) is observed having a field dependence for electric field strengths above 0.5 kV/mm. During the second measurement at 40 ℃ (blue lines), a field independence is observed for measurement in frequency domain while time domain remains field dependent.

Measurements performed at 90 ℃ and 150 ℃, will in both FD and TD be independent of the electric field strength.

Conductivity calculated at from measurement results at 10 mHz in FD have obtained a higher value than those calculated from polarisation and depolarisation currents in TD. This difference can be found to be in the range of one – two orders of magnitude.

For time domain analysis, space charge built-up is observed at high temperatures which can cause an inaccuracy of the calculated conductivity. This can be one reason why the values are deviating.

For frequency domain analysis, the relation $|\varepsilon_r'| \gg |\varepsilon_r''|$ is assumed to apply in most cases, and thus providing $\varepsilon_r' \approx \varepsilon_r$. For dielectric response on a stress control tube, the losses will be high causing the relation to be invalid.

The complex permittivity is calculated from the measured complex capacitance divided by the geometric capacitance of the stress control tube. The values obtained are presented in Figure 74 and Figure 75. From these, the imaginary part of the complex capacitance is found to be much larger than the real part at 10 mHz.

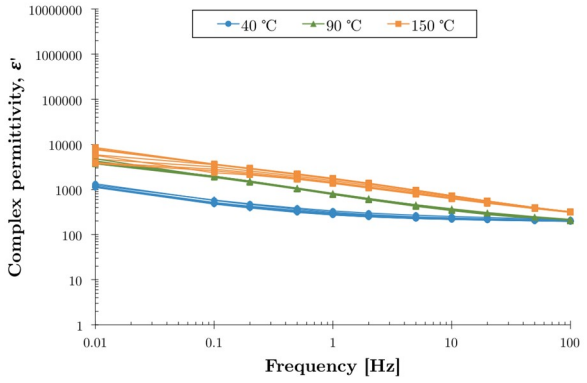

Figure 74. Complex permittivity, ε', for Object S.

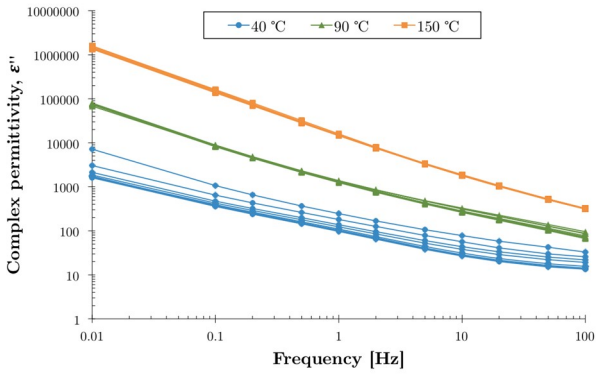

Figure 75. Complex permittivity, ε'', for Object S.

As a result, the conductivity should be calculated from Eq. 4.2 rather than Eq. 4.1. This will provide a reduced value of the conductivity.

$$\sigma = \omega \varepsilon' \varepsilon_0 \cdot \left(\tan \delta - \frac{\varepsilon_r''}{\varepsilon_r'} \right) \qquad \text{Eq. 4.2}$$

4.3.7 Measurement on wet object

In order to determine the effect of an increased humidity, the test object is placed in water for 39 days. Dielectric response measurement is performed on the test object, both before and after being immersed in water. Comparison can thus be performed to identify any changes by an increased humidity.

To lock the water inside the stress control tube, plastic foil and insulation tape is applied. Measurements are performed on a dry object in order to verify that such application will not have an appreciable effect on the results.

All results are given in Appendix C4.

Water content

As water uptake measurements indicate that none of the samples reaches saturation during the experimental work. Water content in the test object after being immersed for 39 days, is determined by using Figure 76. In order to use values from Figure 76, the cylindrical test object has approximated to be a plane plate to be comparable to the test samples.

The yellow curves is defined for samples of stress control tube being exposed to water at both sides ($s = h$). However, when immersing the test object, only one side is exposed ($s = 2h$). Using the cohesion yield in Eq. 2.31, the time required to reach the same concentration is dependent on s^2. This will provide a concentration in the test object that is a quarter of what found during water uptake measurements.

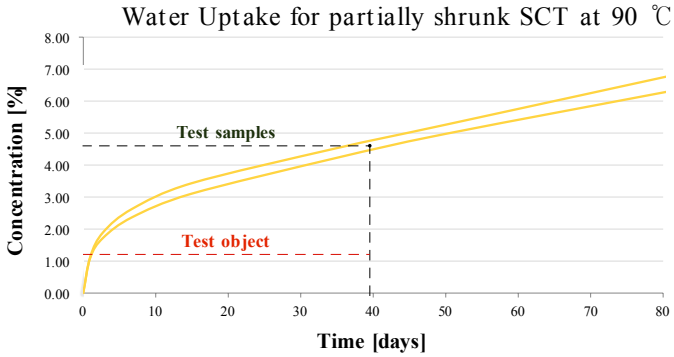

Figure 76. Determination of water uptake for partially shrunk samples. After 39 days, the concentration in the test samples will be approximately 4.6 % and 1.15 % for the test object.

From Figure 76 the water concentration in the samples is found to be approximately 4.6 % after 39 days. Consequently providing a water concentration in the test object of 1.15 % if only exposed at one side. However, as the stress control tube provides a watertight design, water will be present at both sides. The test object can thereby be assumed to have a higher water content after 39 days.

Effect of plastic foil and PVC insulation tape

Measurements indicate that application of a plastic foil and PVC insulation tape will not have a considerable effect on the results. As they have a resistive value much larger than the stress control tube, a marginal current will flow through the plastic foil and insulation tape.

Comparison of dielectric loss tangent and conductivity is presented in Figure 77 and Figure 78. For both parameters, a reduced field dependence is observed for test object with plastic foil and PVC insulation tape. At the highest frequencies the values is approximately identical, while the values will have a minor deviation at the lowest frequencies.

The effect of application of plastic foil and PVC insulation tape is regarded as insignificant and is thus neglected.

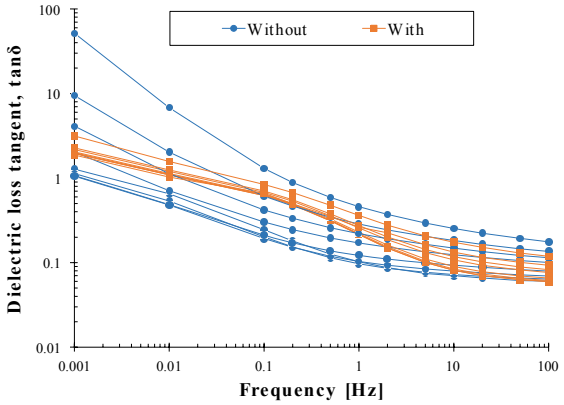

Figure 77. Dielectric loss tangent for test object with and without application of plastic foil and insulation tape.

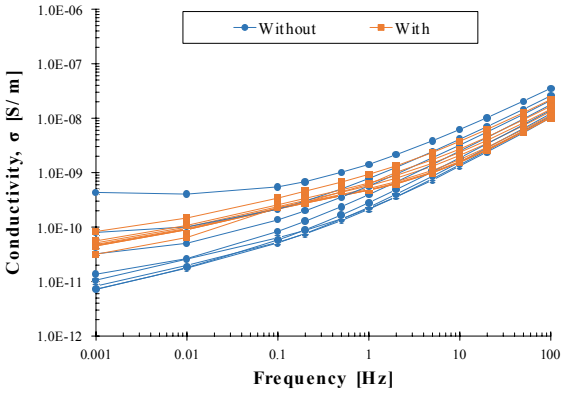

Figure 78. Conductivity for test object with and without application of plastic foil and insulation tape.

Effect of an increased humidity

After being immersed in water for 39 days, the conductivity will have a significant increase. This is illustrated in Figure 79 and Figure 80.

Measurements on a dry test object at 20 °C show a field dependence, where the conductivity increases when the applied field is increased. A field dependence is also observed for the wet test object, this will thus decrease with an increasing electric field strength. The decrease in conductivity is likely due to water diffuse out of the material during the measurements. Additionally, the large currents can cause an increased heat generation that can contribute to drying the object.

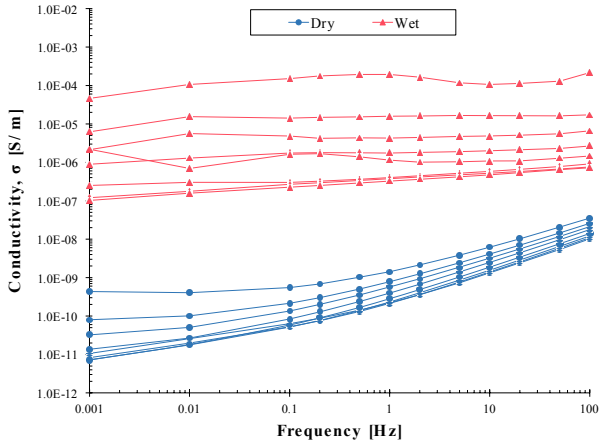

Figure 79. Conductivity for a wet and dry test object calculated for all frequencies.

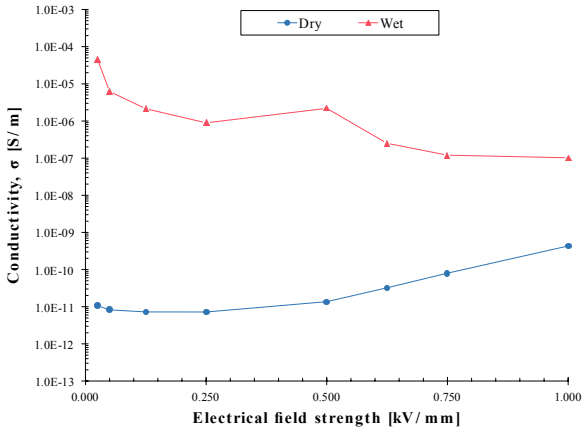

Figure 80. Conductivity for wet and dry test object as a function of electric field strength at 1 mHz.

Conductivity at 1 mHz with an electric field of 0.025 kV/mm is found to be 10.6 pS/m for a dry test object, while increasing to 46 µS/m in wet condition. This provides an increase of almost six orders of magnitude.

An increase of six orders of magnitude can also be observed for the complex capacitances at 1 mHz and 0.025 kV/mm. C' increases from 11.7 pF to 17.2 µF, while C'' will have an increase from 15 pF to 62.6 µF.

Values of the dielectric loss tangent for a dry test object are found to have an electric field dependence from 0.5 kV/mm. Furthermore, the value will increase as the frequency is decreased.

An electric field dependence can also be observed for the wet test object. This is, as found for the conductivity, decreasing with increasing field strength, i.e. with longer expose time with atmospheric conditions. It can then be assumed that the decrease in water content influences the results, providing a decrease in dielectric loss tangent.

Frequency dependence can be observed for the two first measurements, i.e. 0.025 and 0.05 kV/mm. This dependence will decrease when the electric field strength is increased, and a minor frequency dependence can thereby be observed for the highest electric field strengths.

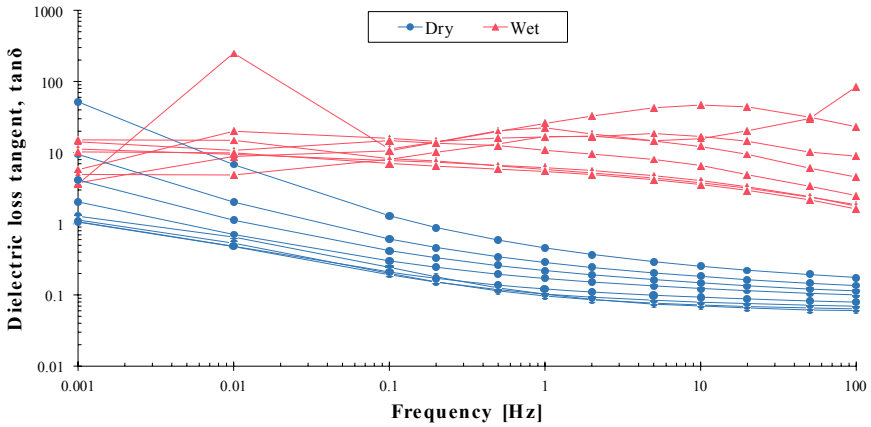

Figure 81. Dielectric loss tangent for a dry and wet test object.

Chapter 5

5 Discussion

5.1 Diffusion

Water saturation of the samples has not been reached during the experimental work of this thesis. A deviation from the Fickian diffusion can be observed as the water uptake follows two distinct phase of diffusion. This is likely caused by a diffusion by the filling materials within the stress control tube. As two phase diffusion is observed, the diffusion coefficient cannot easily be determined by curve fitting. The time required to achieve 99.9 % saturation content have therefore not been determined in this thesis.

The highest water concentration is found for samples kept immersed in water at 90 °C. The free volume in the material will increase with temperature, providing an increased ability to absorb water. After 85 days, the concentration in the samples will be: 7 % (virgin), 6.5 % (partially shrunk) and 5.3 % (fully shrunk). These values are significant, and they all appear to still be increasing.

The water uptake is found to be dependent of the degree of shrinkage. The highest water concentration is found for virgin samples, while the lowest is observed for fully shrunk samples. As the stress control tube is expanded, the free volume will increase. During heated the tube will shrink, causing a decrease in the free volume and potential to absorb water.

When stress control tubes are applied to cable sections, the cross-section of the cable should be close to the stress control tube's fully shrunk diameter. This will reduce the stress control tube's ability to diffuse water.

For wet constructions of XLPE cables, water can be present during service. If the stress control tube is being exposed to an increased humidity for a long time

period, its electrical properties could be expected to start change which eventually could lead to a failure.

5.2 Differential scanning calorimetry

The stress control tube has a phase transition for temperatures below 150 ℃. An endothermic thermal transition is observed in the temperature range of 94 ℃ to 114 ℃, with a maximum melting temperature at 104 ℃.

Local peaks are observed during first measurement on virgin and partially shrunk samples, located at a temperature of 80 ℃. These peaks will disappears during second measurement and are not observed for fully shrunk samples. The local peaks thus assumed to be caused by incomplete shrinking.

The phase transition provides the stress control tube to experience changes from a semi-crystalline to an amorphous state. The semi-crystalline–amorphous interfaces can act like carrier traps. If these regions are heated up to their melting point, these regions can gradually disappear and release these trapped carriers. This will make the material more electrically conductive, increasing the conductivity. [35]

When performing dielectric response measurements on Object S, this can be observed as an increase in conductivity when reaching the thermal transition temperatures. The increased conductivity will be independent of the electric field strength applied. Conversely, an increased conductivity is not observed at lower field strengths for Object L. Here, the conductivity will have a linear increase with temperature.

Thermal transition located slightly above the rated temperature of XLPE cables, causing the conductivity to increase at high electric field strengths. In situation where to have an overload, the temperature for the XLPE cable section can be assumed to increase beyond its rated value. If this endures for a long time period, the electrical properties of the stress control tube can experience an increased conductivity which contributes to an increasing heat generation in the tube. However, as the increase in conductivity is minor, this is not assumed to be causing critical conditions.

5.3 Dielectric spectroscopy

Dielectric loss tangent

Results from dielectric spectroscopy imply that the stress control tube has a high dielectric loss tangent. Values are found to be in the range from 0.1 to 1000, however, large dispersion is observed when reaching at the highest values. This is likely caused by the limit in the measuring range of IDA 200, providing inaccurate results. The electric field dependence observed at the lowest frequencies is thereby assumed to be caused by this inaccuracy.

The effect of the PTFE rod is neglected as the value is below 0.01 for all temperatures, providing a minor influence on the main results. In addition, the object will not observe considerable changes when applying plastic foil and PVC insulation tape. As the resistivity of these is much higher than for the stress control tube, only an insignificant part of the leakage current will in flow there. The test object's configuration can thus be assumed to provide the electrical properties of the stress control tube alone.

Dielectric loss tangent is found to have an electric field dependence at low temperatures. For 40 ℃, this is observed for electric field strengths above 0.5 kV/mm. This dependence cannot be observed for measurements at higher temperatures, and when performing the second measurement after being cooled from 150 ℃.

As proposed in [1], the higher values during the second run is likely caused by desperation of volatiles in the stress control tube. Thermogravimetric measurements have been performed on samples of stress control tube. The result indicates that the weight of the sample is reduced after being exposed 150 ℃ for two hours. Analysis imply that stress control tube will have a desorption of volatile substances at high temperatures, which caused the material to be more conductive [1]. Another explanation suggests have been that the semi-crystalline content in the stress control tube changes after cooling from 150 ℃ to 40 ℃ [1,36]. As the material becomes more conductive, this will explain the increased dielectric loss tangent observed after exposed to temperatures up to 150 ℃.

Increasing the temperature will reduce the relaxation time constant, which causes the local peak in the dielectric loss tangent to appear at a higher frequency. This can provide different shapes of the dielectric loss tangent when changing the temperature.

Complex capacitance

Complex capacitance is found increasing with decaying frequency. The real part, C', will experience a smaller increase than the imaginary part. The value will also be independent of the electric field. The deviations observed is likely caused by inaccuracy and the malfunction caused by a deformation in the current. The imaginary part, C'', obtains a higher value with decreasing frequency as the conductivity causes increasing losses.

The electric field dependence observed for $\tan\delta$ at 40 °C, is also to be seen for C''. This is likely caused by a field dependence in the conductivity, causing increased losses at higher electric field strengths.

Conductivity

The conductivity is calculated at values obtained 1 mHz (Object L) and 10 mHz (Object S). The conductivity is found independent of field for electric field strengths up to 0.5 kV/mm. This field dependence is also observed during measurement in time domain [1]. Increasing the field strength will provide an electric field dependence for measurements at low temperatures, while stay independent at the higher temperature.

The conductivity is dependent on the temperature as the charge carries will observe an increased mobility providing a higher drift velocity. For lower temperatures, the drift velocity will be more dependent of the electric field strength. This can imply why an electric field dependence observed during measurements at 40 °C.

The conductivity will have an increased conductivity when reaching the phase transition. As earlier stated, this can be caused by a transition from semi-crystalline to amorphous state, causing the material to have an increased electrical conductivity. This is observed even at temperatures slightly above the rated temperature for XLPE cables.

After being subjected to high temperatures, the conductivity of the material has increased. By compare both measurements at 40 ℃, the conductivity have increased with a factor of 20 for Object L and 2.3 times for Object S. The deviation in the increase can be caused by the hours exposed to high temperatures. Longer exposure time at high temperatures will increase the desorption of the volatiles in the stress control tube, which causes the material to become more conductive.

Comparing the values found in time and frequency domain, a higher value is observed for the conductivity obtained from the frequency domain. This can be caused by the fact that the relation $|\varepsilon_r'| \gg |\varepsilon_r''|$ will not apply for the stress control tube in the frequency range of 100 Hz to 1 mHz. As the calculation requires this relation to apply, the conductivity can obtain a higher value than intended.

The values obtained from time domain will at higher temperatures experience space charge build-up causing the polarization current to still be decreasing. This provides inaccuracy in the measurements. [1]

Having an increased humidity of the test object, the stress control tube's conductivity will experience a significant increase from 10^{-11} to 10^{-5} S/m for measurements performed at 20 ℃. This increase was observed even though the test object had not reached its saturation level. The water will provide a substantial increase in the charge carriers, which increases the conductivity of the stress control material.

Closer examination of the stress control tube imply that the increased conductivity have caused high heat dissipation at the interface between the electrode and PTFE rod. Signs indicate that water have been accumulated at the interface, however, no signs was found indicating tracking between the electrodes.

The high conductivity will provide a higher current passing through the stress control tube, providing an increased ohmic loss. This ohmic loss will provide heat generation increasing the temperature, which in turn causes the conductivity to increase further, i.e. thermal runaway. If the conductivity becomes too high, the system can suffer from a thermal breakdown.

The temperature increases, the heat will cause the tube to diffuse water and dry up. However, if the design avoids the water to diffuse out of the system, the increased temperature can cause the water to condense and be trapped in the interface between the stress control tube and joint or XLPE-cable.

As implied by [1], the stress control tube can be limited to only cover critical parts of the system with no connection between the insulation screen and conduction, i.e. no connection between ground and high voltage potential. In such configurations, the increased conductivity can cause critical enhancement at the edge of the stress control tube. This can increase the partial discharges leading to lower breakdown strength and damage the insulation, and possibly result in a premature failure in the cable system.

5.4 Sources of errors

1. Exceeding the measuring range of IDA 200

The measuring range of IDA 200 is limited to 0 – 10. This causes a deviation in the measured values causing a field dependence. This dependence can thereby be caused by IDA 200 and not the material.

2. Deformation in the current

As the electric field strength increases above 0.75 kV/mm, current spikes are observed when performing measurements at 40 ℃. These can be caused by discharges, and is observed both at the positive and negative half-cycle.

Additionally, as the frequency decreases, the current's shape will experience a deformation caused by harmonic content in the current. This deformation will increase when the frequency decreases, as the conductivity becomes more dominating.

The current spikes may have caused an inaccuracy, providing a higher value than expected. At higher temperature, these will not be present.

3. Improper water preservation

Paper foil and insulation tape is used in order to avoid the water diffuse out during measurements. Observations made indicate that the material will diffuse water during measurement, proving a field dependence where the values decrease with increasing field strength.

4. Calculation of the conductivity

The conductivity is calculated with a formula that requires $|\varepsilon_r'| \gg |\varepsilon_r''|$ to apply. Measurements suggest that this does not apply for this experiment, which can cause the calculated conductivity to be larger than that originally.

Chapter 6

6 Conclusion

From experimental work in the laboratory, the dielectric loss tangent is found to be significant when reaching lower frequencies caused by the conductivity.

Measurement results imply that the conductivity of the stress control tube will be dependent on the temperature, providing a larger conductivity as the temperature is increased.

A field dependence is observed for the conductivity at 40 ℃. This dependence is identified for electric field strengths above 0.5 kV/mm. For higher temperatures, the conductivity becomes independent of the temperature.

The stress control tube will not have a reversible change from highly conductive to resistive state. After being exposed to a temperature of 150 ℃, the material's conductivity will increase. This implies that the electrical properties of the stress control tube experiences changes in the electrical properties after exposed to high temperatures.

Measurements show that the stress control tube have phase transition on the temperature range of 94 ℃ to 114 ℃. When heating the material to its endothermic transition temperature, the conductivity will experience an increase.

When increasing the humidity, the conductivity experiences a significant increase of almost six orders of magnitude. This implies that the conductivity is strongly dependent on the humidity level.

From the experimental work, changes in the temperature and electrical field strengths performed on a dry test object will not cause any critical changes. The hysteresis effects found in the stress control tube provide a small increase in the conductivity, after exposed to high temperatures for a short time. A minor effect is also observed by the thermal transition phase of the stress control tube.

However, when increasing the humidity level of the test object, the conductivity experienced a significant increase. With an increase of six order of magnitude, such currents can causes critical changes. An increased heat generation can cause the material to suffer from a thermal breakdown.

If the stress control tube is limited to cover parts of the cable system, the increased conductivity can cause critical field enhancement at the edge of the stress control tube which can lead to a breakdown.

6.1 Further work

This master thesis has examined the effect of an increased temperature, electrical field strength and humidity level. Both increased temperature and electrical field strengths did not cause critical changes, while the increased humidity provided significant changes.

Measurement performed on the wet test object indicated that the plastic foil and PVC insulation tape did not provide a sufficient protection against the water diffuse out of the object. In addition, rust was observed at both electrodes. Further work should improve the test object and test setup, avoiding diffusion and rust. If such is achieved, the wet stress control tube can be examined for electric field dependence.

Another interesting situation is to determine how a wet stress control tube will be influenced when increasing the temperature, as this experiment is performed at 20 ℃.

7 Bibliography

[1] Henrik Enoksen, Sverre Hvidsten, Mai-Linn Sanden, and Frank Mauseth, "Temperature and Electric Field Dependence of the Time Domain Dielectric Response of a Medium Voltage Cable Joint Stress Control Sleeve," SINTEF Energy Research and Norwegian University of Science and Technology, Trondheim, 2015.

[2] Walter S. Zaengl, "Dielectric spectroscopy in time and frequency domain for HV power equipment. I. Theoretical considerations," *Electrical Insulation Magazine, IEEE*, vol. 19, no. 5, pp. 5-19, 2003.

[3] Sverre Hvidsten, "Condition assessment of XLPE cable systems installed in the 1980s," 2011.

[4] Erling Ildstad, *TET 4195 High voltage Equipment – Cable Technology*. Trondheim.

[5] Erling Ildstad, *High Voltage Insulation Materials, TET4160.*: Akademika forlag, 2014.

[6] H Faremo, J.T. Benjaminsen, P.B. Larsen, and A. Tunheim, "Service Experience for XLPE Cables Installed in Norway - From Graphite Painted Insulation Screens to Axially and Radially Water Tight Cable Constructions," 1997.

[7] G. Bahder. (1984) Electrical cable joint structure and method of manufacture. [Online]. http://www.google.com/patents/US4487994

[8] N.H. Malik, A.A. Al-Arainy. , M. I. Qureshi, and F. R. Pazheri, "Calculation of Electric Field Distribution at High Voltage Cable Terminations," in *High Voltage Engineering and Application (ICHVE), 2010 International Conference on*, October 2010, pp. 24 - 27.

[9] Hampool Enterprise. Medium Voltage tubing & Tape. Heat Shrinkable stress-control tubing. [Online]. http://www.hampool.com/En/ProductView.asp?ID=34

[10] T. Christen, L. Donzel, F. Greuter, and Switzerland Corp. Res., ABB Switzerland, Baden-Dättwil, "Nonlinear resistive electric field grading part 1: Theory and simulation," *Electrical Insulation Magazine*, vol. 26, no. 6, pp. 47 - 59, 2010.

[11] Eva Mårtensson, "Modelling electrical properties of composite materials," Department of Electrical Engineering, Kungl Tekniska Högskolan, Stockholm, PhD 2003.

[12] X. Qi, Z. Zheng, and S. Boggs, "Engineering with nonlinear dielectrics," *Electrical Insulation Magazine*, vol. 20, no. 6, pp. 27 - 34, 2004.

[13] Steven Boggs and Joe Yingneng Zhou, "Dielectric Property Measurement of Nonlinear Grading Materials," in *Electrical Insulation and Dielectric Phenomena, 2000 Annual Report Conference on*, vol. 2, 2000, pp. 764 - 767.

[14] J.W. Hoffman, "Insulation enhancement with heat-shrinkable components," *Electrical Insulation Magazine*, vol. 7, no. 2, pp. 33-38, 1991.

[15] Lise Donzel, Felix Greuter, and Thomas Christen, "Nonlinear Resistive Electric Field Grading Part 2: Materials and Applications," *Electrical Insulation Magazine*, vol. 27, no. 2, pp. 18 - 29.

[16] Philip Hofmann, Plane plate capacitor.

[17] Oral Büyüköztürk, Tzu-Yang Yu, and Jose Alberto Ortega, "A methodology for determining complex permittivity of construction materials based on transmission-only coherent, wide-bandwidth free-space measurements," vol. 28, no. 4, pp. 349-359, April 2006.

[18] N. A. M. Jamail, M. A. M. Piah, and N. A. Muhamad, "Comparative Study on Conductivity Using Polarization and Depolarization Current (PDC) Test," 2012.

[19] H.Faremo, J.T.Benjaminsen and E.Ildstad S. Hvidsten, "Condition Assessment of Water Treed Service Aged XLPE Cables by Dielectric Response Measurements," *CIGRE Session 2000*, vol. 21-201, pp. 1-8, August 2000.

[20] Y. Fieldman et al., "Time domain dielectric spectroscopy: An advanced measuring system," *REVIEW OF SCIENTIFIC INSTRUMENTS*, vol. 67, no. 9, pp. 3208-3216, SEP 1996.

[21] A. K. Jonscher, "Dielectric Relaxation in Solids," *Chelsea Dielectric Press. London.*, 1983.

[22] Sverre Hvidsten, "ELK-30: Condition Assessment of High Voltage Apparatus. Power Cables: Dielectric response - General description and applied on cables," 2014.

[23] P. Werelius, R. Thärning, R. Eriksson, B. Holmgren, and U. Gäfvert, "Dielectric spectroscopy for diagnosis of water tree deterioration in XLPE cables," *Dielectrics and Electrical Insulation, IEEE Transactions on*, vol. 8, no. 1, pp. 27-42, 2001.

[24] Frank Mauseth, Knut Dahle Hammervoll, and Sverre Hvidsten, "Dielectric Properties of Service Aged Medium Voltage XLPE Cable Joints," *Solid Dielectrics (ICSD), 2010 10th IEEE International Conference on*, pp. 1-4, 2010.

[25] A. K. Jonscher, "Dielectric Relaxation in Solids," 1999.

[26] Anders Helgeson, "Analysis of Dielectric Response Measurement Methods and Dielectric Properties of Resin-Rich Insulation During Processing ," Department of Electric Power Engineering, KTH, 2000.

[27] Daniel Gotz, Hubert Schlapp, and Hein Putter, "Dielectric loss measurement of power cables using hamon approximation," SebaKMT, 2011.

[28] Bruce Duncan, Jeannie Urquhart, and Simon Roberts, "Review of Measurement and Modelling of Permeation and Diffusion in Polymers ," NPL report DEPC-MPR 2005.

[29] M.H. Klopffer and B. Flaconnèche, "Transport Properties of Gases in Polymers: Bibliographic Review," *Oil & Gas Science and Technology*, vol. 56, no. 3, pp. 223-244 , 2001.

[30] Chi-Hung Shen and George S. Springer, "Moisture Absorption and Desorption of Composite Materials ," Department of Mechanical Engineering , The University of Michigan, 1975.

[31] Mettler Toledo. (2013) Mettler Toledo. [Online]. http://us.mt.com/dam/Analytical/ThermalAnalysi/TA-PDF/51724550C_V09.13_TA_Komp_Bro_e.pdf

[32] Mai-Linn Sanden, "Condition Assessment of Medium Voltage Cable Joints," Department of Electric Power Engineering, Norwegian University of Science and Technology, Trondheim, Specialization project 2014.

[33] Programma Electric AB, "User's manual for Insulation Diagnostic System IDA 200," Sweden, 2002.

[34] GE Energy Service. Insulation Diagnostics System, IDA 200.

[35] S. Pélissou, H. St-Onge, and M.R. Wertheimer, "Electrical conduction of polyethylene below and above its melting point," vol. 23, no. 3, pp. 325-333, 1988.

[36] G. Teyssedre and C. Laurent, "Charge Transport Modelling in Insulation Polymeres: From Molecular to Macroscopic scale," vol. 12, no. 5, pp. 857-875.

[37] James E. Mark, *Polymer Data Handbook*, 2nd ed. Oxford: Oxford University Press.

Appendices

Appendix A – Diffusion

A1 – Test procedure for Mass Uptake Measurement

The test procedure was followed point by point to limit the time in which the tube was out of the water container. By following the same procedure for each measurement, there will be formed a basis for comparison. The procedure is followed in 10 steps.

Preparation of equipment in advance of the experiment

1) The tube was cut into thin pieces that hold a weight of less than two grams. Figure 82 illustrates the preferable geometry of the test specimen. The size of *n* and *l* should be much larger than *h*, resulting in a dominating diffusion through the *nl* –surface. The diffusion is then considered to have one-dimensional conditions, $D(t) = D_x(t)$.

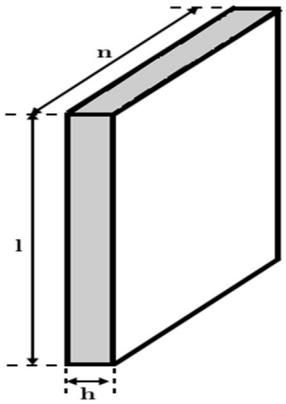

Figure 82: Geometry of test specimen.

2) To achieve a completely dry specimen, the stress control tubes are put in a vacuum drying oven for a week at 70 degrees. 12 hours before measurement of the dry weight, the temperature in the desiccator is decreased to 25 degrees.

3) All the equipment is cleaned with isopropanol to avoid particles and impurities to attach to the specimen and influence the measurement result.

4) Three glass containers should be cleaned and filled with distillate water and placed under different temperatures.
   i. One glass is preheated to the given test temperature in advance of the experiment. This should be used for the specimen to be fully immersed.

   ii. One glass is placed in the refrigerator. Cold distillate water is used to rapidly cool the specimen down to remove convectional currents on the specimen.

   iii. One glass should be kept at room temperature. The specimen is placed in this container for couple of seconds to decrease its temperature. It should hold approximately the same temperature, thus giving a better comparable value.

5) Mettler Toledo UMX2 is internally calibrated, and preformed automatically by the gauge. Both the temperature and humidity of the environment is considered when calibrating. This should be performed when the time since last measurement becomes significant large.

6) Static charges in the surface of the test specimen are removed by moving it a few times through an electrostatic precipitator. The static charge built up on the surface will attract dust and by moving it through the precipitator, the dust can be removed. The cancel of the charge should be performed before placement on the weigh gauge.

Mass Uptake Measurement

7) The specimen is taken out of the desiccator and immediately placed in UMX2 for measurement. The date, time and dry-weight should be noted before placing the object in the water container.

8) The container with test specimen is placed in a heating cabinet exposed to a constant temperature. The specimen should at all time be entirely immersed in the distillate water.

9) The moist material should be continuously measured. Typically, diffusion characteristic has a higher water uptake in the beginning, but as time pass, the weight will approach the saturated value M_m. A test measurement is executed to determine the suitable period between each measurement.

10) For each measurement, the following procedure is carried out.
    i. Equipment and working area are cleaned with isopropanol before the test specimen is taken out. This to avoid impurities.
    ii. Two glass containers with respectively cold water (4 ℃) and room temperate water (□ 25 ℃) as well as paper sheets are made ready.
    iii. The specimen is taken out of the water container at test temperature and immediately placed in the cold water.
    iv. The measurement program is started with a delay of one minute. This gives a minute to prepare the object before an automatically measurement is performed and saved in an Excel sheet.
    v. The specimen in then placed in the room temperate water for a couple of seconds before its surface is dried with paper sheets. The first paper sheet wipes away the largest part of the water. A second paper sheet is used for making sure that the object does not have water left on its surface.
    vi. For removal of the surface charge, the specimen is moved a couple of times through the electrostatic precipitator.

vii. The specimen is placed on the UMX2 for measurement. The date, time and weight is saved in an excel document when the delay has reached one minute. The specimen is then placed back in the water container.

11) The measurements are plotted as the water uptake (in percentage of the total weight) versus the time. The curve will then give the characteristic of the diffusion, and thus giving the possibility to proceed tentatively to find the diffusion constant, D_x.

The tests are repeated for each test specimen at the different experimental temperatures.

A2 – Curves for diffusion

One sample at each degree of shrinkage is shown in the figure for water uptake at 30 ℃. The curves for the water uptake are not reaching saturation within 110 days.

The virgin sample has the highest water uptake, with a concentration of 1.2 % after 110 days. The partially and fully shrunk sample has both a lower value, with 0.92 % and 0.85% respectively. This provides an increase in water uptake as the degree of shrinkage decreases.

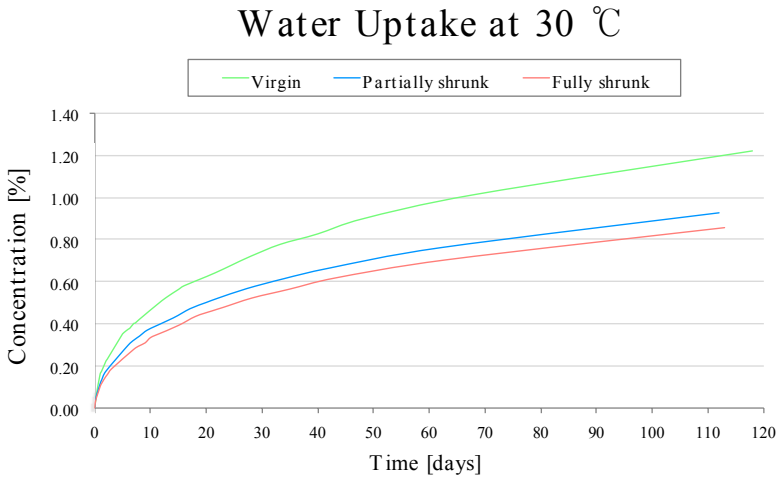

Figure 83. Water uptake at 30 ℃. One sample at each degree of shrinkage is shown in the figure.

Results from measurement at 60 ℃ have a similar shape as found for 30 ℃, but with a higher level of concentration. Saturation is not reached for any of the samples after 95 days.

The highest degree of water uptake is still found for the virgin sample, and the lowest is found for the fully shrunk sample. Water uptake by the partially shrunk sample is found to be approximately the mean value of the result from virgin and fully shrunk samples.

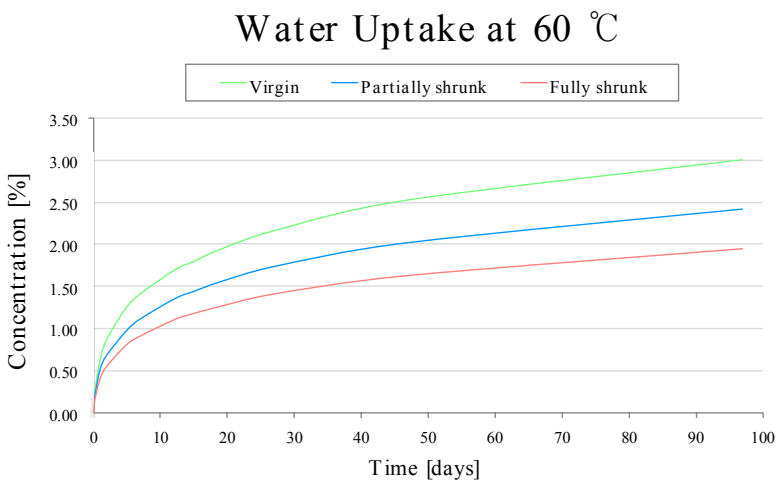

Figure 84. Water uptake at 60 ℃. One sample at each degree of shrinkage is shown in the figure.

Measurement at 90 ℃ shows a linear increase after 10 days, and saturation is not reached. As for 30 and 60 ℃, the water uptake increases with a decreasing degree of shrinkage.

For a virgin sample kept at 90 ℃, the water uptake after 105 days is found to be 8 %. Both the partially and fully shrunk sample have lower water uptake, but evince signs of increasing as seen for the virgin sample.

Water uptake for a stress control tube kept at rated temperature for an XLPE cable can be significant.

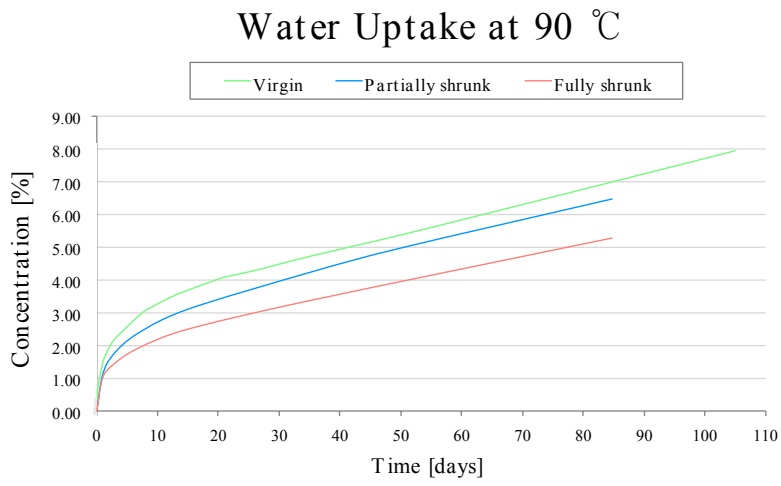

Figure 85. Water uptake at 90 ℃. One sample at each degree of shrinkage is shown in the figure.

When analysing the samples with the same degree of shrinkage, result indicate that the water uptake will increase with temperature.

Figure 86 presents the water uptake by six virgin samples. Samples kept at the same temperature have an approximated equal water uptake, and can be seen by the overlap of the curves.

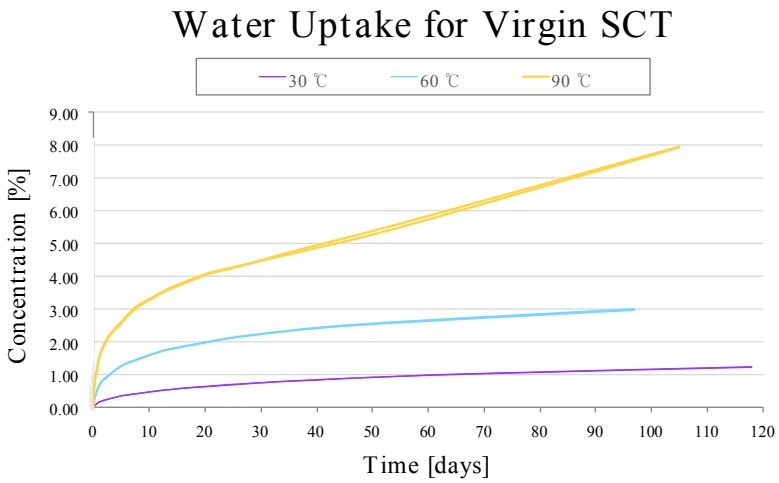

Figure 86. Water uptake by a virgin stress control tube. Two samples at each temperature are shown in the figure.

Analysis of the partially shrunk samples show curves with a greater dispersion for samples kept at the same temperature. This is likely due to an uneven shrinkage of the samples.

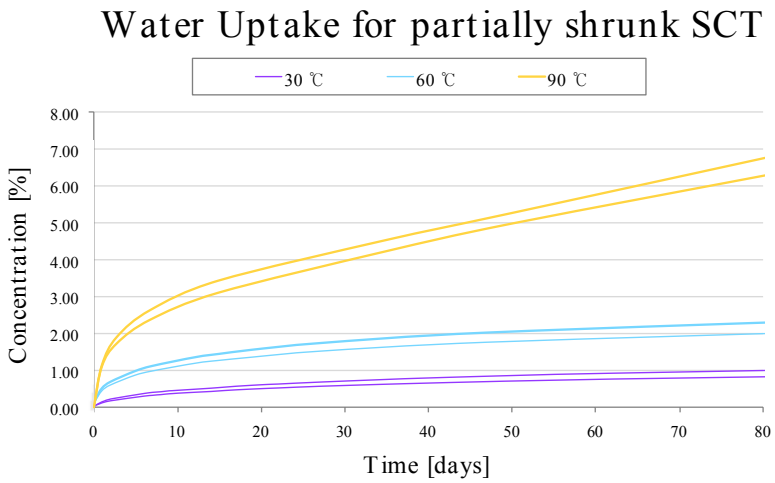

Figure 87. Water uptake by a partially shrunk stress control tube. Two samples at each temperature are shown in the figure.

Result from fully shrunk samples is presented in Figure 88. The curves for the water uptake have a similar shape to the result found for virgin test samples, but a lower value.

Samples kept at the same temperature have approximately equal water uptake, given by the overlap of the curves.

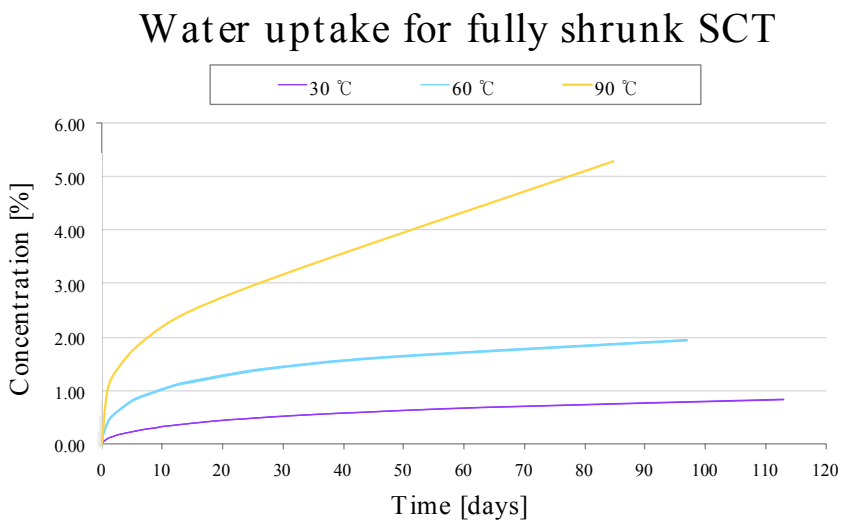

Figure 88. Water uptake by a fully shrunk stress control tube. Two samples at each temperature are shown in the figure.

Appendix B – Differential scanning calorimetry

B1 – Test procedure DSC

The procedure for preparation of the DSC sample is performed in the following steps.

1. The stress control tube is heated to the desired degree of shrinking for the DSC measurement, and then cut into smaller pieces around one cm^2.

2. These pieces are conditioned at 70 °C for a week in a vacuum drying oven, and then held at 25 °C until removed. This procedure is performed as for the diffusion experiment giving comparable results.

3. The tube is removed from the desiccator and immediately taken for preparation for limitation of the influence from the surroundings. Gloves and a forceps should be used when preparing and to moving the sample.

4. The crucible used for the DSC measurement has a volume of 40 µL and the samples of tube need to be cut into smaller pieces. The crucible is used as a pan during measurement, and is heated from beneath. The sample's height should not be too large in order to avoid a temperature gradient. Furthermore, the sample should be evenly distributed along the bottom of the crucible.

5. The DSC measurement program is set up for measurement. A temperature interval is chosen and the measurement is named with the shrinking degree in addition to the number of sequence. Furthermore, the test specimen must be weighed and typed into the measurement program.

6. The weight is found by placing the aluminium crucible on the scale and reset to show zero weight. The specimen is placed in the crucible and its weight is noted in the test program. A weight of 10mg is a suitable amount of sample for the analysis.

7. An aluminium lid should be placed on the top, sealing the crucible. Nitrogen is used during the DSC measurement and since it is desired to have gas intrude into the crucible, three holes are made in the lid before sealing. A needle is used to make holes penetrating entirely through the lid.

8. Forceps is used to place the lid on top of the pan containing the specimen. The crucible is then placed in an encapsulating press for sealing.

9. An empty crucible is made as above and used as a reference sample in the measurement.

10. The test- and reference crucible are placed separately in the measuring device on each heating plate. Furthermore, both water-cooling and the nitrogen gas are checked to be in open position.

11. DSC-measurement is started from a computer, and is self-serviced during the whole test period. Afterwards the measurement can be analysed using the analysing program STARe Excellent.

B2 – DSC measurement results

Virgin stress control tube

Measurement 1

Results from the first DSC measurement on a virgin stress control tube show that during the first run, the specific heat transfer to the sample is quite unstable.

The curve show both endothermic and exothermic peak. The maximum peak temperature occurs at approximately the same temperature as the two other measurements.

The specific heat transfer is in the range of –0.2 to -0.46 W/g.

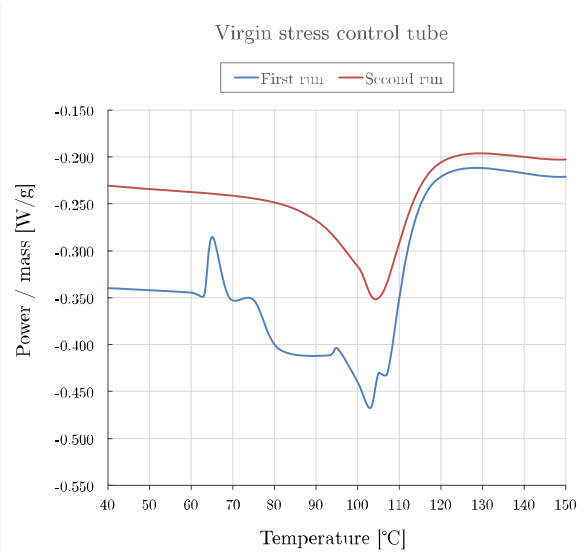

Figure 89. Result from DSC measurement 1.

Measurement 2

The second measurement has a more stable specific heat flow than the first measurement. However, a local peak can also here be found at 80 °C.

During second run, the specific heat flow is lower than the first run, and the local peak has disappeared.

The specific heat transfer is in the range of -0.23 to -0.47 W/g.

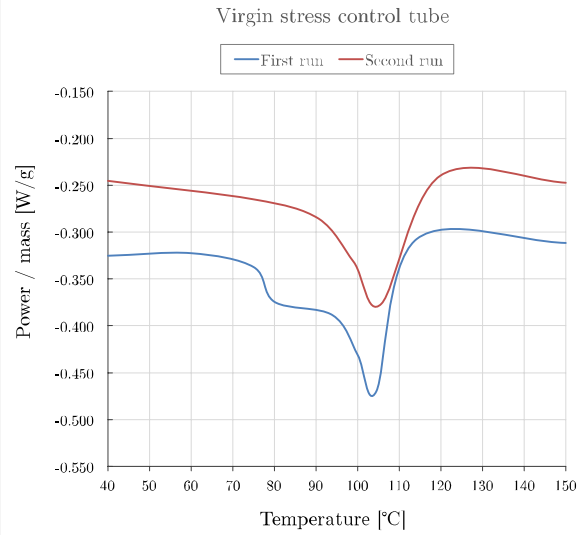

Figure 90. Result from DSC measurement 2.

Measurement 3

The third measurement is similar to the second measurement with a local peak at 80 °C.

The second run has a much smaller specific heat requirement than the first run. This is also the lowest specific heat requirement by all samples. The local peak will also here disappear during the second run.

The specific heat transfer is in the range of -0.19 to -0.5 W/g.

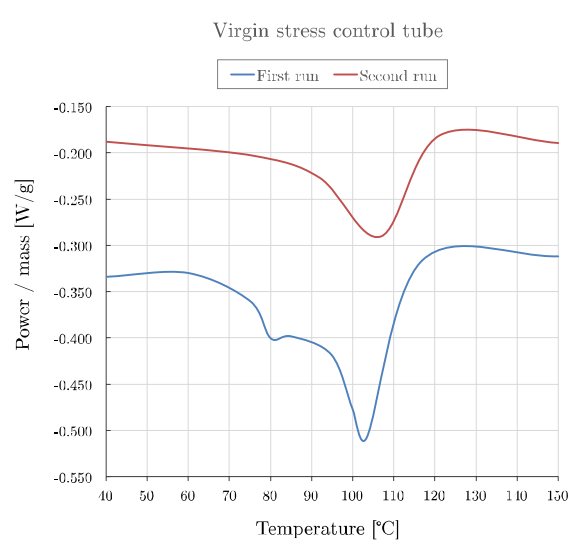

Figure 91. Result from DSC measurement 3.

Partially shrunk stress control tube

Measurement 1

The first measurement of a partially shrunk sample show that the first and second run is more similar than for a virgin sample.

A local peak is found during the first run. However, this peak is smaller than the one found in the virgin samples. This peak disappears during the second run.

The specific heat is in the range of -0.37 to -0.6 W/g.

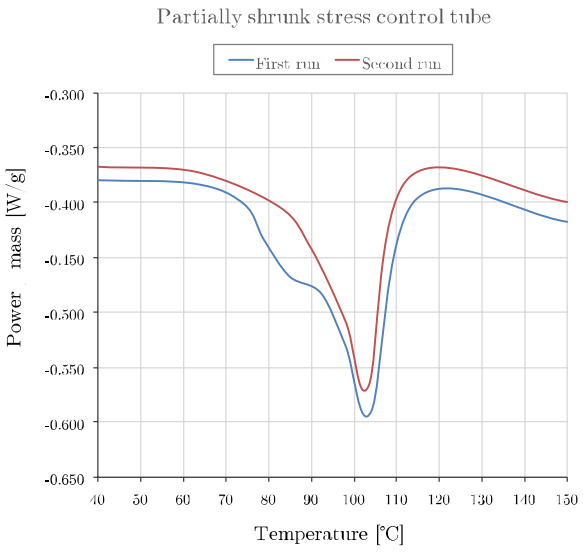

Figure 92. Result from DSC measurement 1.

Measurement 2

Results from the second measurement are similar to the first.

The values in the first and second run are similar, but with a little higher heat requirement during the first run.

A local peak is found in the first run and disappears during the second run.

The specific heat is in the range of -0.32 to -0.55 W/g.

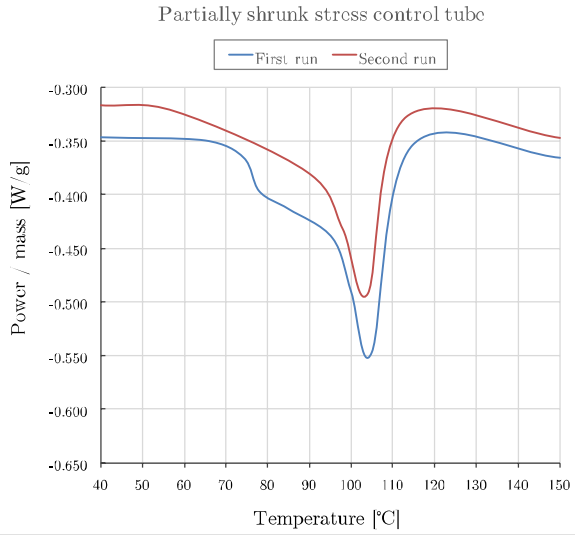

Figure 93. Result from DSC measurement 2.

Measurement 3

The third measurement has almost identical specific heat transfer during the first and third measurement. A local peak during the first run is the difference that distinguishes them.

The specific heat is within the range of -0.38 to -0.61 W/g. This is the highest for three measurements, and the range with the fully shrunken. The sample is likely a higher degree of shrinkage than the two previous.

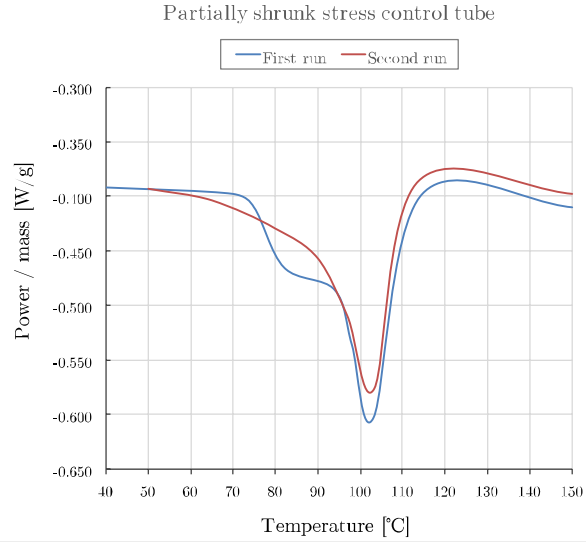

Figure 94. Result from DSC measurement 3.

Fully shrunk stress control tube

Measurement 1

Results from the first DSC measurement of a fully shrunk stress control tube shows that the specific heat during first and second run is approximately identical.

No local peak is present during this measurement.

The specific heat for the measurement is within the range of -0.35 to -0.6 W/g.

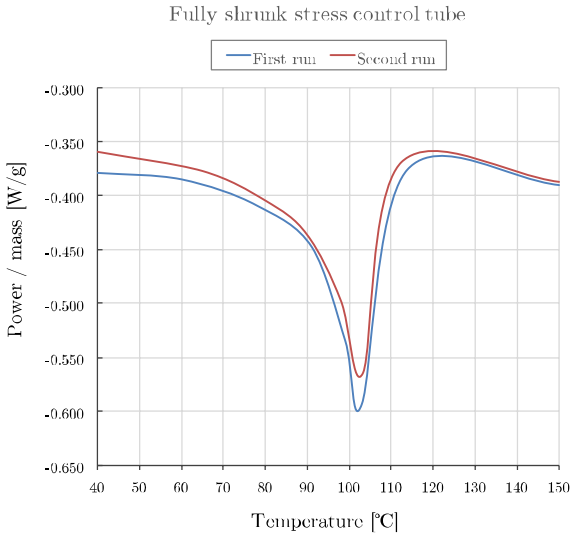

Figure 95. Result from DSC measurement 1.

Measurement 2

The second measurement is similar the first.

The first and second run is almost identical and no local peak is observed.

The specific heat flow during the measurement is within the range of -0.35 to -0.56 W/g.

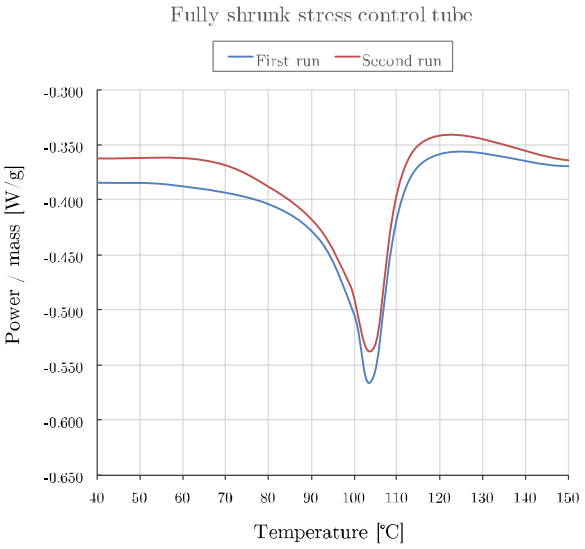

Figure 96. Result from DSC measurement 2.

Measurement 3

The third measurement differs out from the previous two. The first and second run is similar, however, a local peak can be observed.

This measurement is similar to the third measurement of a partially shrunk sample. The local peak is therefore likely caused by an incomplete shrinking.

The specific heat range is within -0.38 to -0.63 W/g.

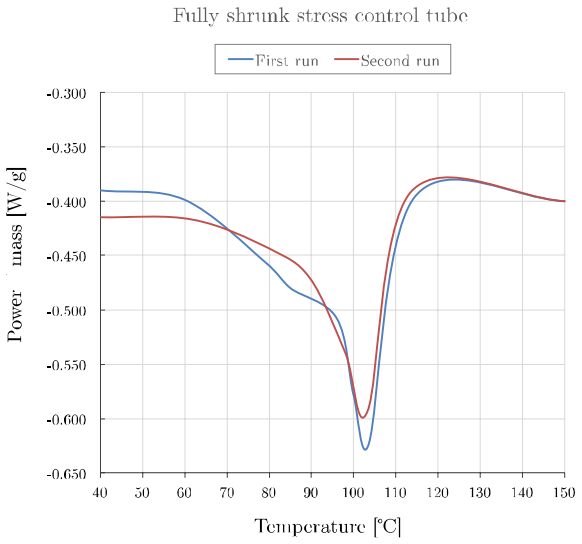

Figure 97. Result from DSC measurement 3.

Appendix C – Results from dielectric response measurements

Results from dielectric response measurements on Object S are here provided as figures. The figures presents the values of the dielectric loss tangent, complex capacitances and the calculated conductivity for all measurements performed.

First, the results for measurements at 40, 90, 150 and 40 ℃ are given for Object L and Object S. Furthermore, the results from measurements at DSC temperatures are presented. At last, the measuring results from examination of an increased humidity are given. Results from the dry object, with and without plastic insulation, in addition to results from the wet object measurements are presented.

C1 – Measurement result, Object L

Measurement at 40 °C

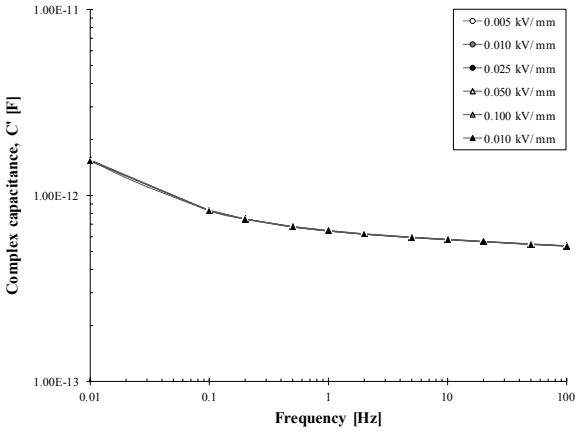

Figure 98. Complex capacitance, C', for Object L measured at 40 °C.

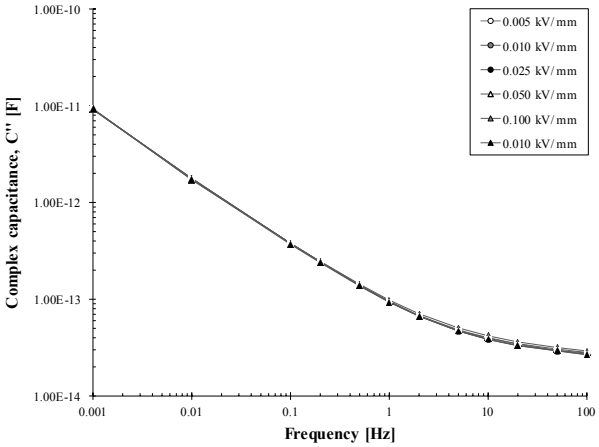

Figure 99. Complex capacitance, C'', for Object L measured at 40 °C.

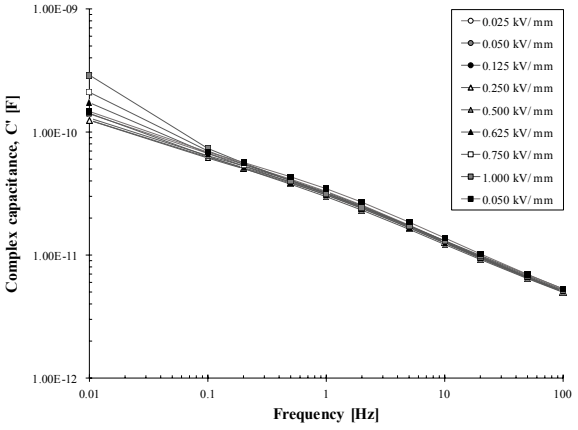

Figure 100. Dielectric loss tangent for Object L measured at 40 °C.

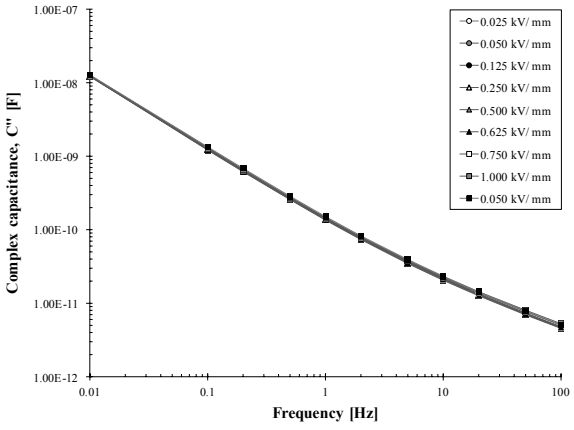

Figure 101. Conductivity for Object L calculated from measurements at 40 °C.

Measurement at 90 °C

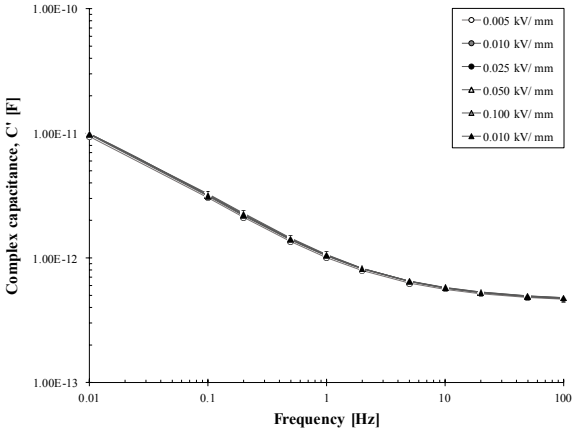

Figure 102. Complex capacitance, C', for Object L measured at 90 °C.

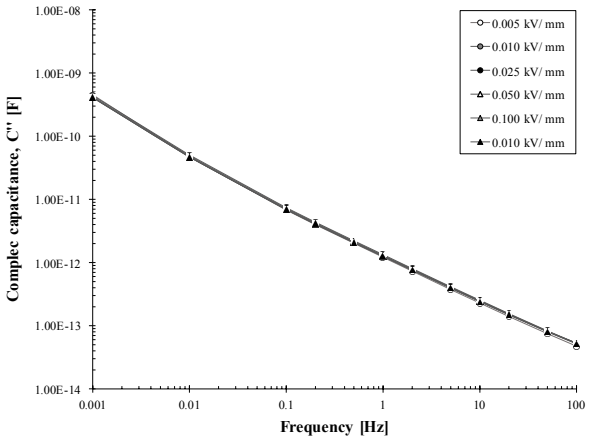

Figure 103. Complex capacitance, C'', for Object L measured at 90 °C.

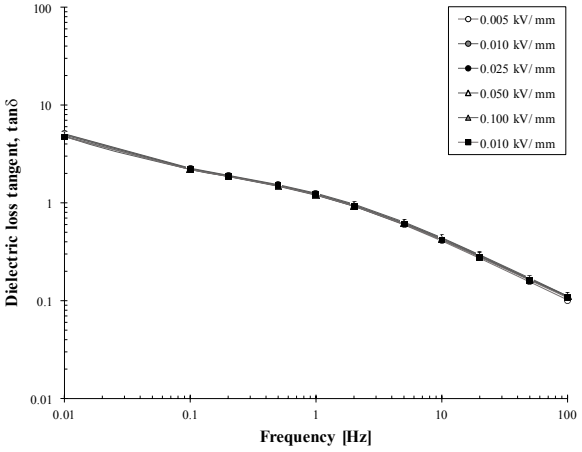

Figure 104. Dielectric loss tangent for Object L measured at 90 °C.

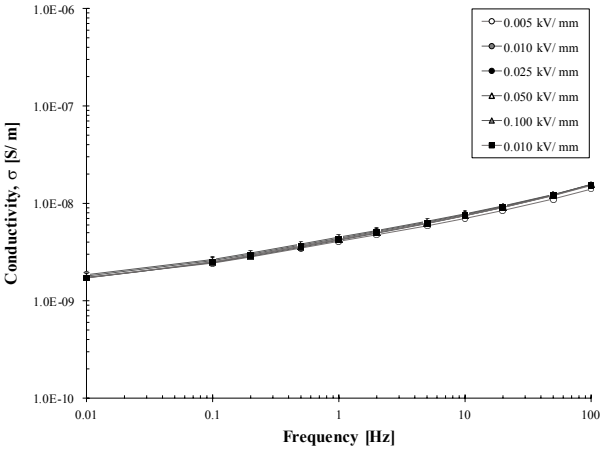

Figure 105. Conductivity for Object L calculated for measurements at 90 °C.

Measurement at 150 °C

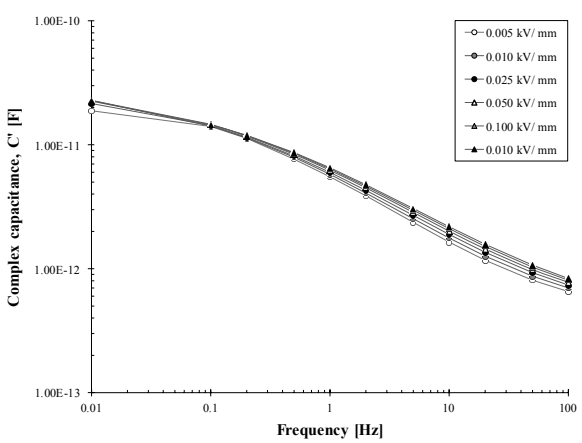

Figure 106. Complex capacitance, C', for Object L measured at 150 °C.

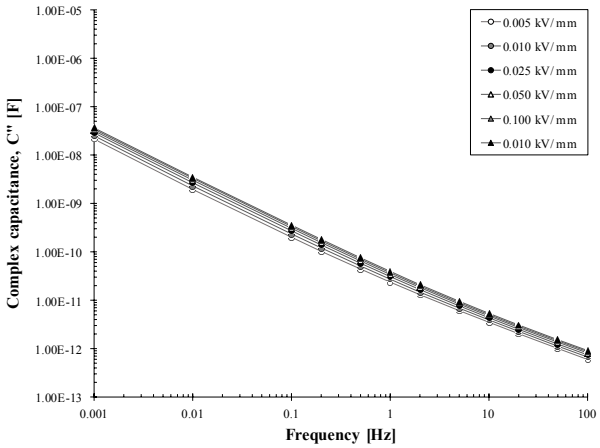

Figure 107. Complex capacitance, C'', for Object L measured at 150 °C.

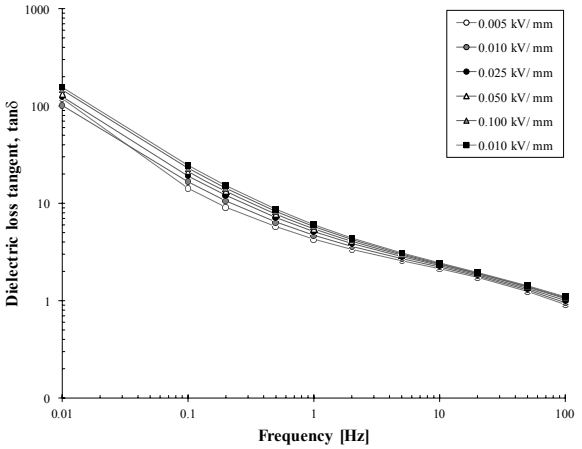

Figure 108. Dielectric loss tangent for Object L measured at 150 °C.

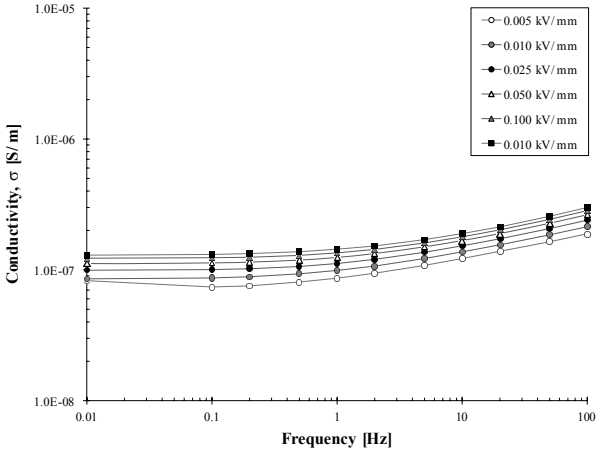

Figure 109. Conductivity for Object L calculated from measurements at 150 °C.

Measurement at 40 °C, second run

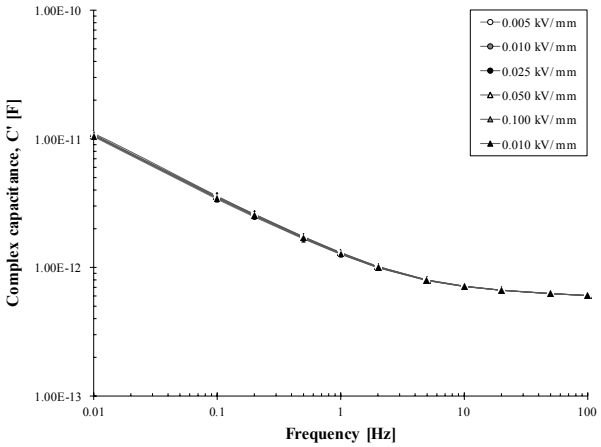

Figure 110. Complex capacitance, C', for Object L measured at 40 °C.

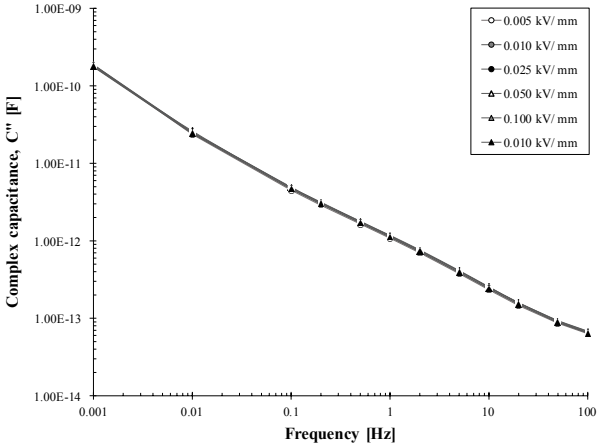

Figure 111. Complex capacitance, C'', for Object L measured at 40 °C.

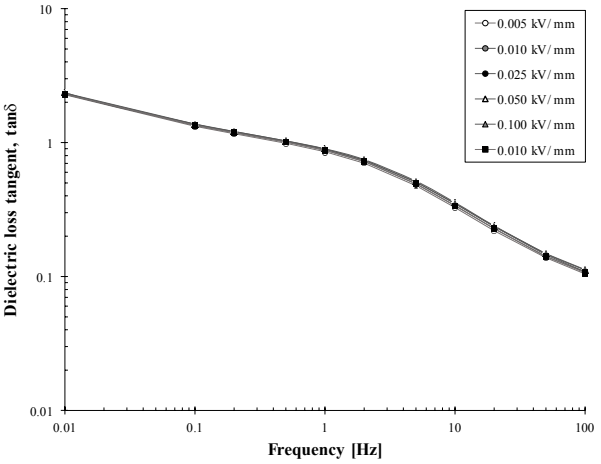

Figure 112. Dielectric loss tangent for Object L measured at 40 °C, second run.

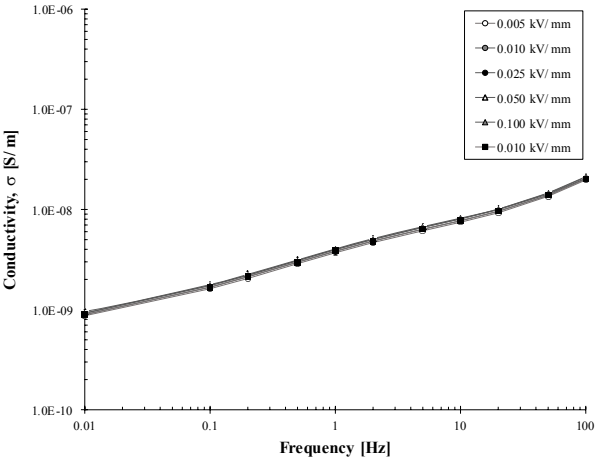

Figure 113. Conductivity for Object L calculated from measurements at 40 °C, second run.

C2 – Measurement result, Object S

Measurement at 40 °C

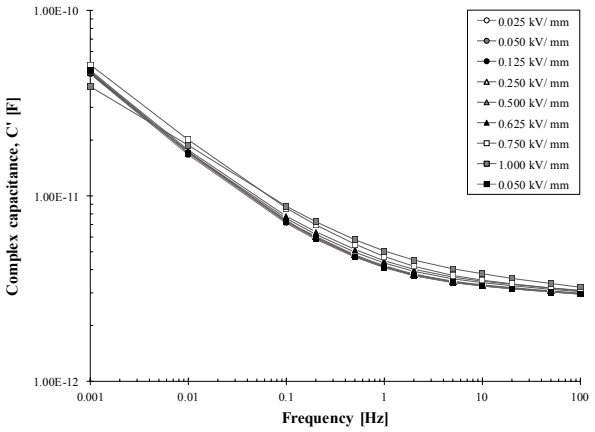

Figure 114. Complex capacitance, C', for Object L measured at 40 °C.

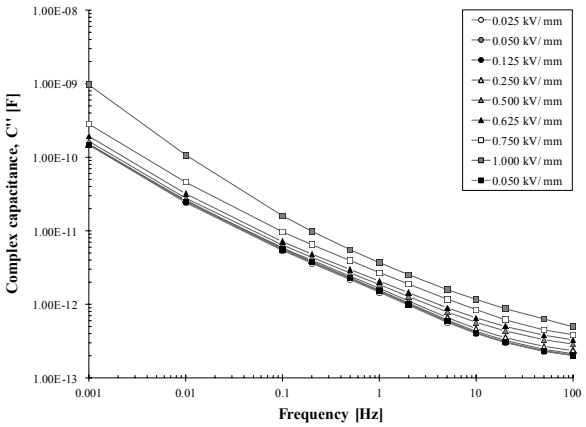

Figure 115. Complex capacitance, C'', for Object L measured at 40 °C.

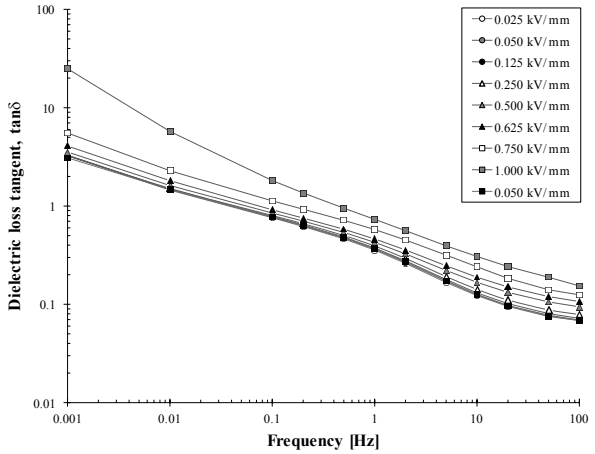

Figure 116. Dielectric loss tangent for Object S measured at 40 °C.

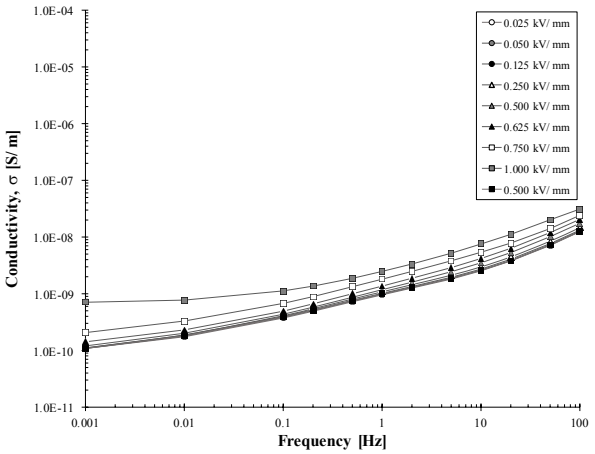

Figure 117. Conductivity for Object S calculated from measurements at 40 °C.

Measurement at 90 °C

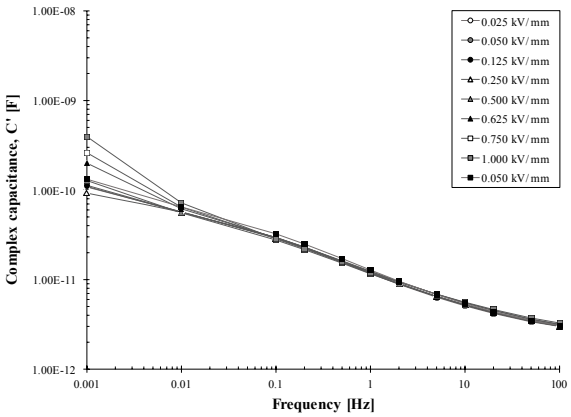

Figure 118. Complex capacitance, C', for Object S measured at 90 °C.

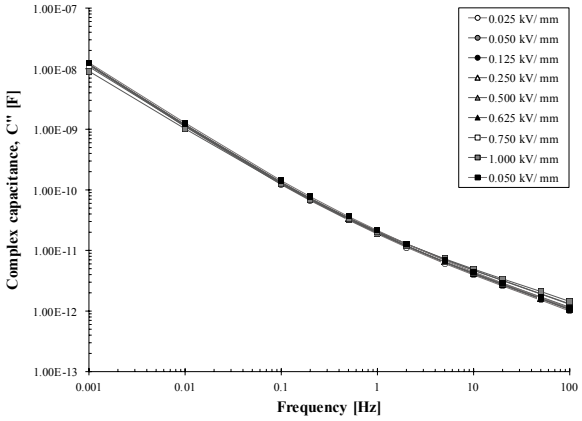

Figure 119. Complex capacitance, C'', for Object S measured at 90 °C.

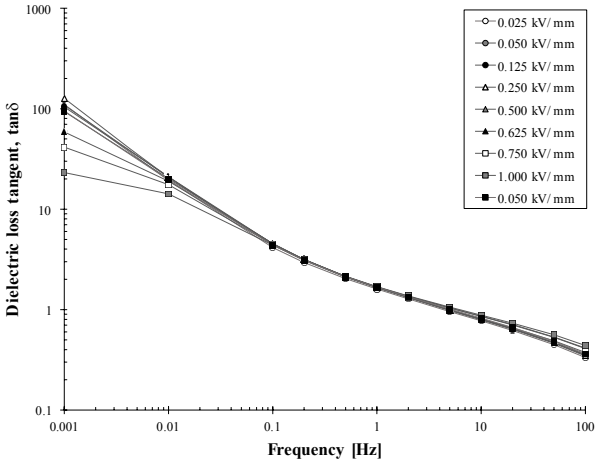

Figure 120. Dielectric loss tangent for Object S measured at 90 °C.

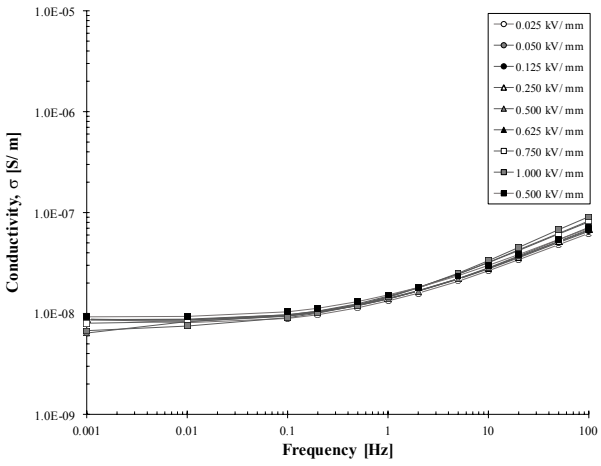

Figure 121. Conductivity for Object S calculated from measurements at 90 °C.

Measurement at 150 °C

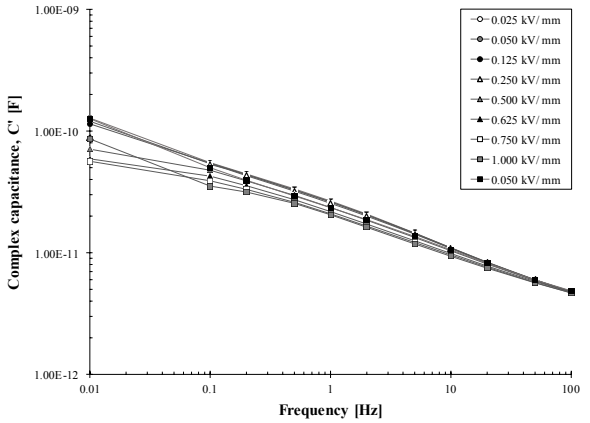

Figure 122. Complex capacitance, C', for Object S measured at 150 °C. Limited to 10 mHz as the losses becomes too large.

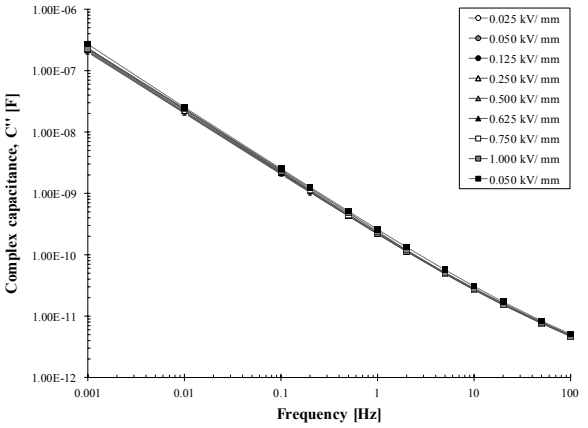

Figure 123. Complex capacitance, C'', for Object S measured at 150 °C.

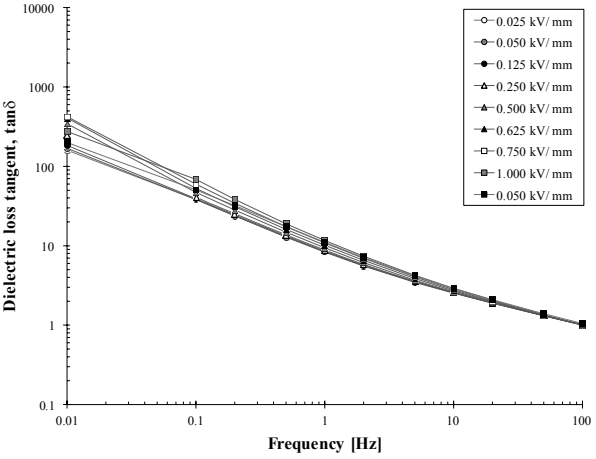

Figure 124. Dielectric loss tangent for Object S measured at 150 °C. Large dispersion in values as accuracy range is exceeded.

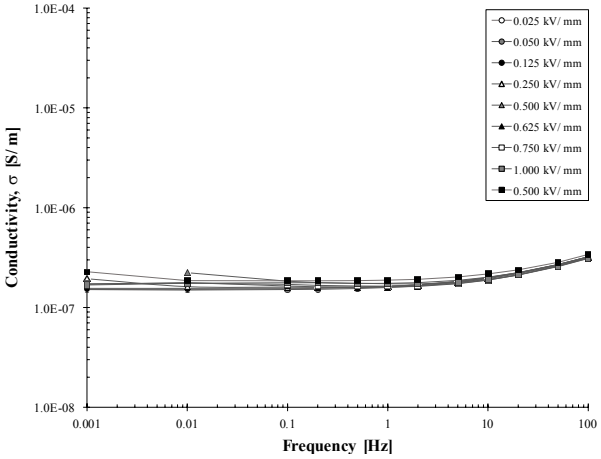

Figure 125. Conductivity for Object S calculated from measurements at 150 °C.

Measurement at 40 °C, second run

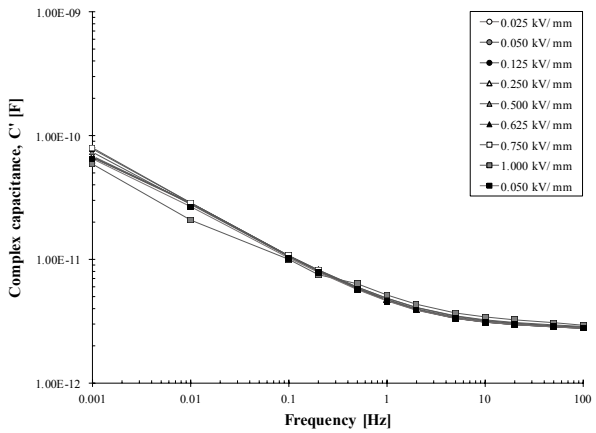

Figure 126. Complex capacitance, C', for Object L measured at 40 °C.

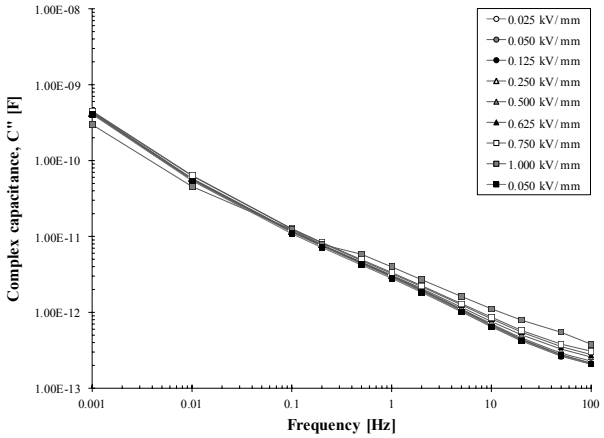

Figure 127. Complex capacitance, C'', for Object L measured at 40 °C.

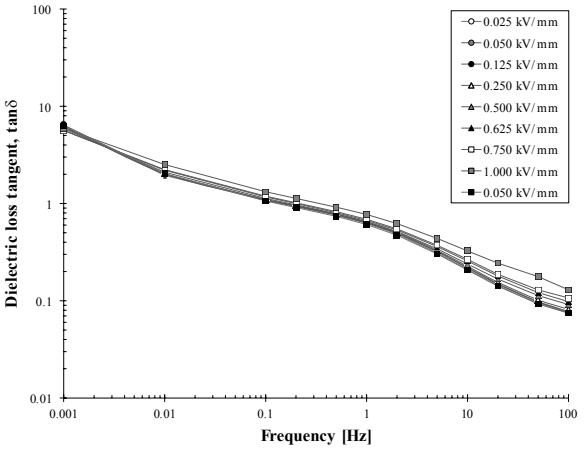

Figure 128. Dielectric loss tangent for Object S measured at 150 °C. Large dispersion in values as accuracy range is exceeded.

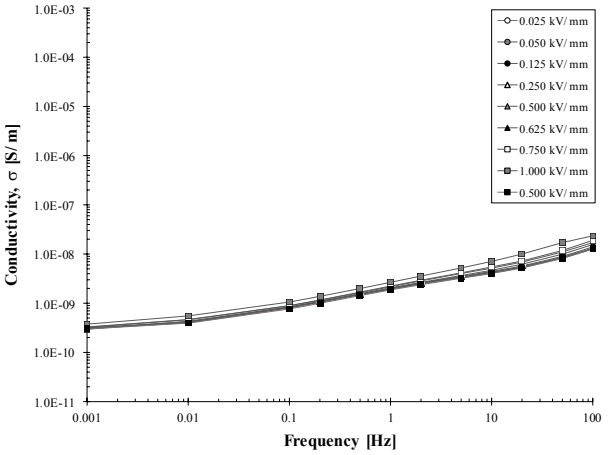

Figure 129. Conductivity for Object S calculated from measurements at 150 °C.

C3 – Results at DSC temperatures

Object L

Measurement on Object L at 94 °C

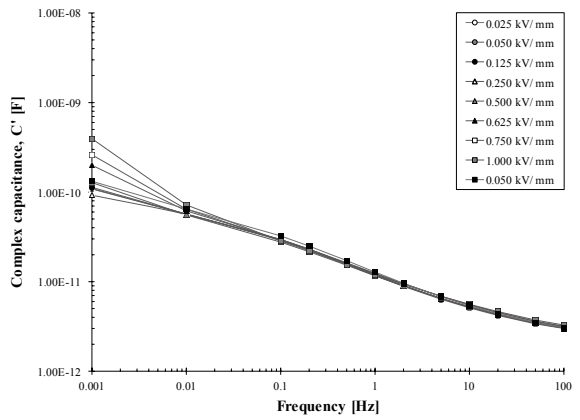

Figure 130. Complex capacitance, C', for Object L measured at 94 °C.

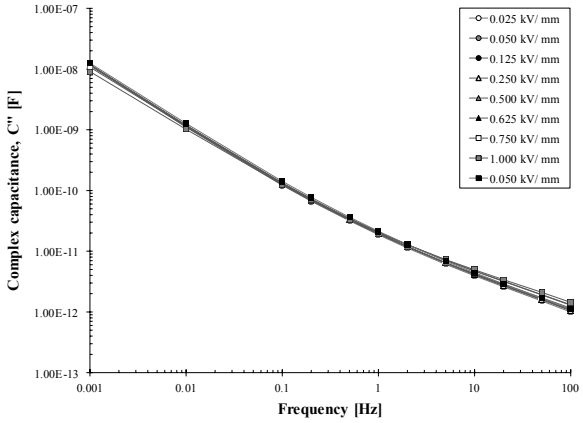

Figure 131. Complex capacitance, C'', for Object L measured at 94 °C.

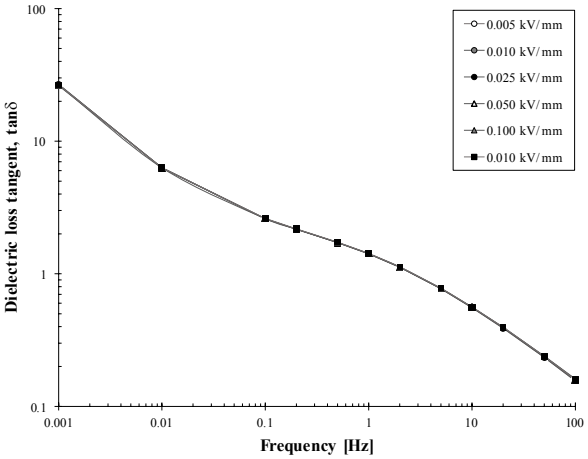

Figure 132. Dielectric loss tangent for Object L measured at 94 °C.

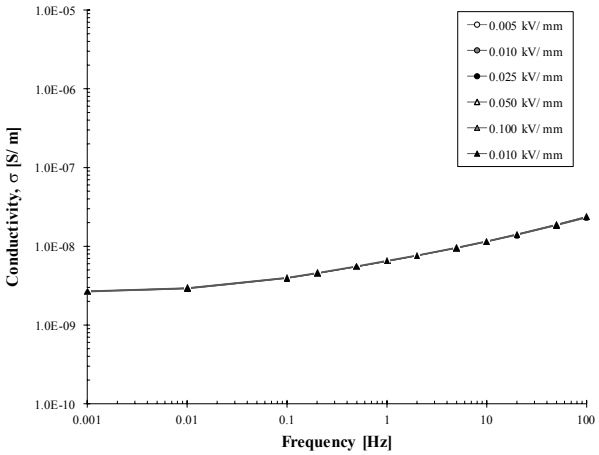

Figure 133. Conductivity for Object L calculated from measurements at 94 °C.

Measurement on Object L at 104 °C

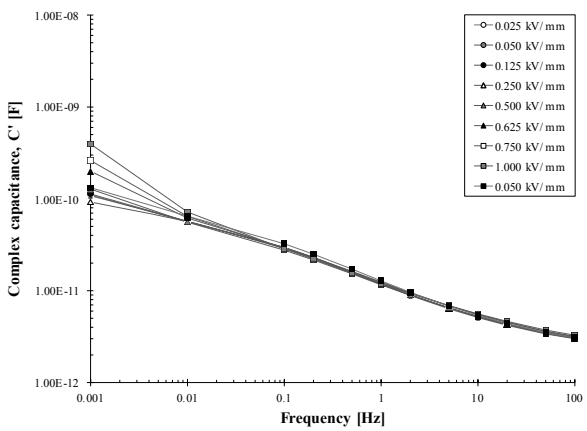

Figure 134. Complex capacitance, C', for Object S measured at 104 °C.

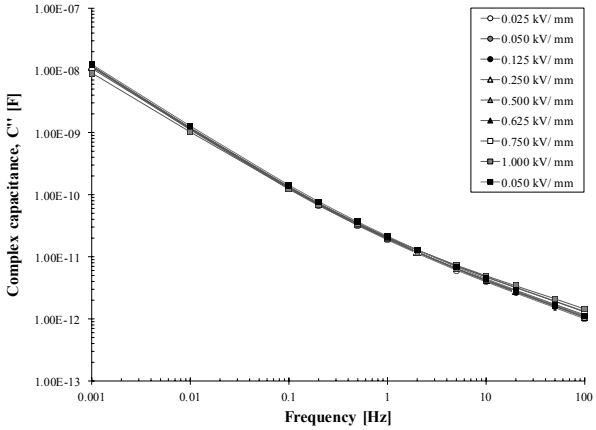

Figure 135. Complex capacitance, C'', for Object S measured at 104 °C.

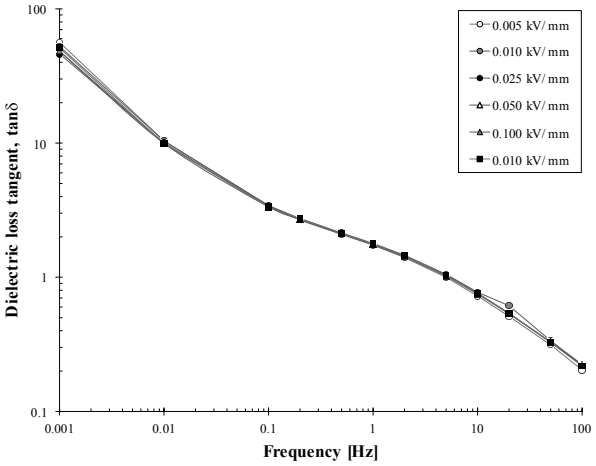

Figure 136. Dielectric loss tangent for Object S measured at 104 °C.

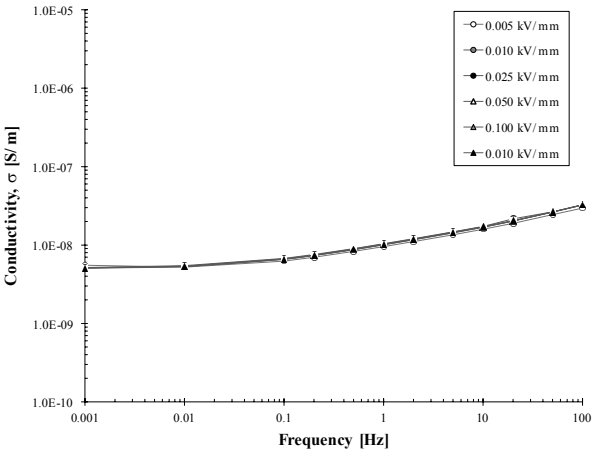

Figure 137. Conductivity for Object S calculated from measurements at 104 °C.

Measurement on Object L at 114 °C

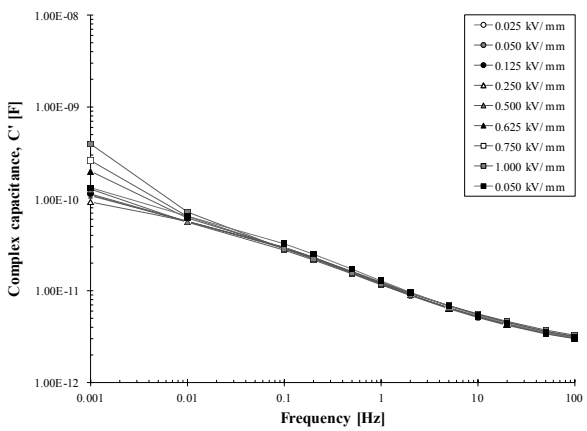

Figure 138. Complex capacitance, C', for Object S measured at 114 °C.

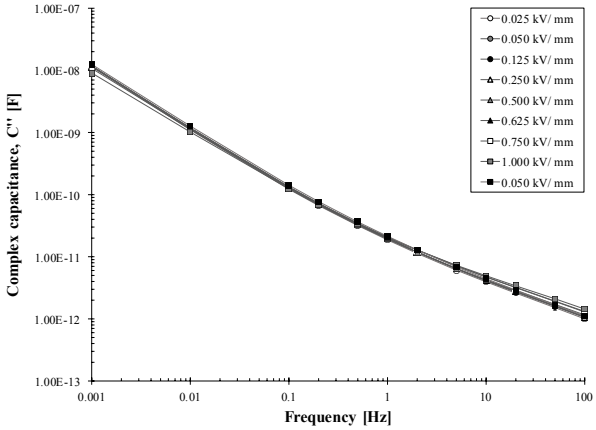

Figure 139. Complex capacitance, C'', for Object S measured at 114 °C.

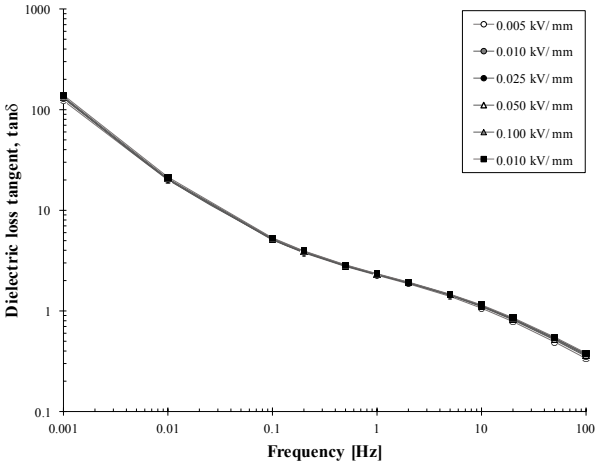

Figure 140. Dielectric loss tangent for Object S measured at 114 °C.

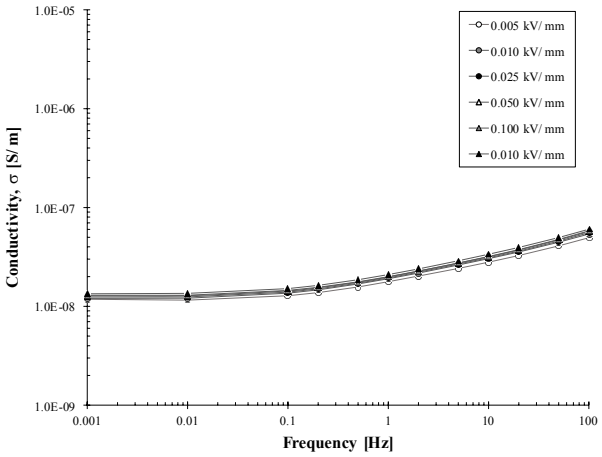

Figure 141. Conductivity for Object S calculated from measurements at 114 °C.

Object S

Measurement on Object S at 94 °C

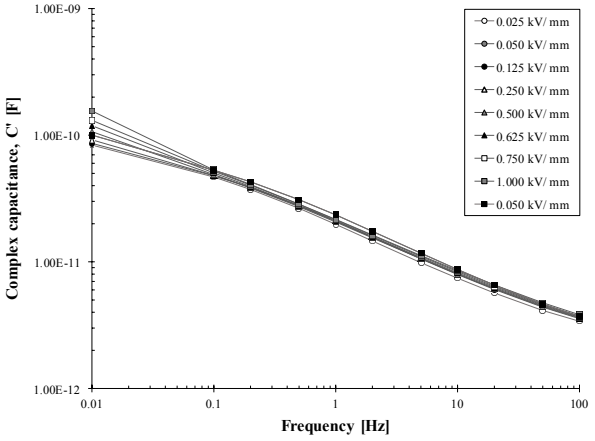

Figure 142. Complex capacitance, C', for Object S measured at 94 °C.

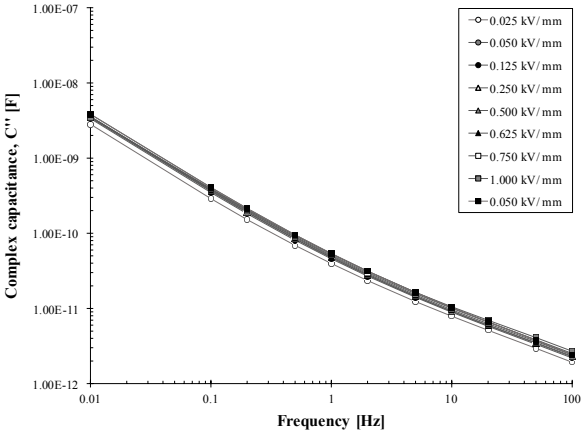

Figure 143. Complex capacitance, C'', for Object S measured at 94 °C.

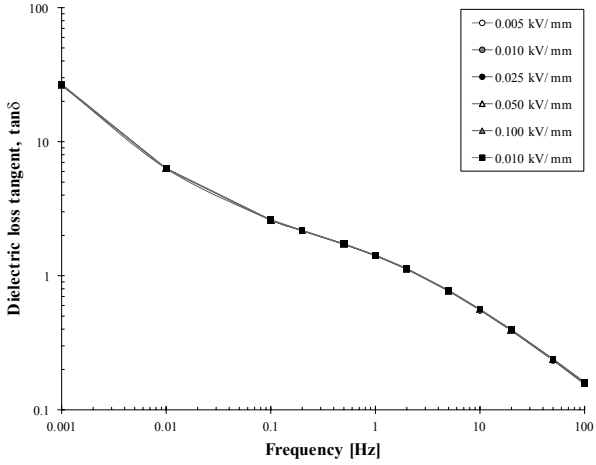

Figure 144. Dielectric loss tangent for Object S measured at 94 °C.

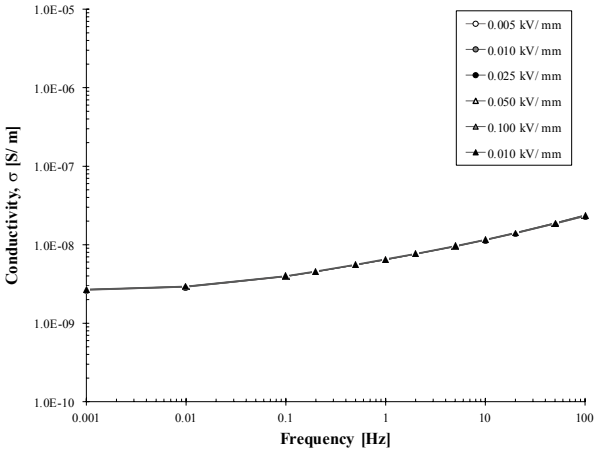

Figure 145. Conductivity for Object S calculated from measurements at 94 °C.

Measurement on Object S at 104 °C

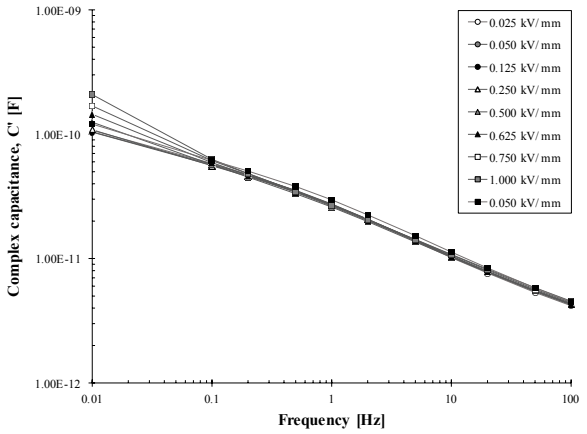

Figure 146. Complex capacitance, C', for Object S measured at 104 °C.

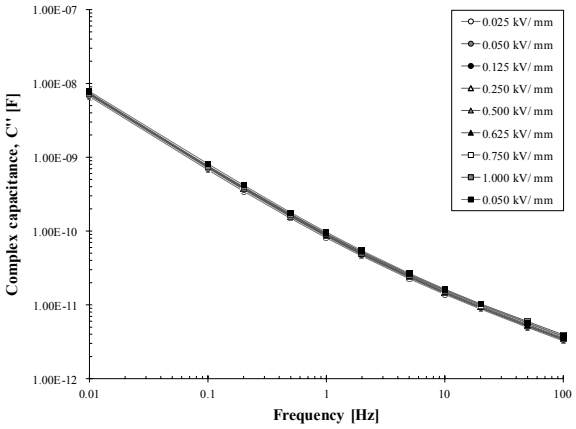

Figure 147. Complex capacitance, C'' , for Object S measured at 104 °C.

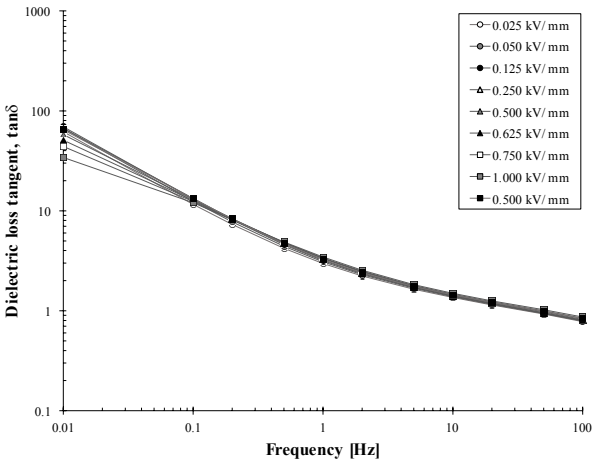

Figure 148. Dielectric loss tangent for Object S measured at 104 °C.

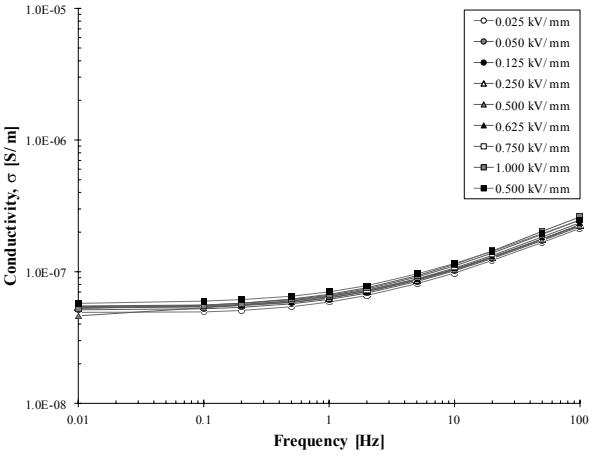

Figure 149. Conductivity for Object S calculated from measurements at 104 °C.

Measurement on Object S at 114 °C

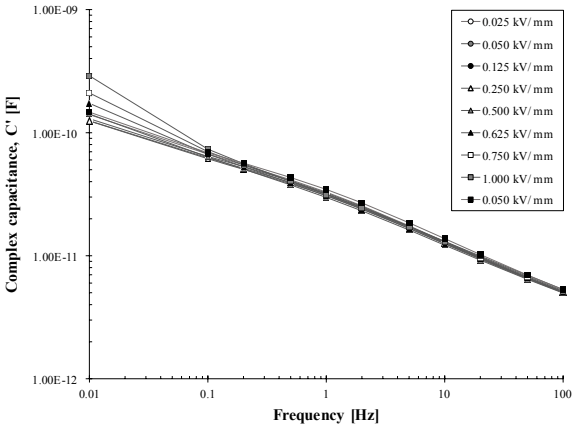

Figure 150. Complex capacitance, C', for Object S measured at 114 °C.

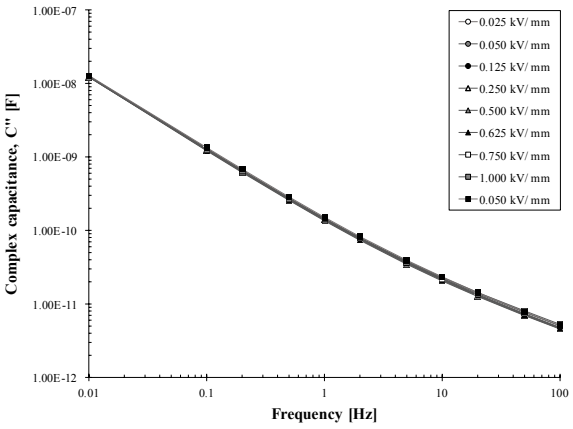

Figure 151. Complex capacitance, C'', for Object S measured at 114 °C.

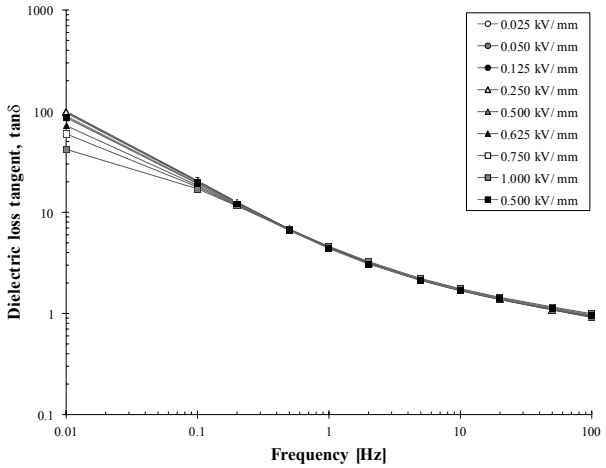

Figure 152. Dielectric loss tangent for Object S measured at 114 °C.

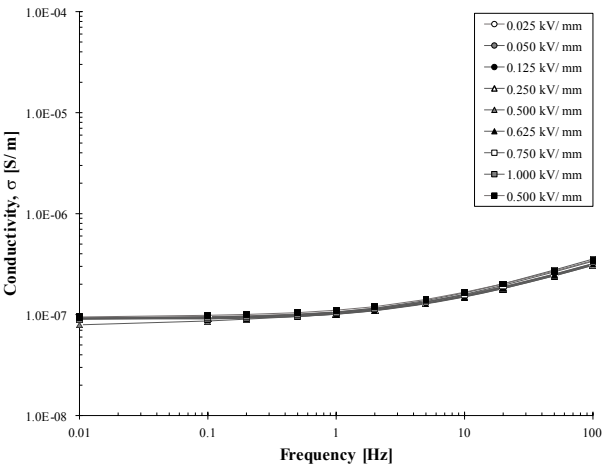

Figure 153. Conductivity for Object S calculated from measurements at 114 °C.

C4 – Measurements results examine effect of increased humidity

Measurement on a dry test object

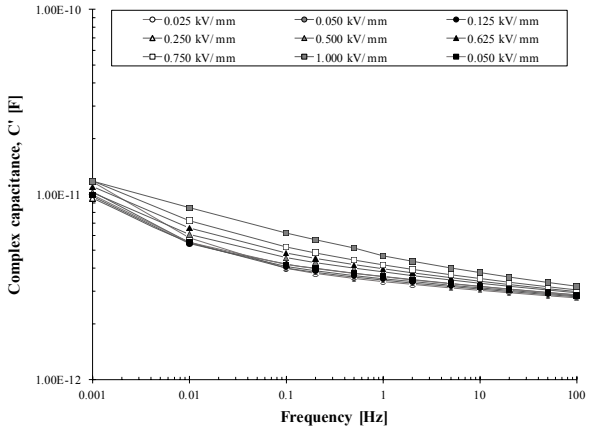

Figure 154. Complex capacitance, C', for a dry test object measured at 20 °C.

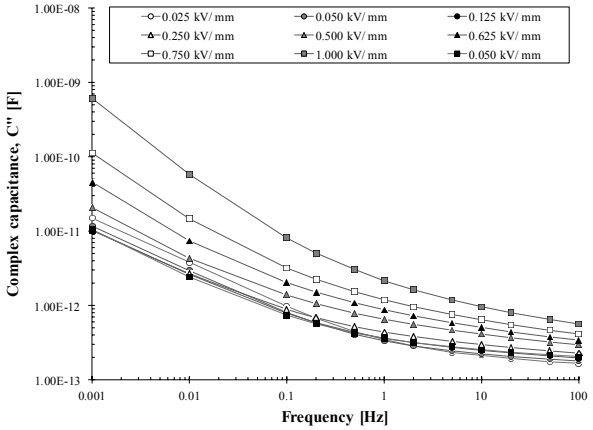

Figure 155. Complex capacitance, C'', for a dry test object measured at 20 °C.

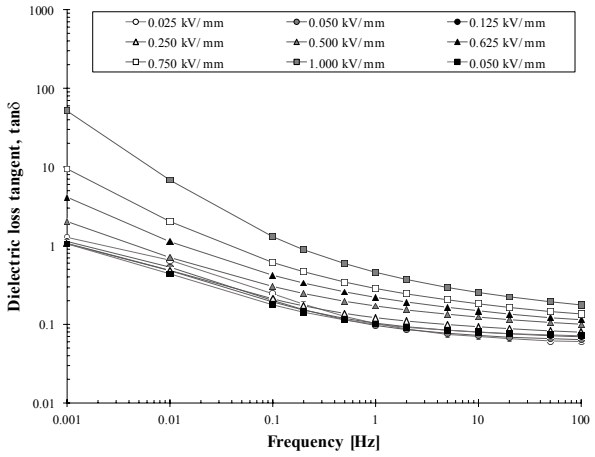

Figure 156. Dielectric loss tangent for a dry test object measured at 20 °C.

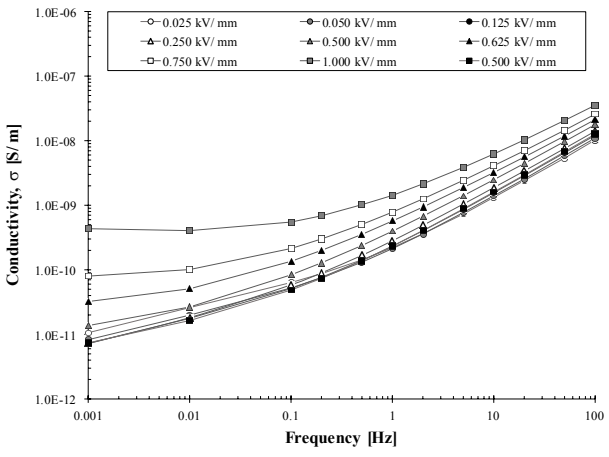

Figure 157. Conductivity for a dry test object calculated from measurements at 20 °C.

Measurement on test object wrapped in plastic foil and insulation tape

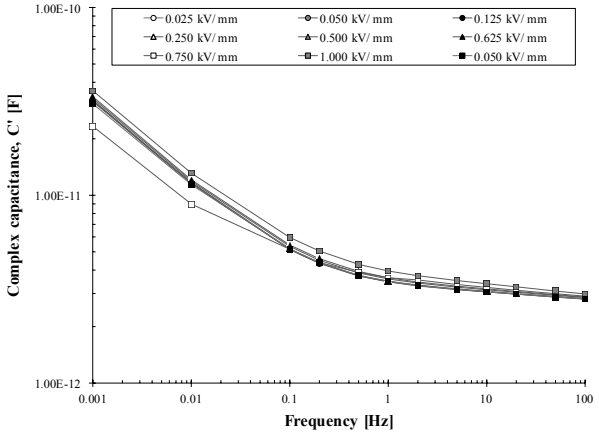

Figure 158. Complex capacitance, C', measured at 20 °C.

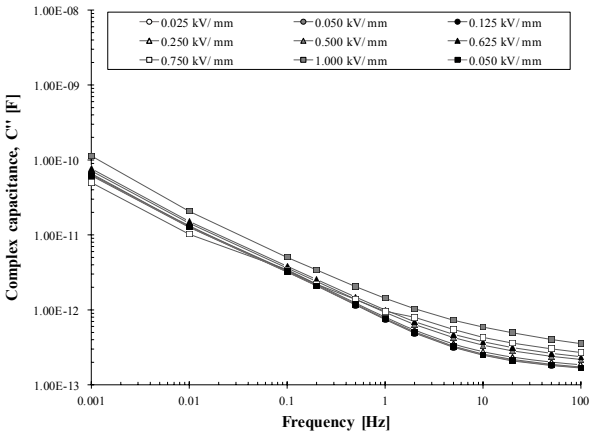

Figure 159. Complex capacitance, C'', measured at 20 °C.

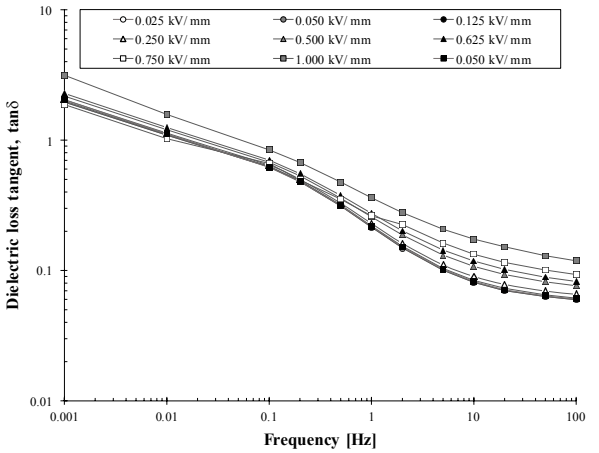

Figure 160. Dielectric loss tangent measured at 20 °C.

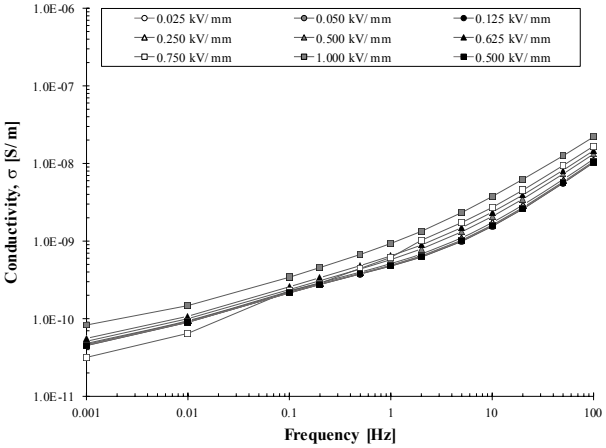

Figure 161. Complex capacitance, C'', measured at 20 °C.

Measurement on wet test object

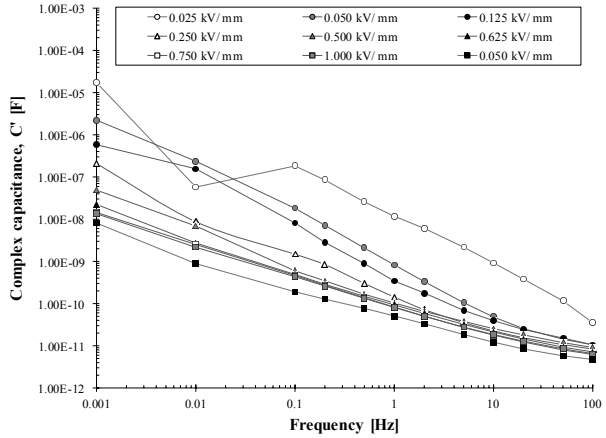

Figure 162. Complex capacitance, C', for a wet test object measured at 20 °C.

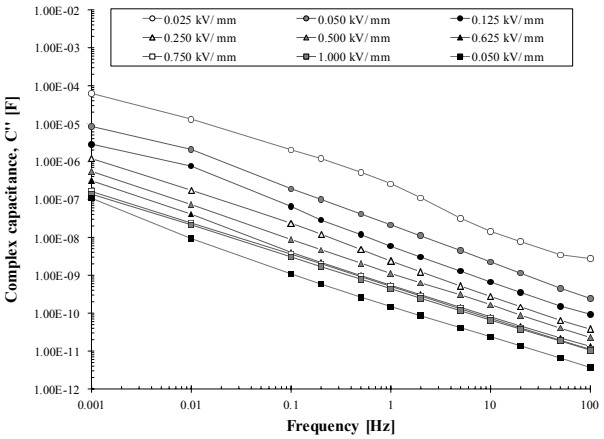

Figure 163. Complex capacitance, C'', for a wet test object measured at 20 °C.

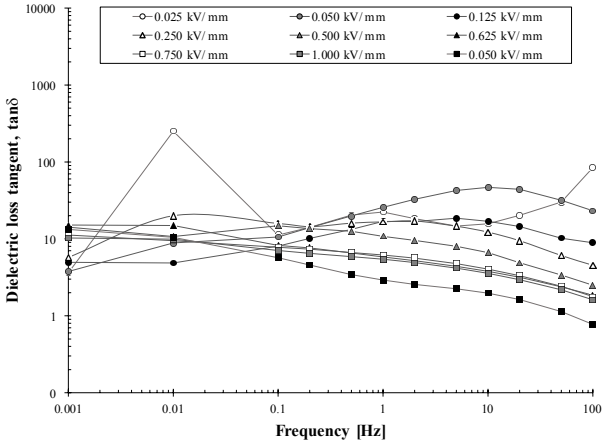

Figure 164. Complex capacitance, C', for a wet test object measured at 20 °C.

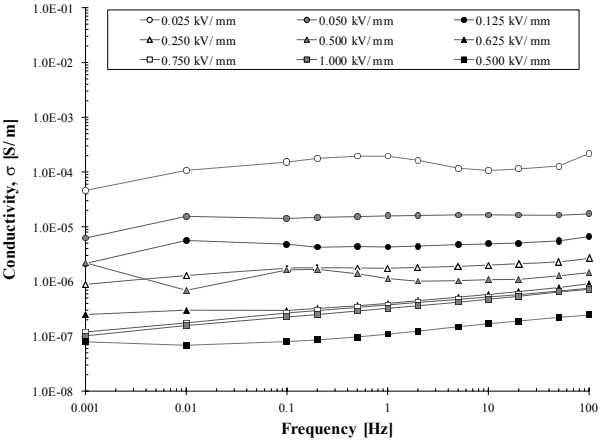

Figure 165. Complex capacitance, C'', for a wet test object measured at 20 °C.

Appendix D – Formulas used for calculation of the conductivity

The conductivity of the test object can be calculated with the parameters found in dielectric spectroscopy measurements. The relationship between dielectric loss tangent, permittivity and conductivity is seen in Eq. 2.3, and can be rewritten as in Eq. D.1.

$$\sigma \approx \tan\delta \cdot \omega \varepsilon' \varepsilon_0 \qquad \text{Eq. D.1}$$

This equation is an approximation and will apply when the relation $|\varepsilon_r'| \gg |\varepsilon_r''|$ is fulfilled.

At low frequencies, the losses in the test object will be dominated by the conductivity. Utilizing this relation, the conductivity of the stress control tube can be calculated using Eq. 4.1 with dielectric loss tangent found at the lowest frequency.

As the capacitance measured by IDA 200 is the equivalent for both the PTFE rod and SCT, calculations are necessary for determination of the complex permittivity. The equivalent circuit is illustrated in Figure 166, and is given as a parallel coupling.

Using the relation from Eq. D.2 for the parallel coupling, complex permittivity for the stress control tube can be determine as yield in Eq. D.3.

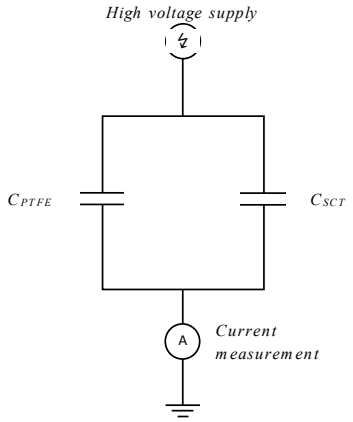

Figure 166. Equivalent circuit for measurement of the total capacitance in the test object.

$$C = C_0\,(\varepsilon' - j\,\varepsilon'') \qquad \text{Eq. D.2}$$

$$\varepsilon'_{SCT} = \frac{C'_{eq} - (C_{0,PTFE} \cdot \varepsilon'_{PTFE})}{C_{0,SCT}} \qquad \text{Eq. D.3}$$

The complex permittivity of the PTFE rod is for this thesis used as 2.1 [37]. The geometric capacitance, C_0, is determined for each of the materials. Additionally, the value of C_0 is required determined for both Object L and Object S as their distance between the electrodes is different.

After determined the relative permittivity, conductivity can be calculated with values found at the lowest frequency.

Object L

$$C_0 = \varepsilon_0 \cdot \frac{A}{d} \qquad \text{Eq. D.4}$$

$$C_{0,PTFE} = 8.85 \cdot 10^{-12} \cdot \frac{\pi \cdot 0.0125^2}{0.1} = 4.344 \cdot 10^{-14}\ [F] \qquad \text{Eq. D.5}$$

$$C_{0,SCT} = = 8.85 \cdot 10^{-12} \cdot \frac{\pi \cdot (0.0145^2 - 0.0125^2)}{0.1} = 1.501 \cdot 10^{-14}\ [F] \qquad \text{Eq. D.6}$$

Object S

$$C_{0,PTFE} = 8.85 \cdot 10^{-12} \cdot \frac{\pi \cdot 0.0125^2}{0.02} = 2.172 \cdot 10^{-13}\ [F] \qquad \text{Eq. D.7}$$

$$C_{0,SCT} = = 8.85 \cdot 10^{-12} \cdot \frac{\pi \cdot (0.0145^2 - 0.0125^2)}{0.02} = 7.507 \cdot 10^{-14}\ [F] \qquad \text{Eq. D.8}$$

Appendix E - Dissection of the wet test object

Dissection of the wet test object was performed after dielectric response measurements. The stress control tube was closely examined for tracking on the surface towards the electrodes.

Tracking is a formation of carbonaceous layers or lines on the surface of organic insulators [5]. As water is present in the test object, they can form conductive paths on the surface. If these conductive paths expand from one electrode to the other, they will short circuit the electrodes. Dielectric response measurement results will thereby not be referred to the stress control tube.

Close examination of the stress control tube indicate that tracking have not been present during measurements. A picture of the stress control tube can be found in Figure 169. Observations made indicate that large heat generation have been formed at one electrode as illustrated in Figure 170.

As the electrodes also have been immersed in water, rust has been formed at both electrodes. However, as tracking is not observed, the presence of rust is assumed to not influence the measurement results.

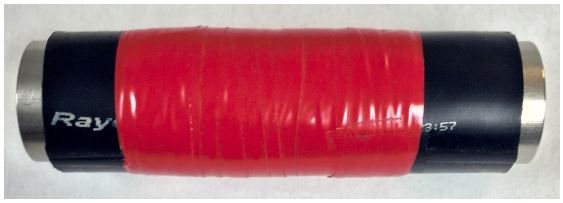

Figure 167. Wet test object with plastic foil and PVC insulation tape.

Figure 168. Wet test object wrapped in plastic foil.

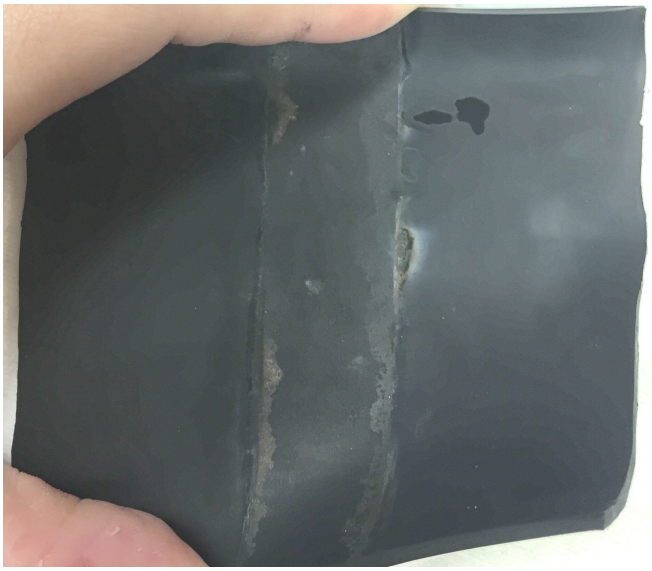

Figure 169. Dissection of the wet stress control tube after measurements.

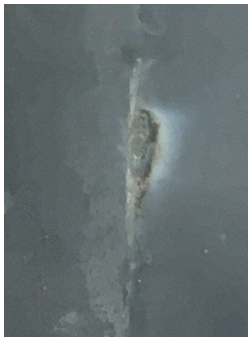

Figure 170. Closer look at a point where a heat generation have made a mark on the stress control tube.

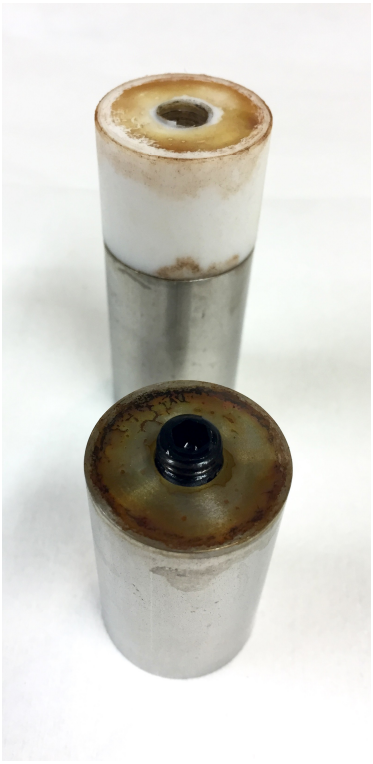

Figure 171. Metal electrodes and PTFE rod from the wet test object. Rust is observed at each electrode.

Appendix F – List of figures

Appendix G – List of tables